7-12-2014

A Standalone High Frequency Receiver System

Orlando Leone Jr.

Orlando Joseph Leone, Jr.

Candidate

Electrical and Computer Engineering

Department

This thesis is approved, and it is acceptable in quality and form for publication:

Approved by the Thesis Committee:

Mark Gilmore , Chairperson

Greg Taylor

Christos Christodoulou

A Standalone High Frequency Receiver System

by

Orlando Leone Jr.

B.S.E.E., Florida International University, 2010

THESIS

Submitted in Partial Fulfillment of the
Requirements for the Degree of

Master of Science
Electrical Engineering

The University of New Mexico

Albuquerque, New Mexico

May, 2014

Dedication

I dedicate this and all my future work to the peaceful research of scientific and human discovery, whether terrestrial or cosmic.

Acknowledgments

I would like to acknowledge the help of Joseph Craig, UNM systems engineer and Jayce Dowell, astronomy research professor. These two individuals took up the responsibility to assist a graduate student on a systems-level research project. They persevered through the barrage of questions, software issues, and troubleshooting. Jayce especially has been present as a contributing member and thus a core reason why the project is a success. I would like to acknowledge all the graduate students who had to put up with the hundreds of cups of instant soup and green tea, as well as the random barging in with occasionally pertinent topics of discussion. Finally, Dr. Greg Taylor offered the project to me and I am deeply grateful. As a result, my career goals and profession has changed to suit more interesting and enjoyable adventures. He has helped my character by making it clear what is expected of any professional during crunch time - one must do what is needed to get the project done. In addition, I like to thank and give praise for the at-large open-source community and groups that make GNU/Linux, GNU Radio, software defined radio, and Python possible and tangible. In addition, the open-source community expresses advice and tips via forums which demonstrate many ways of doing things. In the beginning of my project, all this was a daunting task but I now have a great respect for open-source software and the culture behind it. Without such things, this project, along with other educational and recreational projects would be slower, bulkier, and probably more expensive.

A Standalone High Frequency Receiver System

by

Orlando Leone Jr.

B.S.E.E., Florida International University, 2010

M.S., Electrical Engineering, University of New Mexico, 2014

Abstract

The High Frequency Receiver System (HFRS) is a mobile, autonomous, Linux-based RF recording system that is designed to pick up ionosonde sounding signals from 1–10 MHz. Systems are designed for quick deployment and capable of remaining deployed in the field for up to a month. The design motivation was for ionospheric sounding campaigns in New Mexico organized by the Air Force Research Laboratories (AFRL). The systems are calibrated to selected sites and thus require Radio Frequency Interference (RFI) characterization of the sites. The project includes building and using four standalone systems with associated power, antenna, RF, and remote control subsystems that are capable of streaming timestamped quadrature (I/Q) data straight to storage.

Contents

List of Figures

List of Tables

Chapter 1

Project Introduction and Proposal

The AFRL specified several goals which the systems need to meet, and through these goals a list of requirements can be drawn up. Once the project requirements have been quantified, different approaches and technologies are considered. The systems engineer has to consider many possible avenues of technology, techniques, and implementation in order to fulfill the project requirements on time, on budget, and safely. This chapter will divide the project into subsystems for a generalized discussion of what needs to be considered. Chapter 2 will further detail the research that went into the antennas considered for the HFRS, Chapter 3 expands on the HFRS via its subsystems, and Chapter 5 exemplifies another use of the HFRS system: Radio Frequency Interference (RFI) surveying.

1.1 Project Objective

The campaign objective is to obtain raw RF data from these machines for delivery to the Air Force Research Laboratories (AFRL) by creating four standalone antenna-to-disk recording systems that are robust, modular, and transportable. The

device comprises a majority of commercially available parts with custom fabrication as needed. This chapter establishes system requirements and considers possible implementations. Additional processing beyond basic quality assurance is beyond the scope of this project.

1.1.1 Scope

A number of primary parameters have been identified:

- The HFRS will acquire signals in the range of 1–10 MHz, and will be able to select center frequencies with a minimum bandwidth of 390 kHz. The data will be written directly to storage.
- The system will use two 50Ω RF channels for dual polarization. This will allow for determining polarization of signals.
- Antennas will have a gain pattern and geometry optimized for near vertical incidence skywaves (NVIS).
- A GPS synchronizer will discipline the RF system clock and interleave timestamps into the data. This will allow for direction of arrival with multiple units.
- Data will be provided in time series complex voltage data.
- Remote command will be sent via an ongoing 3G cellular data connection.
- The HFRS will be autonomously powered by a battery-backed photovoltaic (PV) system for field deployments up to a month.
- The HFRS system's enclosure will be adequately shielded both from outside interference as well as self-generated interference.

- The HFRS will be resistant to the outdoor environmental extremes found in New Mexico. These environmental hazards include solar irradiance, winter temperature lows, summer temperature highs, strong winds and blowing dust, precipitation, snowfall burden, and possible animal intruders.
- Data storage will be sufficient for month-long deployments.
- Each HFRS not to exceed $16,800 in costs.

1.2 Antenna Design

The chosen antenna needs to receive Near Vertical Incidence Skywaves (NVIS) primarily from 4–10 MHz, and preferably down to 1 MHz. This consists of Medium Frequency and the lower portion of High Frequency radio bands. Commercially available antennas can be designed for this general range of frequencies, and require a large footprint, up to 100 ft x 100 ft. An ideal antenna can be designed with a voltage standing wave ratio (VSWR) of 2:1 or better throughout the entire spectrum, but is not entirely necessary. Due to the strength of ionosonde signals and the minimal contribution of system noise, antennas with far worse VSWR throughout the bands of interest can still be suitable.

A balun is used to prevent common mode signals on the coaxial line as well as to adjust the antenna impedance. Rather, better VSWR is attained by adjusting the characteristic impedance of the antenna as close to 50Ω as possible. The balun turns ratio is determined by the antenna geometry, its characteristic impedance, and intended broadband behavior.

To achieve a dual-feed system, there are two dipole-like antennas sharing a single structure positioned orthogonally to each other. In this way, North-South (Y) and East-West (X) data can be used to determine polarization of signals. The structure

has to be easily deployed and withstand wind, ice, and other extreme New Mexican weather occurrences. Two types of antennas were considered for this project:

- A custom manufactured, half-wavelength inverted-V folded dipole(forming a vertical triangle).
- The existing LWA antenna, which is an inverted-V forked/fan dipole design with a ground screen.

Further considerations to the HFRS antenna are to add a series resistor to achieve broadband VSWR performance at the sacrifice of gain, lumped reactive elements to help change the resonance frequencies of the antenna, and digitally-controllable switchable tuning circuits which would include reactive and non-reactive components. These modifications can dramatically increase the complexity of the system design. The advantage of an optimized antenna is that it can be a completely passive design, negating the necessity of pre-amplification or otherwise sending power to the antenna. Furthermore, components on the RF chain can be nothing more than passive in-line filters and attenuators. Design, simulation, physical testing, and results are in the antennas chapter, Chapter 2.

1.2.1 Modified LWA Antenna

The LWA antenna[5] is an antenna designed specifically for the Long Wavelength Array. This is a radio telescope that uses a pseudo-random array of dipole-like antennas for low frequency astronomy and ionospheric physics. The LWA antenna was designed by the Naval Research Laboratory along with its associated front end electronics (FEE) for the 10–88 MHz range. Satisfying the HFRS requirement of dual polarization, four dipole antenna elements are attached to a single two-sided circuit board that provides two separate RF feeds.

Since the physical space allotted at the field sites are unlikely to accommodate a true broadband antenna, the existing LWA antenna design will be considered and modified in order to work at lower frequencies. UNM currently has dozens of LWA antenna kits ready to be built, including the front-end electronics.

1.2.2 Optimized Antenna

There has been an antenna constructed specifically designed for NVIS signals in the range of 1–10 MHz. Although it might simplify the electrical portion of the system design, the footprint and added complexity of transporting and deploying such a large antenna has proven a considerable detriment. Nevertheless, design, simulation, physical testing, and results are in the antennas chapter, chapter 2.

1.3 RF/Analog Section

The analog portion of the system holds a critical role in getting clear and undistorted data into the system. Essentially, the RF/Analog section is the RF line up to the digitizers. System design needs to consider calibration, amplification, filtering, and power transfer throughout. Since the system will have passive and active RF components inside the enclosure and next to the antenna, separated by a cable run, the RF section is divided into the analog front-end and the analog back-end to refer to components on both sides of the cable run. Figure 1.1 displays the placement of key components of the analog section.

1.3.1 Analog Front End

The front end consists of the analog components attached to the antenna, prior to the cable run. Ideally, these components will be enclosed in an RF-shielded metal box and will be at some distance from the main enclosure and as close as possible to the receiving antenna structure. This close placement is due to amplifying the signal before it travels through any medium that can inject noise, including transmission lines or coaxial cable. The goal is to maximize the signal-to-noise ratio with the use of low noise amplifiers and filters. Fortunately, due to the terrestrial nature of the observation, low frequencies of interest, and RF-quiet deployment locations, shielding components of the front end is of less concern than in applications regarding much higher frequencies and RF-dense locations.

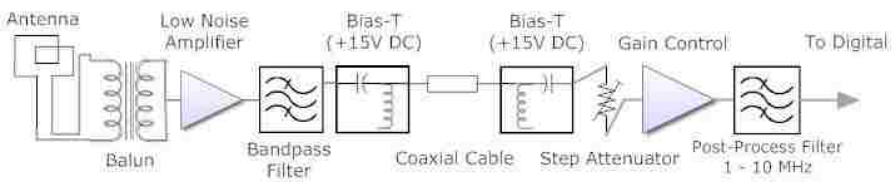

Figure 1.1: Generalized components of an ideal, robust analog system

In the front end chain should be a balun which will reduce the two antenna feedpoints into one and also act as an impedance transformer, reducing the characteristic impedance of the antenna structure down to as close to 50Ω as possible. This is the point where all RF feeds share a common ground. The balun was also placed as close to the antenna structure as possible.

Low noise amplifiers (LNA) should also be one of the first components following the antenna structure, and should be placed as close as possible to the antenna feedpoints. This assures as little noise as possible is being injected before the weak signals of interest are amplified. LNAs by design exhibit a low noise figure but might not have a high gain or compression point. This is where chaining amplifier together

can increase gain and compression point while minimizing the noise introduced into the chain. Additionally, the LNAs need to provide linear amplification throughout the frequencies of interest and avoid saturation from impinging RFI signals.

Noise Factor

Minimizing noise is important to any RF design, and the task is primarily assigned to analog RF electronics. When selecting amplifiers from industry, two important values to consider are gain and noise figure values. Integrated circuit amplifiers, attenuators, and others are certainly easier to design with as opposed to creating them from scratch, since the work of impedance matching, stability, and fabrication have already been optimized for specific purposes, detailed in the associated datasheet. However, it is still important to consider the noise figure and gain of each element, whether passive or active, to assure the best design. According to the Friis noise formula,

$$F_{noise} = F_1 + \frac{F_2 - 1}{G_1} + \frac{F_3 - 1}{G_1 G_2} \cdots \frac{F_n - 1}{G_1 G_2 .. G_n}$$

where F and G are the respective noise figure and gain of the component. It is easy to see here that the noise figure of the first amplifier in the chain will dominate the noise figure. It is important to maintain sensitivity of the HFRS system to be dominated by the sky noise.

Eventually the RF chain should integrate filters in order to prevent RFI from compromising the downstream amplifier linearity and throwing the system into compression. Specific values of these components will be highly influenced by the electromagnetic environment at the remote sites and thus spectrum surveys will be required to maximize immunity of RFI to the system. Finally, all powered components located on the Front End will receive power from a Bias-T (device to inject power onto the RF cable). A Bias-T eliminates the need for running a separate power cable and keeps the RF signals biased well above ground. DC voltage will be at 15V to allow for a 12V voltage regulator and to account for voltage drop in the cable run.

1.3.2 Analog Back End

On the other end of the transmission cable will be another Bias-T, which delivers the power to the Front End and decouples the RF signal towards the final stage of analog electronics. Here, the HFRS will provide a final stage of amplification, attenuation, and filtering before it enters digitization(by way of analog to digital converters). All amplifiers are at a constant rated gain per frequency, but using an attenuator in series can adjust that gain. To keep system complexity down, a fixed attenuator was selected for this campaign, however a digital step attenuator could also be used with the requirement of control circuitry. This final stage gain is primarily for maximizing dynamic range for the analog to digital converters. Following the attenuator/amplifier pair will be another filter which is designed to suppress higher frequencies that can alias into the band of interest. Out of band signals are desired to be rejected by at least 20 dB, and the cutoff frequency (low-pass or high-pass) or frequencies (bandpass) is determined by the sampling rate of the digitizers.

The coaxial run will be 100' in order to reduce self-generated electromagnetic interference (EMI) getting into the receiver chain.[1] The analog back-end components will be placed inside the weatherproof and RF-shielded HFRS enclosure.

1.4 Digitization

The digitization of the RF signal allows for lossless manipulation of the signal. Such manipulation can include downconversion or upconversion, additional filtering, modulation/demodulation, and many other digital-signal processing(DSP) techniques. Digitization can be implemented in a number of ways. For this proposal, digitization

[1]EMI, in this thesis, is defined as RFI emitted from the system itself. This can be produced by system clocks, power supplies, communication chips, and other more mysterious sources.

hardware options are divided into *on-board* and *off-board* capture, meaning whether the digitizer is a standalone system or part of an existing architecture. A host of software applications can streamline GPS timestamping, recording commands, and data storage. Due to a wide assortment of commercially available hardware systems, the digitizer, computer system, GPS receiver, and additional DSP hardware can be individually selected or a package solution can be sought.

1.4.1 Off-Board Capture

An off-board device combines the analog-to-digital converter (ADC), mixing, down-conversion, and some digital processing on a separate platform that can be sent to a computer via a data link. The Universal Software Radio Peripheral (USRP)[2], made by Ettus Research, exemplifies the evolution of such a device. Categorized as a Software Defined Radio, the device is capable of being programmed for a variety of transmission and reception purposes using powerful DSP programs such as GNU Radio, Labview, and Matlab/Simulink. The system includes a GPS digital oscillator which automatically locks and disciplines the internal oscillator of the USRP system. Signals are digitized with the 100 Msps ADCs and sent to the Field-Programmable Gate Array (FPGA). The FPGA performs DSP such as downconversion, decimation, and filtering. The FPGA also interleaves header information and prepares the data over UDP/IP transmission. Data transfer from the capturing device to the computer is via gigabit ethernet and the USRP system can also interleave timestamps into the headers, on the fly, before it is sent over ethernet. Thus,the USRP system streamlines the project inventory and operations. DSP can also be done on the computer, but the point of off-board capture is to minimize the load of the CPU as much as possible. For this project, the off-board capturing option requires:

[2]Throughout the project,the Ettus USRP model N210 has been used.

- Dedicated gigabit ethernet port.
- A computing system that supports SATA II/III (capable of 300 MB/s).
- CPU and memory that can pipeline significant amounts of streaming data from ethernet to a hard disk drive (HDD).

A possible disadvantage of this system is the additional power consumption and distribution requirements for an external device. For a space-limited application, there are also the dimensions of the device that have to be accounted for.

1.4.2 On-Board Capture

The alternative, On-Board Capture, has the aforementioned hardware on a platform designed to be integrated into a computer. For example, the ADC card is attached to a CPU motherboard with supporting architecture, and any processing can be done on that card or computer. Host programs running on the computer can be streamlined to the specific task. This configuration requires:

- An ADC Card via PCIe bus. PCIe is capable of at least 250 MB/s.
- A motherboard that supports PCIe, SATA II / III.

Disadvantages of this system:

- Available ADC cards are expensive and can offset the projected budget. Such cards are, even in the least equipped models, designed beyond the scope of this project.
- Computing platform selections are limited to those that support PCIe buses and thus limit enclosure design to larger, bulkier, more power-consumptive systems.

- The majority of on-board capture systems prohibit the use of open-sourced software and architectures, instead preferring towards licensed, generalized, expensive software.

Due to the project disadvantages in seeking an on-board capturing device, the project will utilize the USRP off-board capture system because it is affordable, flexible, and does not require an oversized computing system. Figure 1.2 details the off-board capture system in a direct-to-disk configuration.

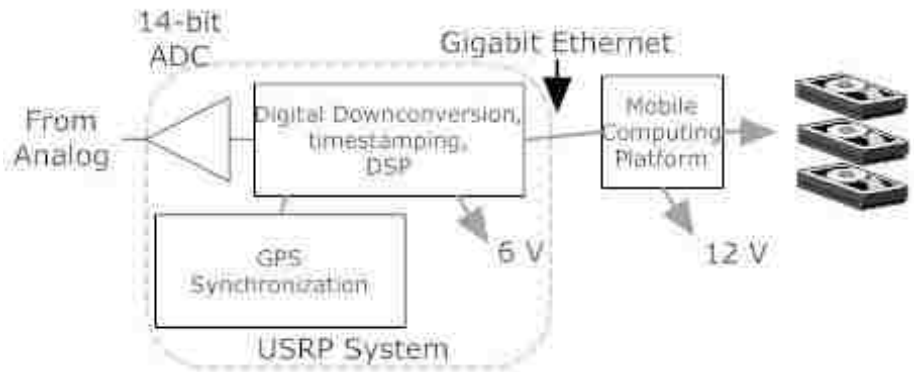

Figure 1.2: HFRS data-to-disk flowchart

1.5 USRP and System Specifications

The USRP can satisfy the following RF parameters for the campaign:

- **Passband**: The system's passband needs to be tunable between 4 and 100 MHz. During the campaign, the system will not be required to observe below 4 MHz and above 10 MHz, however, other uses will need it to observe at the higher frequencies.
- **Sampling Rate and Downconversion**: The maximum sampling rate should be 6.25 Msps for a 3.125 MHz bandwidth observation. This is due to the

Nyquist sampling criteria where the sampling rate needs to be at least twice the bandwidth of observation. The USRP's analog-to-digital converters operate on a constant rate of 100 Msps. The USRP's FPGA can downconvert to any frequency, but bandwidth can only be selected in factors of 2 (e.g. 50, 25, 12.5, 6.25 Msps).

- **Resolution**: RF signals will be digitized to 14 bit resolution, the USRP's maximum. Transmission over ethernet, however, will have to be in multiples of bytes, so samples will be increased to 2 bytes. The USRP records I/Q pairs sent over the wire as complex numbers consisting of two signed 16-bit integers.
- **Dual Feed System**: Two separate RF feeds for each polarization are required. The USRP is equipped with two receiving channels.

1.5.1 Computing Platform and Operation

The USRP will be connected to a computing platform, which will act as the central control for the HFRS. Since the USRP performs digitization, downconversion, timestamping, and data packaging via FPGA hardware, the burden of the computing system is reduced to the following:

- Hardware must be rugged, consume little power, and operate within $0\,^\circ$ to $80\,^\circ$ Celsius, at the CPU cores.
- Accept incoming UDP/IP packets via gigabit ethernet from the USRP and dump to external SATA storage.
- Interface and configure the USRP for observations of varying durations, frequencies, and bandwidths.
- Accept and transmit commands and queries via a 3G cellular connection.

- Connect to the charge controller to monitor the power system.
- Maintain internet connection and recover from power failures.
- Switch on and off loads to minimize power consumption while not recording.

Preliminary ethernet calculations can determine the load of the data stream going through the CPU:

- For dual 390 kHz BW recording, 11.3 Gigabytes/hour or 3.12 Megabytes/second.
- For dual 3.125 MHz BW recording, 90 Gigabytes/hour or 25 Megabytes/second.
- For dual 6.25 MHz BW recording, 180 Gigabytes/hour or 50 Megabytes/second.

Such transfer rates are within the capabilities of gigabit ethernet (125 MB/s) and SATA II (300 MB/s) and so any bottlenecks in data transfer will be within the computing platform. The selected computing platform is an Intel Atom N2600 dual-core processor on a Pico-ITX form factor. The physical computer is equipped with a number of onboard features such as serial, USB, 12V power, SATA-II ports, and VGA. The Atom CPU was selected because it offered a drastic reduction in power consumption compared to the i3 processors of comparable processing ability by 25W. The maximum safe transfer speed from USRP to hard drive has been determined to be 25 MBps, or dual-polarization observations at 3.125 MHz BW, before the computer produced overflow errors due to limited CPU resources. The CPU also allows to observe on a single polarization (Rx channel) at 6.25 MHz BW before overflowing. Therefore,

$$2 \text{ feeds} * 6.25 \frac{samples}{second} * 2 \frac{bytes}{sample} = 25 \text{ MB/s}$$

This is considered a broadband observation and will fill up a 4TB drive in about 41 hours (assuming 3.7 TB formatted) if run continuously.

The operating system will be Linux based because it has proven to be a stable operating system in the UNM Department of Physics and Astronomy. The USRP driver is native and stable on Linux, and open-sourced software allows for streamlined, in-house system development. The project requires replicable results due to a demanding flow of data that might need to run for days at a time. In addition, previous versions of the USRP radio has been used successfully in the department in past experiments. Thus, Linux has proven to be an operating system that provides a high level of user control, minimal process and power overhead, and proven stability in user operations.

1.5.2 GPS Sub-System and Metadata

A GPS synchronizing sub-system is necessary for precise timestamping. The data can then be combined in later analysis from multiple systems. The USRP comes equipped with a built in GPS synchronizer. It will generate a 10 MHz reference, which will then be multiplied to discipline the USRP clock. The USRP will then be phase-locked to this signal before timestamps are interleaved to streaming data. When locked-on, timestamps will be accurate to within 25 ns. The HFRS project has configured the USRP to interleave a header file that contains more than just precise time into the datastream. Called metadata, this header data is 171 bytes in size and includes sample rate, size of each sample in bytes, center frequency, and number of bytes until next header data. This header information is used in the post processing software to assure accuracy of data. By also giving information about a large file of millions of otherwise arbitrary complex numbers, it makes the development of post-processing scripts less tedious, once the headers are de-interleaved. An exterior GPS antenna will have to be affixed to the enclosure. The computer module will need not be synchronized, as the timestamping procedure has already been done by the time it reaches the computer.

1.6 Storage

Hard drive storage is needed in this project. There is an onboard 8GB solid state drive (SSD) for primary operations which run the operating system and control scripts. For storage of the raw data, both SSD and conventional hard drives were considered.

SSD can be as much as $1,000/TB, where mechanical drives are $50/TB. SSD take up less physical space and there are enclosures available to stack them to achieve multiple terabytes of storage. However, there are plenty of in-house 1 to 4 TB mechanical drives available. Size, cost, and temperature constraints did not warrant SSD purchases and RAID controllers, in this application. Table 1.1 shows data rates per hour and total storage for the two observation types expected during the HFRS operation. Since 4 TB drives are easily obtainable commercially, the project will equip each HFRS with that size of a hard drive. Since most of the observations will be narrowband and on an intermittent schedule, a mechanical 4 TB hard drive will be sufficient and provide a good safety margin for extra storage. The drive enclosure is selected to be metallic and equipped with a vent fan so that it can be affixed to the interior of the enclosure. There will be a SATA-II connection directly to the computer.

Bandwidth	Rate	Monthly Requirement
390 kHz	5.61 GB/hr	4 TB
3.125 MHz	90 GB/hr	64.8 TB

Table 1.1: Data rates and storage for various dual-channel bandwidth captures

1.7 Power System

Since the primary source of power will be solar panels and battery storage, it is imperative that this project utilize low power consumption devices. A DC-distribution system will power the components. The lack of an AC inverter will eliminate the conversion losses experienced from going from DC to AC and back to DC again. These losses can be up to 20% and might lead to oversizing the photovoltaic array. In general, the power distribution system will include:

- A PV panel that is properly sized to power the system.
- A 24 V battery system that will feed three switched mode power supplies: 6V, 12V, and 15V and provide power during times of no solar irradiation.
- A charge controller to charge and monitor the batteries, handle a PV input, and provide status/health of vitals to computer.
- Batteries should act as an anchor for the system, withstand temperature extremes, and be sufficient to allow for 24 hours of continuous operation without recharge.

1.7.1 Battery Sizing

A battery bank will be sized depending on the power budget, desired days of autonomy, and the level of charge depletion. Estimated regular depletion of the batteries is usually a trade-off between battery bank size and battery lifetime. If a bank is designed for a shallow depth of discharge, this would mean longer lifetime for the battery, a larger safety margin for extended cloudy weather, but at a cost of a larger battery bank. Additional factors to be considered are weight vs. cost vs. functionality. Absorbed Glass Mat (AGM) batteries were selected because of the

affordability and stability. AGM batteries are sealed lead-acid batteries, but capable of withstanding shock, a deep level of discharge, wide temperature fluctuations, and achieving longer lifetimes than the standard lead-acid batteries. Weight is an advantage in this system because it will add resilience against wind by keeping the center of gravity low. Selecting AGM batteries, or any lead-acid batteries for that matter, will require a properly sized enclosure. Alternative battery types to the AGM type were considered. Lithium-based batteries have a much higher energy density and can reduce the enclosure size but they are costlier, still experimental in deployable types of applications, and require special battery chargers that do not have solar panel, load control, and monitoring capabilities. Lithium-based batteries can be upwards of $1/Wh whereas AGM batteries cost about $1/Wh.

1.7.2 PV Sizing

The total power supplied by the PV system will be determined by the power budget and desired days of autonomy. Considerations that go into the PV sizing include DC losses, temperature de-rating, and utilization of nominal operating cell temperature (NOCT) values on the PV datasheet instead of Standard Testing Conditions (STC). NOCT offers more realistic power output of the PV when the cells are heated and the solar radiation is not at its max. Some basic requirements for the system:

- A single PV panel per system. This will keep mechanical complexity down.
- The selected PV panel should charge a depleted battery bank and maintain power to loads within a daily cycle.
- Panel sizing should not exceed 3' X 5' and be reasonably priced for this project. 250 W panels can be found with similar or less area. Single panels exceeding 320W are also available, but as of 2014, are still priced at a premium.

1.8 Physical Implementation

The entire system is designed to fit in a light- to medium- duty truck or SUV and requires a single person to set up. Thus, the size and weight of the enclosure and components have moderate importance. For the system to be easily deployable, only a few parts should be manipulated during installation and removal. For example, the batteries will to be removed and carried separate from the enclosure, as well as any external antennas. The electronic parts of the enclosure will be affixed to an interior metal plate that can be removed for shop maintenance. This will also provide a chassis ground to as many parts as possible. This metallic plate will be placed behind the batteries, computer, and USRP. The Analog back-end will be attached to its own metal plate on the interior side of the enclosure. Finally, the entire system should be able to be tested, configured, and commissioned at each site well within a day.

1.8.1 Enclosures and Physical Placement

The enclosure should be a NEMA Type 3R or 4 rated box. This will assure adequate protection against the elements. Although the batteries will need to be removed during transport, the solar panel will be affixed on top of the enclosure. This will reduce the number of movable components, provide shade and covering over the enclosure, and maximize normal solar irradiation to the solar cells. To create a more modular system, the PV is designed to be removed if necessary. All components and enclosures should be commercially available, weatherproof, metallic, and vented while being well RFI-shielded. Cattle and other animals are a concern with equipment in remote New Mexico locations. A fence around the antenna may be required if placement will be on ranch land. Plastic fencing with fiberglass rods can be posted in and put up around the perimeter of the antenna and enclosure. Metal fence

components should be avoided due to possible coupling to the antenna elements.

1.8.2 Deployment Plan

The system will be tested and adjusted at UNM first in parts, then as a complete system. All systems will be checked to be functioning properly with an assortment of testing equipment that will not remain at the site, such as a laptop, multimeter, RFI meters, and a spectrum analyzer. Each chosen field site will have a RFI survey performed and this information will influence small customizations made in the hardware and software of each system. RFI surveys are detailed in Chapter 5. Field sites include:

- North Arm: A plug-in version will be placed in an EMI-eliminating electronic enclosure near the north terminus of the VLA array.
- Sevilleta: A small section of Sevilleta National Wildlife Refuge has been reserved for future LWA projects.
- Kirtland AFB: One of the systems will be placed near the southern corner of the base, near the border of the Isleta Indian Reservation.
- National Solar Observatory: Located in the mountains south of Cloudcroft, New Mexico.

Firstly, the antenna is assembled, staked, and oriented. The enclosure will be placed 100' away and turned on. The fence, if needed, will be installed around the antenna and the cables run. The system will be checked for internet connectivity and working subsystems. There will be a test run with a laptop ready to process data. In addition, a handheld spectrum analyzer will assist in confirming system functionality. Before leaving, a remote SSH connection will be established.

1.8.3 Timeline

The prototype will be completed by August 2013 with a deployment of 4 systems in January 2014. The UNM development engineering resources include a RF / systems engineer, a EE graduate student, and an astronomy researcher.

- Spring 2013: Power budget of system set. PV and battery sizing and selection. DC distribution design and selection. LWA vs. Idealized Antenna simulations and testing. Initial equipment purchases.
- Summer 2013: Equipment Purchases. Experiments with USRP radio, GPS timestamping, and computer storage. Extensive Python-based software development to process RFI data taken with USRP radio.
- Fall 2013: Final purchases for equipment. Tests at the VLA's reverberation test chamber for examining RFI emission from the enclosures. Test deployment at Sevilleta, since it's the best combination of quiet radio environment and distance from Albuquerque.
- January 2014: 4 Systems deployed for campaign.

1.9 Conclusion

This chapter outlines the design for a portable High-Frequency receiver system. Sufficient research in commercially available parts will maximize the balance between cost, weight, and functionality. The system must be able to pick up the desired signals from the ionosonde, be ready to record at any time, and be able to run autonomously for about a month.

Chapter 2

Antenna Analysis and Design

2.1 General

This chapter details the two types of antennas considered for the project. The first antenna covered is the HF-optimized antenna whose size provided both the desired RF characteristics and undesired large physical footprint. This antenna is designed to provide a low VSWR (2:1 or better) for 1–10 MHz and a beam pattern optimized for NVIS. The second antenna is the LWA antenna, which was selected for the project. It was not optimized for frequencies below 20 MHz, however LWA antennas are readily available, ionosonde signals are loud, electronics are able to work down to 2 MHz, and the footprint made the package far more portable and capable of dealing with cattle and other animals with use of a small perimeter fence, if needed. The HF-optimized antenna is still used for RFI measurements and various gain/SWR/reception comparisons with the LWA antenna. Figure 2.1 shows both the LWA and HF-optimized antenna at the North Arm site, with a scenic VLA antenna in the background:

Figure 2.1: Left background: The 25-meter VLA dish antenna. Center: 35' high, 95' wide HF-optimized antenna. Right: LWA Antenna.

2.2 HF-optimized antenna

For any project that has specific RF requirements, it is best to create an antenna that is optimized for the mission. The design process had these considerations in mind:

- 2:1 or better VSWR for 1–10 MHz.
- An E & H beam pattern optimized for NVIS with minimal gain loss (in terms of dBi).
- Mechanical structure designed for two orthogonally placed antennas that can withstand wind, rain, and its own weight.

2.2.1 Theory and Simulation

The inverted-V folded dipole design offers relatively simple theory, simulation, and construction over other types of broadband antennas. This design was selected due to broadband performance over a regular dipole. The antenna run is center fed and anchored at three points, sloping towards and parallel to the ground, forming a vertical triangle. This decreases peak gain, but achieves a wider band of reception. The antenna wire length is designed so that its base run length is a half-wavelength at 5 MHz. This produces significantly less characteristic impedance than if classically configured as a folded dipole. As a result, an in-line resistor of 800Ω is used along with a 16:1 balun to match to a 50Ω line. The geometric design, balun, and resistor was configured in order to increase broadband reception. The beam pattern is also optimized to receive NVIS below 15 MHz.

A program called 4NEC2 was used for its accuracy for designing similar antennas. The program uses the Numerical Electromagnetics Code (NEC-2) engine, developed by Lawrence Livermore National Laboratories. There are more powerful engines available, but licensing is necessary and the engine is useful only to microwave applications. The geometry of a desired antenna can be drawn, along with any lumped elements (resistive, inductive, and/or capacitive). Desired simulation outputs are the gain patterns and the VSWR performance for 1–15 MHz. This antenna type was selected also because of the ease of manufacture and construction. Many small companies cater to amateur radio enthusiasts and frequently develop similar antennas.

Figure 2.2 shows a comparison of gain patterns of the E field of both antennas in the 4NEC2 simulator. With these antennas, the E-field and H-field are very similar and hence the H-field lobes were omitted. The lobe shapes change little throughout the frequencies of interest, and are focused towards zenith.

The gain patterns hold stable up to 15 MHz, where the lobe patterns start to

change dramatically. Above 15 MHz, the lobe patterns change and grate, and reception for particular frequencies from particular directions can become unreliable. VSWR simulations show better than 2:1 throughout a large spectrum, as simulated in Figure 2.3b. Thus, the limiting factor would be the gain as the frequency of interest increases.

2.2.2 Physical Tests

We contracted out the manufacture of the antenna to a company that has made NVIS antennas, but none as tall as 35'. The antenna package includes the antenna wire, baluns, resistors, and structure. The antenna wire itself doubled as guy wires. As it turned out, the received antenna was not sufficient for a sound mechanical structure. Upon receipt of the antenna, it was found that the 3/4" diameter fiberglass rods are not structurally sound enough to hold its own weight vertically. As a result, the mast broke during the first installation. Although it would have been ideal to create a non-metallic structure, we used an existing 3/4" steel pole for the first 20' of the antenna and the remaining 13' with the unbroken fiberglass mast pieces. We then affixed four guy wires at the 20' height to further stabilize the structure. This has worked out well; it has been set up at the North Arm for nine months.

2.3 The LWA Antenna

The LWA antenna can also be considered a variation of the inverted-V dipole, but with forked elements and a ground screen. This design achieves good broadband reception between 20–88 MHz. It is designed in conjunction with an electronics board that is connected to all four blades (two per polarization). The LWA antenna was considered for use with this project because of the available inventory and the

robust nature of the electronics included with the antenna (the FEE). Both the antenna and the FEE were designed and developed by NRL. The terrestrial nature of the signals of interest was also assumed to be significantly more powerful than the cosmic sources it was originally designed to detect. Fortunately, powerful ionosonde signals proved to offset $\geq$ 10:1 VSWR in the sub 10 MHz regime.

2.3.1 Theory and Simulation

Like the HF-optimized antenna, the LWA dipoles are designed to have a beam pattern that covers most of the sky with a constant lobe shape throughout 1–88 MHz. Figure 2.2 shows the simulated lobe shape for 1 MHz, 5 MHz, 10 MHz, and 15 MHz. This shows that around 10 MHz, the gain performance of the LWA antenna start to exceed that of the HF-optimized antenna. The peak sensitivity is at zenith and the half power beamwidth is between 40 to 45 $^\circ$ from zenith. Unlike the HF-optimized antenna, the LWA antenna continues its singular, non-grating lobe pattern up through 88 MHz, as it is designed and simulated to do[3]. This is because for dipoles, there is mainly a singular lobe until the size of the dipole approaches one wavelength ($l \geq \lambda$). At 88 MHz is the 3.41 meter band, the dipole is not long enough to encourage grating at an unbent length of 3 meters. Simulations and measurements have also been done on the receiving efficiency of the LWA antenna. Figures 2.4a and 2.4b show similar results from simulations as well as a field VSWR test. VSWR exceeds 10:1 around 28–30 MHz and gets progressively worse. However, this should not be a disqualifying factor for this project, since the signals of interest are strong and the system noise is low.

2.3.2 Front End Electronics

The FEE board is actually two boards connected together, so that each polarization has their own antenna, electronics, and cable yet share only the antenna structure and electrical ground. A 2:1 active balun helps in broadband gain, with an amplifier on each unbalanced side placed as close as possible to the antenna. After the filter and 2nd stage amplifier, the RF signal is coupled to a 15 V DC signal before it is sent out on coaxial cable. The FEE is powered due to the three low noise amplifiers that are on board. Two of them are the Gali-74s, that provide 25 dB of parallel gain. These are placed on the unbalanced side. The second stage amplifier is the Gali-6 that provides 12 dB of gain, and is located on the balanced side of the system. This is good for distant signals but might have limitations with trying to receive louder signals of interest. The LWA antenna's dipoles are not designed for frequencies below 10 MHz but fortunately the FEE's components are designed to pass frequencies down to 1 MHz. Although designed for 10–88 MHz, the FEE has been tested for use between 1–10 MHz and found it provides about 37 dB across the spectrum using a calibration method shown in Figure 5.1.

2.3.3 LWA Resonance Test

An attempt has been made to modify the LWA antenna for resonance at 7.5 MHz, and achieve a lower broadband VSWR in that range. This was done by adding lumped elements to a prototype FEE board, with a 4:1 balun, as shown in Figure 2.5a. The test point was on the balanced side of the balun. Using a smith chart and a VSWR meter, one can determine the reflection coefficient (Γ) of the antenna at a given frequency, plot it on the chart, and then determine what types of capacitors and/or inductors are needed to match the impedance. In the case of an antenna, this is changing its resonant frequency. Since the LWA antenna is electrically short

(capacitive) at these low frequencies, inductors were added with 20Ω series resistance in an attempt to explore the new antenna resonance characteristics. However, methods using lumped elements with an electrically short dipole had narrowband results eg. $\leq$ 500 kHz for 2:1 VSWR or better. Figure 2.5b shows the VSWR of the LWA antenna with 17.2μH series inductance and 3.2nF shunt capacitance.

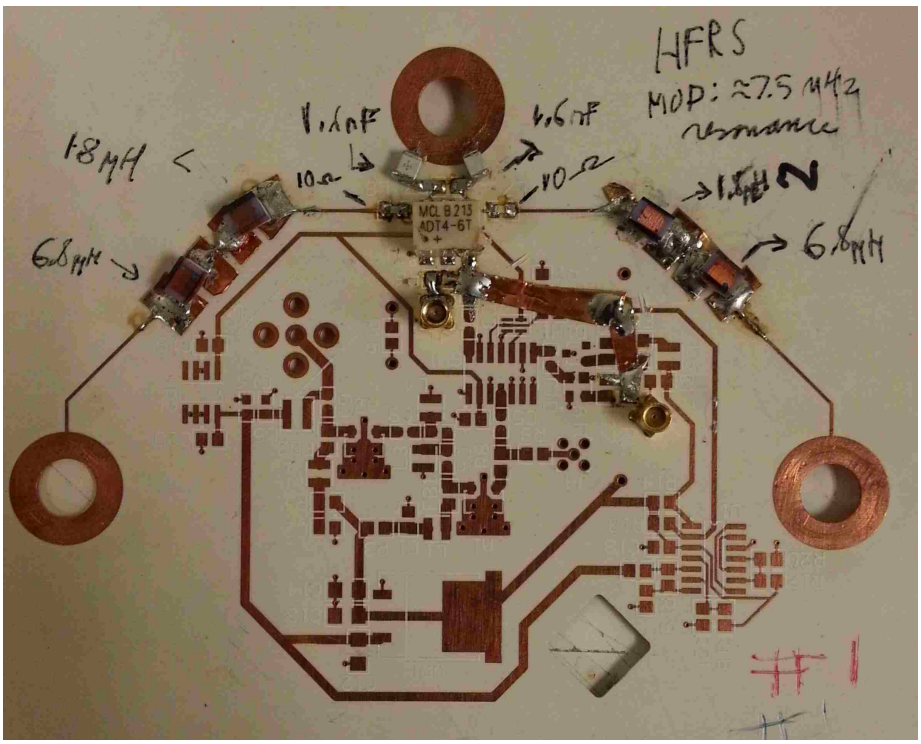

(a) A blank FEE with a 4:1 balun and lumped elements.

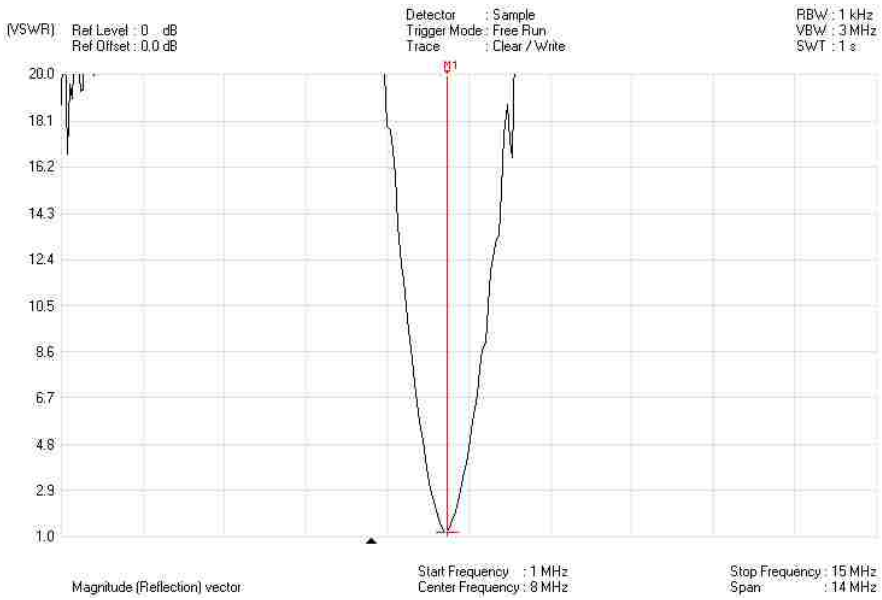

(b) Measured VSWR showing about 1.3 MHz Bandwidth for 10:1 VSWR or better, centered at 7.5 MHz

Figure 2.5: Changing the Resonance of the LWA Antenna.

However, due to the complexity of the modification to the circuit board, which includes changing the balun and adding large inductors to an already densely packed FEE board, an observation of signals at 5 MHz and 10 MHz were done to see how well the existing LWA and FEE setup can receive signals in this frequency range. In addition, bad VSWR does not necessarily mean lost signals if the FEE's system noise is low enough[4].

2.3.4 WWV Tests

In order to confirm that an impedance-transforming alteration was not necessary for the FEE, a timekeeping signal was recorded and visually inspected at 5 and 10MHz, which almost straddles the frequencies of interest for the campaign. These time signals are a few of the National Institute of Standards and Technology's WWV timekeeping signals, transmitted from Fort Collins, CO. At the 1000 Hz upper sideband, there is an audible marker tick on every second and minute. The minute mark is .8 seconds long. Successful observations of both minute and second signals signify sufficient resolution and sensitivity for reception of ionosonde signals which would be transmitting much closer (within the state) and at similar frequencies. An applied FFT integration time of .15 seconds would be fine enough to distinguish these signals. Figure 2.6 shows the successful reception:

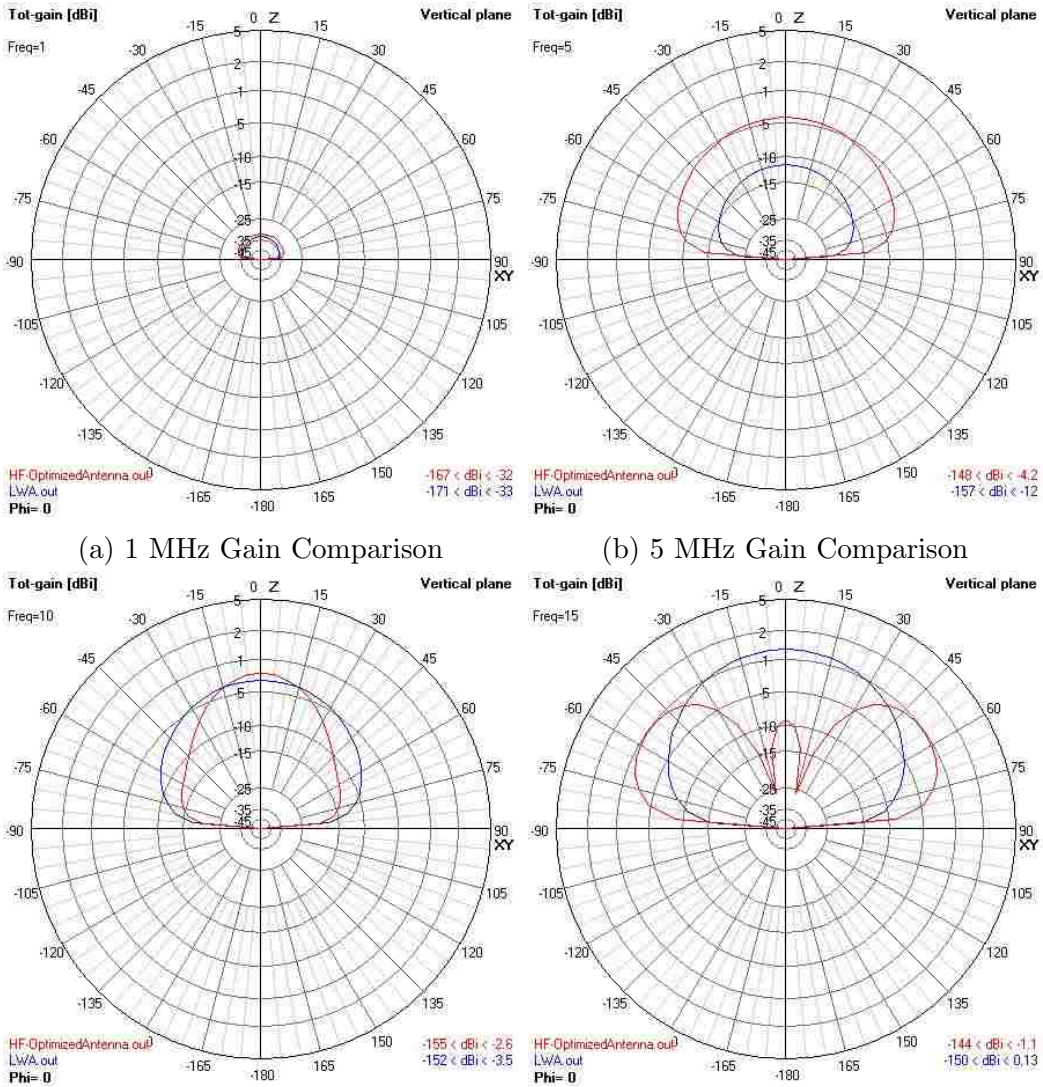

(a) 1 MHz Gain Comparison (b) 5 MHz Gain Comparison

(c) 10 MHz Gain Comparison (d) 15 MHz Gain Comparison

Figure 2.2: Gain pattern simulations that compare the HF-optimized antenna to the existing LWA antenna. E field $\approx$ H field.

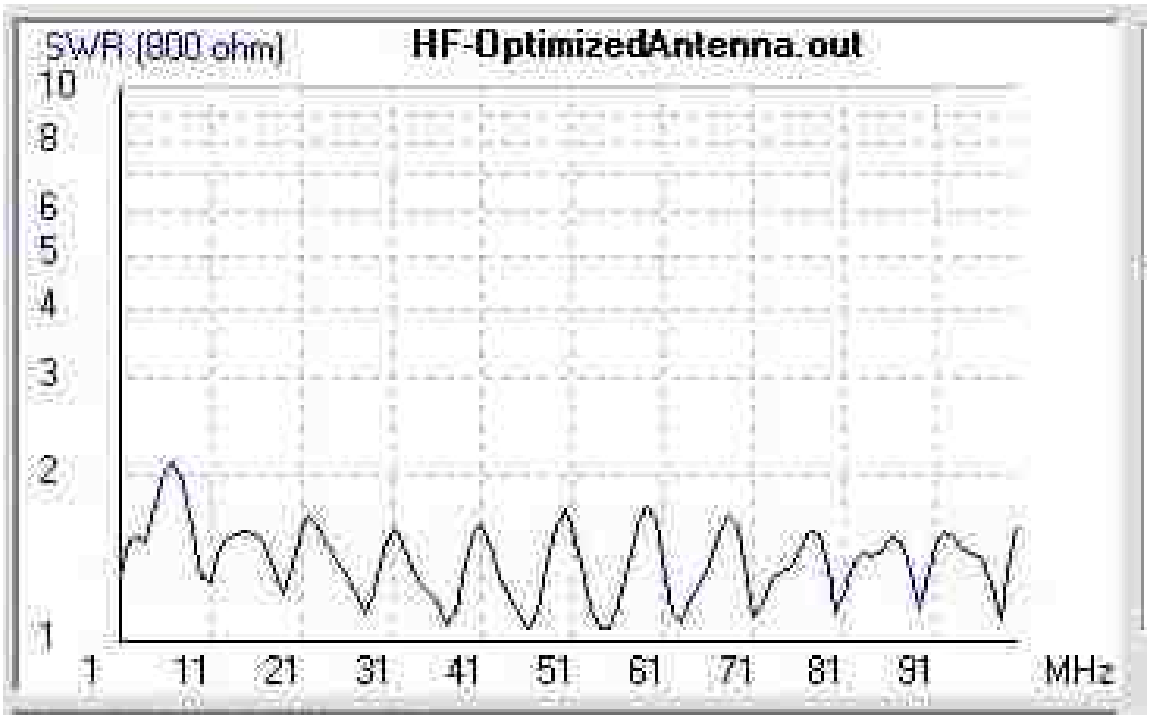

(a) Simulated VSWR of HF-optimized antenna.

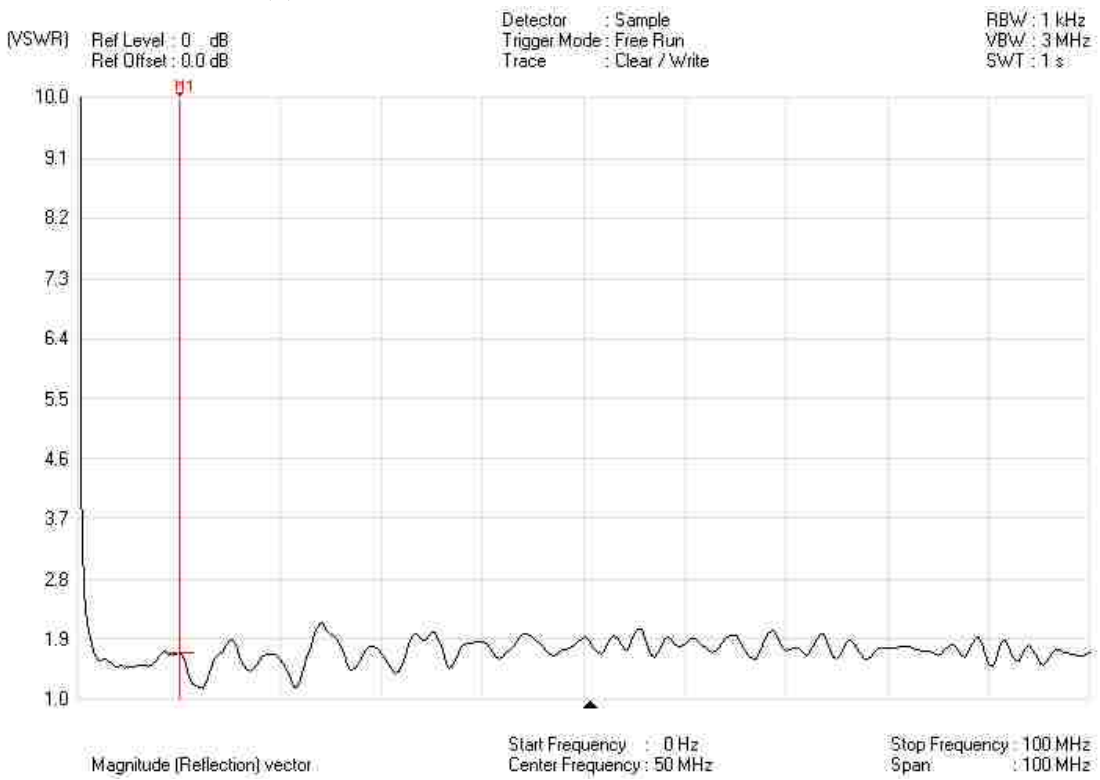

(b) Measured VSWR of HF-optimized antenna.

Figure 2.3: Simulated and field-tested VSWR of HF-optimized antenna.

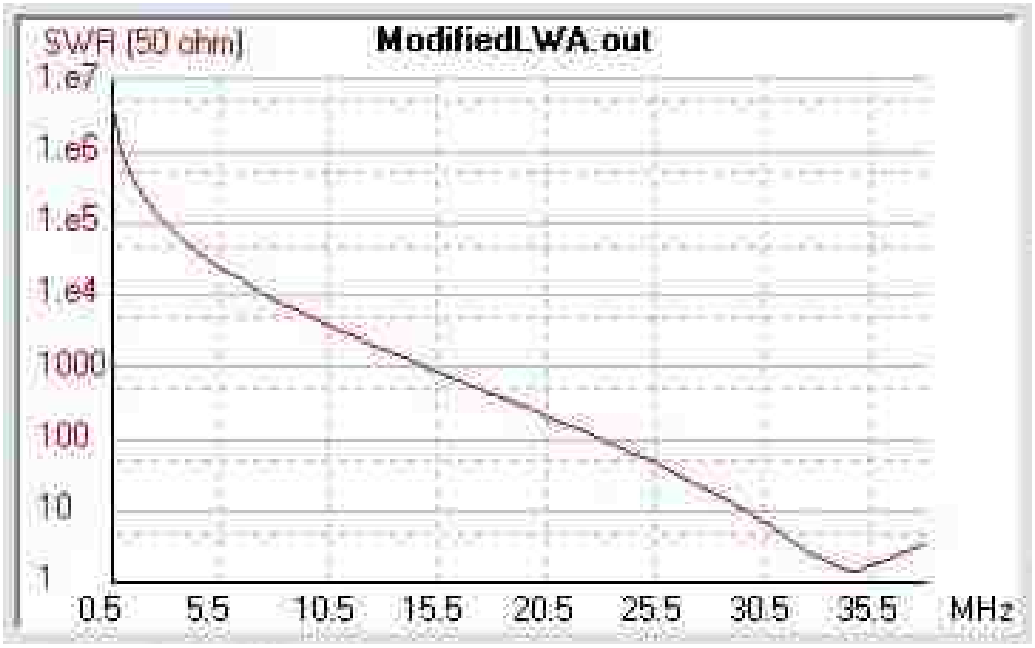

(a) Simulated LWA Antenna VSWR.

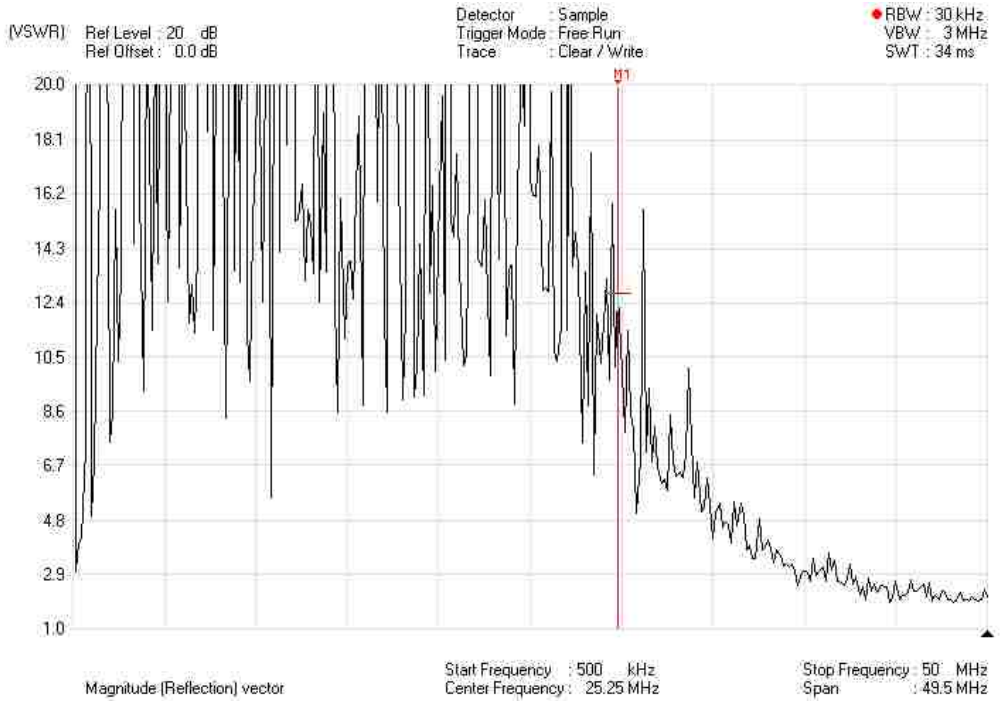

(b) Measured LWA Antenna VSWR.

Figure 2.4: Simulated and actual VSWR for the LWA antenna.

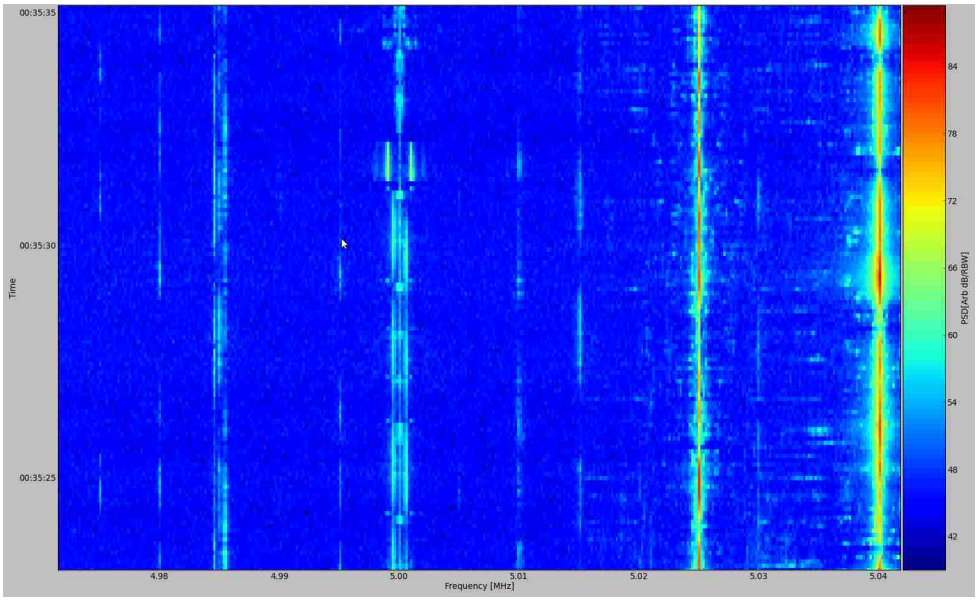

(a) Reception of the 5 MHz WWV signal.

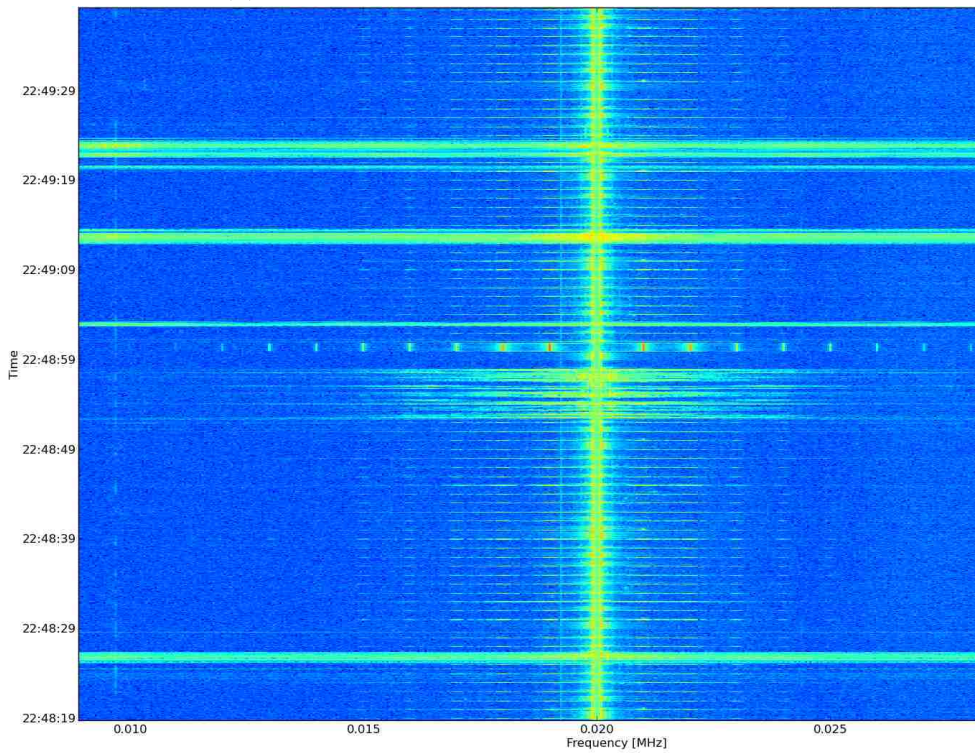

(b) Reception of 10 MHz WWV signal.

Figure 2.6: Successful reception of the 5 and 10 MHz WWV signal using the unmodified LWA antenna and FEE. The seconds and minute tick can be seen at their appropriate lengths.

Chapter 3

System Design

The system design can be divided into the hardware power system, RF electronics, and software operating environment.

3.1 Power Distribution

The HFRS systems are designed to be a DC-based system, where power is sourced off of a solar panel and batteries. The system voltage is designed to be 24 Volts to avoid boosting voltages and reduce DC current. A controller was selected to perform the following tasks:

- Charge and maintain a 24V deep-cycle battery bank.
- Accept solar panel inputs and distribute power both to the system and batteries.
- Be equipped with intelligent charging techniques.

- Be able to communicate charger status, temperatures, and other statistics to computer.

3.2 Energy Budget, PV and Battery sizing

The first step in sizing the DC power system is estimating the power consumption. Although in practice the HFRS system will power off loads when not in use, a worst-case, continuous full-power scenario is considered. The power budget per system is listed in Table 3.1. Maximum power values are listed, however some of the devices can be throttled back in power consumption as well as being powered off completely. However, the sizing of the system's power components will take in full power values.

Component	Voltage (Volts)	Current (Amps)	Power (Watts)
Front End(2)	15	.46	7
Final Stage Amplifier(2)	12	.12	2.88
USRP	6	3	18
Computing Platform	12	.8	10
Computer Fan	12	.25	3
Disk Drive	12	1	7.5
Enclosure Fan	12	.6	6
Total			55 Watts

Table 3.1: Power Budget

The campaign observation schedule was not clear in the beginning of the HFRS development, however it was determined that about 24 hours of continuous full-power needs to be guaranteed. For standalone system designs, the power budget is accompanied with an energy budget, which together sizes the components of the system to the desired capacity. The energy budget in this case requires 24 hours of full power operation before recharge. Indeed, system sizing should consider worst-

case scenarios where a number of consecutive days might occur where there is little to no sunlight, so designing for a 48 hour period would offer a better safety margin. Fortunately, the New Mexico has sunshine over 78% of the year. The daily charge for the HFRS system on a 24V DC bus is 55 Ah.

3.2.1 Battery Bank

Deep cycle AGM batteries were selected due to the the ability to recharge from a deep state of discharge, better lifetime, more rugged handling limits, and an abundant availability of charge controllers. Battery sizing is determined by the energy budget of the HFRS system. Sizing the bank also considers a 90% DC to DC conversion efficiency throughout the system and a discharge depth of 50%. Ideally, a 80% or above discharge depth would be best for maximizing battery lifetime but this is a short term project with size/cost/weight constraints. So designing for a deeper discharge depth will decrease total battery bank size requirements as well as offer a safety margin for slightly less sunnier days. Battery lifetime is measured in charge-to-discharge cycles before the cells in the battery are no longer able to hold reasonable charge. Since a 24V DC bus was selected, and 24 hours of autonomy is desired,

$$\frac{55Ah}{.5 \text{ discharge depth} * .9 \text{ conversion loss}} * 1\text{day} = 122Ah$$

The above equation indicates that a battery bank operating at 24 V with a capacity of 122 Ah will suffice for the aforementioned criteria. The project uses 2 Deka 8A31DT-DEKA AGM sealed lead-acid batteries, which are 12V 110Ah each. They are placed in series. The physical dimensions of these batteries were critical in determining the size of the enclosure. Lead-acid technology is still experiencing improvements, but the energy density of this type of battery is mature, so shopping around based on physical size only is not likely fruitful. The more energy capacity a lead-acid battery is rated, the larger it's going to be. These lead-acid batteries weight 69 lbs. each, and

the combined weight of 148 lbs. will help keep the center of gravity of the enclosure low to the ground and eliminate the need for physical anchors to guard against windy conditions.

Another concern that needs to be considered in battery sizing is the derating involving the rate of which the battery is discharging. The capacity of the battery is reduced not only by ambient temperature or depth, but also on the rate the battery is being discharged. Most datasheets base the "nameplate" charge capacity on an 100 hour discharge. A more realistic value to look for is the 20- or 10- hour discharge. For the Deka batteries, there is only a 5% derating from a 100 hour rate to a 20 hour rate.

3.2.2 PV Selection

After sizing the battery bank, the PV panel can be sized. The full-power energy draw of 55W over 24 hours is 1,320 Wh/day. Accounting for 90% efficiency losses, the draw increases to 1,466 Wh/day. One way to size a PV array to a system incorporates peak sun hours. Peak Sun Hours (PSH) estimates the effective amount of hours per day the solar irradiation is at $\frac{1kW}{m^2}$ in a region. PSH relates geographical location to solar irradiation intensity to give an averaged length of time per day where rated PV power levels are realized. The value of $\frac{1kW}{m^2}$ can only be approached during solar noon at any location, so solar irradiation is summed throughout the solar day to find solar insolation: $\frac{kWh}{m^2}$). Since PV manufacturers rate their PVs based on $\frac{1kW}{m^2}$ intensity, solar insolation doubles as PSH. In Albuquerque, a value of 5.5 peak sun hours (PSH) is set. PSH can be obtained per a monthly basis, and to account for worst-case scenario, the minimum monthly value can be used, but this project uses 5.5 hours, which is an annual average for Albuquerque. Fortunately, the high desert's solar irradiation deviates down by a small amount during winter months. Therefore,

combining PSH and daily required charge, a PV capacity size can be estimated: 267W.

A single PV panel setup would simplify connections and mounting. A single PV panel can be mounted above the enclosure to provide shading and a weather shadow over the enclosure itself. The PV's mounting will be custom fabricated so that it can be removed using Allan wrench tools. Finally, the PV will be tilted towards the south by 15 ° to maximize normal solar irradiation on the PV cells and the PV will be shifted forward to maximize shading onto the enclosure. Of course, the enclosure will therefore be oriented south.

A 250W PV panel from Canadian Solar has been selected, with monocrystalline cells. At slightly less than 3' X 5', it is sizable and will definitely provide plenty of shade for the enclosure. A PV with a higher rating could have been purchased that can cover extended days of inclement weather, however, 1) Loads can be switched off during non-operation hours to a minimum of 12 Watts, 2) multiple days of cloudy weather are rare in New Mexico, 3) the PV still produces power in cloudy weather, and 4) 250W PV panel retail prices are $1 per watt at the time of purchase.

3.2.3 DC System Design

The voltage and current characteristics of PV panels vary depending on solar insolation and change throughout the day. Standard practice by PV manufacturers list open-circuit voltage and short-circuit current values which can be used to match to an appropriate charge controller rated for a certain power level and PV open-circuit voltage. It has been determined that the system will run at 24 V, at least at the battery bank. Thus, the charge controller needs to output this voltage at the load terminals. To maximize the power harvested from the PV panel, only maximum power point tracking (MPPT) charge controllers are considered. MPPT is a

functionality found on premium models that incorporates a continuously changing DC/DC converter that maximizes power draw to the system from the PV. This is because for every arbitrary increment of solar irradiation, different voltages offer the highest power draw from the PV. The charge controller also acts as a battery charger, using special algorithms to maintain a healthy charging technique that maximizes battery life.

Although the charge controller outputs 24V to the system, the components of the system need to run off 6V, 12V, or 15V. Thus, external fixed DC/DC converters called switched-mode power supplies (SMPS) are required. Switching converters are known to be noisier than linear converters but are much more efficient, up to 95%. In addition, modern modular SMPS's are very quiet and have a minimal ripple in the power line. For this design, we have used switching converters because most of the components have internal linear regulators. Only the power lines to the final stage amplifier have an additional linear regulator. 15V is sent through the cable to power the FEE's 12V linear regulator. Figure 3.1 shows the general DC distribution for the system.

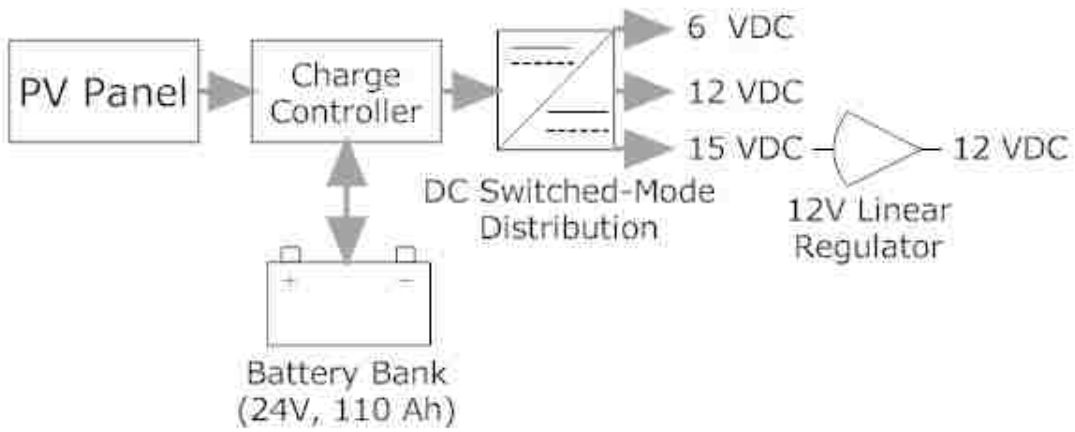

Figure 3.1: DC Distribution

In order to size the charge controller and SMPS, we need to add up the power

requirements for each voltage line per the power budget in Table 3.1.

- **12V**: 26.5 W
- **6V**: 18 W
- **15V**: 9.88 W

This has led to 3 SMPS modules purchased from Vicor rated at 50 W, 25W, and 25W , respectively. They are encased such that all share the same input rail. They also come with a TTL input signal to turn them off. Part of the load control, the USRP and FEE can be shut off this way. Since the computer shares the 12V SMPS with the fan and hard drive, it would not be a good idea to shut off the 12 V SMPS. Instead, external relays were used to target the vent fan and the hard drive.

3.2.4 RF Components

As described in 1.3.1, the analog RF section is both the antenna as well as some components inside the enclosure. For the campaigns, the project uses the FEE as-is. The RF components inside the enclosure are selected and customized for the project - they all have to work between 1–10 MHz, and are equipped with SMA-style connectors. Minicircuits have provided all of these connectorized components. As the cable passes through the enclosure's bulkhead, it connects to a Bias-T which separates the RF signal and DC power. This is what powers the FEE via sending 15V from the SMPS over the 100' cable run. The RF signal then passes through to the final-stage amplifier and attenuator pair. This adds a final stage gain up to 24 dB. The value of the attenuator is selected depending on the RFI survey as well as how well the WWV signal can be seen at each field site. Between the final stage and the USRP is the low-pass 50 MHz filter. The same 50 MHz LPF used for the RFI surveys is used here because at 10 MHz and below, aliased signals from 90 MHz and

upwards are attenuated over 50 dB. Since there are two polarizations, there are two cable runs and two of each RF component.

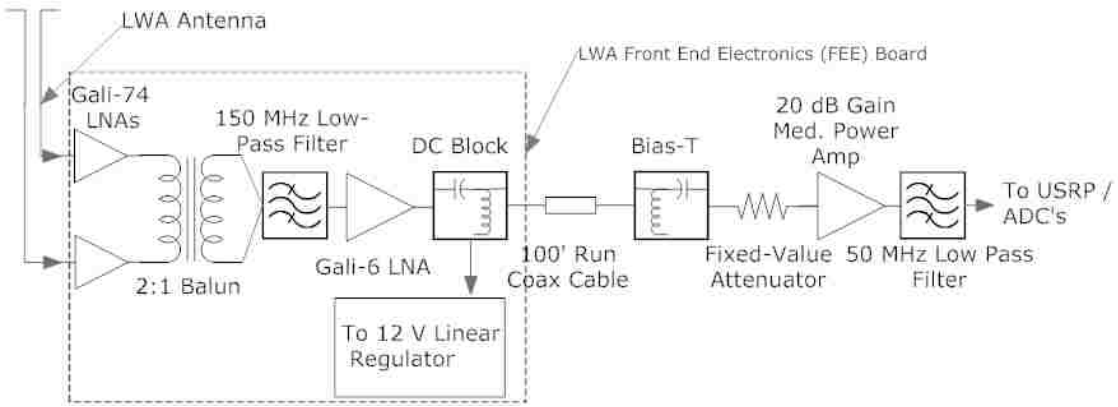

Figure 3.2: Analog RF chain, as used.

3.2.5 Overcurrent Protection

The HFRS system has implemented over current protection, shown in Figure 3.3, to prevent catastrophic damage to the entire system or individual components and keep the system communicating as long as possible after a over current trip occurs. According to the charge controller's specifications, the chassis, PV negative, battery negative, and the load output negative share a common earth ground by use of a grounding rod. There are three DC breakers that are placed on the rear of the enclosure (in an enclosure of its own) that double as main switches for the system. That way, the user can individually disconnect the PV, loads, and/or battery from the rest of the system. Using this, the only major electrical hazard when servicing the enclosure is shorting the battery directly to itself while installing or removing the batteries.

Additionally, there is an in-line fuse for the purpose of isolating the 15V output. This is due to the exposed circuitry inside the enclosure and antenna and increased

risk of short. Figure 3.3 details the overcurrent protection scheme.

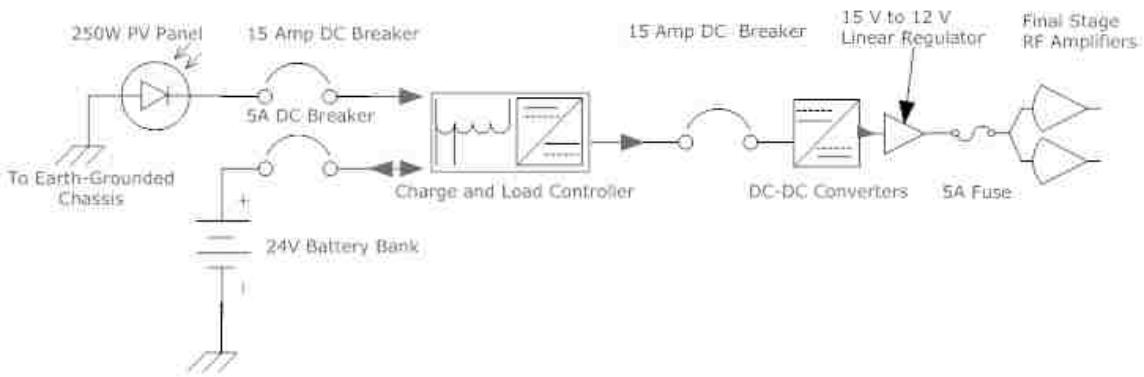

Figure 3.3: Breaker Schematic

3.2.6 Enclosure

Knowing the size of the PV and batteries helps greatly in determining the size of the enclosure. The project went with a OEM BBA-3 NEMA 3R battery enclosure box. The USRP, computer, and analog back-end will take up the space of the third battery. The enclosure comes equipped with a detachable rear panel that can hold the rest of the electronics, such as the charge controller, hard drive, switched-mode power supplies (SMPS), miscellaneous circuits boards, fuses, and various wire trunking devices. In the end, it is a cramped space inside, but the design allows for adequate ventilation. The rear panel also doubles as a heat spreader for the charge controller, hard drive, and SMPS. Several penetrations had to be created. Three evenly spaced SMA bulkheads will allow for the 3G mobile broadband antenna, and the two polarization feeds. A 1/2" diameter hole on top of the enclosure will allow the GPS antenna to face towards the sky. A 1" diameter hole on the back of the enclosure allows for the routing of power wires through the breaker box, also affixed on the rear.

3.3 Operating Environment

The computer within the HFRS system runs on Ubuntu Linux Server, 12.04 LTS (Long Term Support). This was selected because it is a highly customizable and open-sourced operating system that has been used extensively in the UNM Department of Physics & Astronomy Department. Going open-sourced might mean more investment in software development, but usually gives the designer a more intimate understanding of what is going on throughout the system.

3.3.1 Connectivity

Each HFRS system has a 3G mobile broadband modem with Verizon data service, which currently has the best coverage in the New Mexico area. Each HFRS is assigned a static IP address, and each modem was selected based on 1) the firmware's capability to allow incoming SSH connections, 2) being equipped with an external antenna port, and 3) known compatibility with Linux. Thus, the project went with two models: the USB 760 and the more modern UML290. The GPS system and 3G modem need their own antennas because 1) The enclosure shields internally-generated RFI from transmitting to the outside, including cellular transmissions. 2) Rural areas need a high-directivity (towards the horizon) antenna. 3G was selected over 4G due to the guaranteed SSH tunneling and 3G coverage proven by past projects. In addition, there has been reported problems with SSH tunneling with 4G networks within the Linux open-source community.

To establish the connection, the Point-to-Point protocol daemon and wvdial program, made "dialing out" easy, and a service-level script was developed around that to maintain connectivity (by "redialing") in the case of dropped connections.

Cellular Antenna

Another design point was to minimize the amount of penetrations into the metallic HFRS enclosure original and a selection of a dual purpose GPS/Cellular antenna was desired and purchased. Unfortunately, The gain pattern for the cellular side of the antenna was not ideal for such rural areas, where a very high gain (and directivity) was needed in the close-to-horizontal elevation and the Taoglas dual-purpose antenna proved to be too omnidirectional (see Figure 3.7a). A second penetration in the form of a SMA bulkhead was installed, and a high-directivity antenna, shown in Figure 3.7b, was placed on top of the enclosure instead.

GPS Antenna

The dual-purpose Taoglas antenna was kept for the system since the radio regularly maintained lock to the GPS satellites. The USRP radio biases the GPS line at 3V, and the Taoglas antenna takes advantage of it to power LNAs that provide over 20 dB of gain.

3.3.2 Data Recording

The main purpose of the HFRS system is to record I/Q data to disk. Since the USRP runs on a Linux operating system, a special driver and framework is needed to 1) configure the USRP for data capture, 2) interleave and timestamp the data stream, and 3) save interleaved, timestamped data to hard disk. Fortunately, the USRP is well-supported on Linux through the manufacturer-supplied "UHD" driver. In order to command the CPU to direct and prepare data for storage, the GNURadio software suite is used. GNU Radio is effectively a software driven DSP framework similar to Labview. The scope of GNU Radio reaches far beyond the purpose of this project,

as we use it only to direct and prepare RF data and configure the USRP. Although GNU Radio has a graphical user interface, it is primarily a Python and C++ based program. To best streamline the entire HFRS recording operation, GNU Radio has been integrated into custom Python scripts for recording. In addition, the project is further streamlined due to the ability to manipulate the system via system-level services, augmented by various Linux OS capabilities (crontab, logrotate, etc.). As a result, a host of in-house scripts were developed for the HFRS system.

Capturedata.py

This is the Python script that configures the USRP and records data to disk. Capturedata.py directly interacts with the USRP via the UHD driver and the GNU Radio framework. Threads are used to help with the recording process. The program incorporates threading to help with monitoring the recording part of the process. It will record the data to hard disk after configuring the USRP for center frequency, sample rate, and single or dual channel operation.

Powerloads.py

This Python script powers on/off the hard drive, USRP, vent fan, and front/back end RF electronics. Aided by Bash sub-scripts, this program also automatically mounts or dismounts the hard drive, assuring no damage is done to the data from simply switching it off if mounted. The program interacts with the GPIO hardware in order to control loads.

Modbus.py

This Python script queries a number of HFRS subsystems and saves metadata to three .CSV files to be used for logging. First, it queries the charge controller via the Modbus protocol and retrieves information regarding various charges, voltages, and temperatures. It also has the ability to reset certain charge-level fields as well as shut off all system loads. That would turn off the computer as well, and is thus left in a non-operational state until manually reset. In addition, the script queries computer hardware temperatures and hard drive temperatures. The program is run automatically and the log files are routinely rotated and uploaded to a central server for both web-based and detailed graphical representation.

Fancheck.py

Simple Python script that checks system temperatures and determines whether to turn on the main vent fan.

PostHFRSStatus.py

This script extracts information from the log files and current system status and uploads it to a central server for viewing on a monitoring website.

3.4 Pile-of-parts cost and Selection

A list of the major purchases for the HFRS systems are found in Table 3.2. Table shows prices listed for quantity of each item ordered, per HFRS. Slight differences in the DC/DC power supplies, placement of hardware, and computer could have provided operational difficulties in the future, but fortunately did not occur. The

HF-optimized antenna was omitted since the LWA antenna was used, but for informational purposes it cost $750.

3.5 Health

The health of the system is observed regularly to assure timely warnings and to observe patterns that might warrant future system modifications or operations to be handled differently. To do this, two main scripts have been developed: one to gather data to post to a web page, and another to produce more detailed .CSV log files that are sent to a central server. The objective is to record temperatures, location, software states, battery charges, power states of sub-components, and other data on a regular basis. Both scripts ran regularly on each system. The statistics are saved in three comma-separated-values (CSV) logs, which are archived once a week. These three log files can then be used to produce three detailed graphs, representing one week. A number of sources within the system are used to gather data:

Modbus Communication

The Charge Controller was selected partially because it included a Modbus communication port. The manufacturer also supplied a Modbus-to-RS232 converter, which is how the computer communicates to the charge controller. Information such as heatsink temperature, voltages, currents, and charge states of the batteries, PV, and loads are queried. With this information, we can determine how much charge is remaining in the batteries and better characterize the power consumption of the various components of the system.

S.M.A.R.T. Hard Drive Statistics

Most hard drives have a "Self Monitoring, Analysis and Reporting Technology" feature, where a myriad of information can be extracted. For this project, we

extracted only the HD temperature.

CPU and Computer Heatsink Temperature Sensors

The computer has a temperature sensor on each of its two cores and can be extracted from the command line. The CPU temperatures have been determined to fluctuate the most and exhibit the highest value than all other temperatures. Thus the CPU temperatures are the most often observed and have their place on the monitoring website. In fact, it has been determined that a small on-board CPU fan was needed to be placed on the heatsink to keep the temperature down. This fan runs 24/7 and drastically reduces the core temperatures by over 40 ° Celsius.

USRP GPS

The USRP's onboard GPS, if locked, provides coordinates of the system and can then be mapped on a webpage using Google Maps. Since the GPS cannot be accessed while data is being recorded through the USRP, a separate GPS-polling script is used and is run manually. Besides, the HFRS system is not designed to be moved frequently so polling the location for the webpage once after deployment is usually good enough.

GPIO Relays

Turning the hard drive, front end, vent fan, and USRP on or off is currently a manual operation to be done before and after scheduled observations. The external GPIO boards can also be queried for on/off status, and can be seen on the webpage what is currently powered at any one time.

Recording Processes

The main function of the HFRS system is, of course, to record RF signals at various recording settings. Thus, using the command line, we can extract when a recording is about to run, and at what settings (e.g. frequencies, duration, sample rate, polarizations) the command is run with.

Free Space

The system is regularly queried for remaining free space on the recording disk.

3.5.1 System Vitals

The charge controller's firmware continuously monitors the charge delivered into the batteries from the PV and the net energy draw from the batteries. The values, in Amp-Hours, are incrementally added up inside the firmware, until it is manually reset. Figures 3.8 and 3.11 show detailed graphs of a week-long vitals observation of the HFRS3 system, during an RFI observation at Sevilleta. An active observation means all components are on. Figure 3.8 show how the PV panels sporadically charge throughout the day and how seldom the panels actually achieve 250W power throughput. This is one reason why, when sizing PV panels, NOCT values should be used instead of the nameplate (STC) values. Regardless, during consecutive days of constant sunshine as was experienced during late February and early March, the PVs produced enough charge to almost break even. Between February 27th and March 2nd, the PVs injected 110 Ah while the system consumed 120 Ah - a deficit of 10 Ah. This is shown in Figure 3.10. This period shows a minor deficit to recharge from since loads can be powered off. The deficit will be greater if in cloudy or inclement weather, and might compromise extended-length observations.

Another series of collected data to consider is the battery voltage drop between daily solar insolation of the PV. A healthy 24 V battery bank can be charged anywhere from 25–28 V. In the case of AGM batteries, if the voltage drops below 24V, the batteries are becoming exhausted before recharge. Another way to detect this is to sum the load charges between nightly PV inactivity. If the battery bank is designed to supply 55 Ah between charges, then no more than 55 Ah should be expended between charges in order to extend battery life. An extra detail about the

HFRS system can be found in Figure 3.9, where it shows about a 5 Watt difference between recording and non-recording states. This is the extra power required from the USRP, CPU, and the hard drive when recording data.
Finally, it is also important to assure overheating of the system is not occurring. The temperatures in Figure 3.11 show an acceptable diurnal variation.

For on-the-fly status of the system, a php-based website shown in Figure 3.12 provides a quick-check of all operating HFRS systems simultaneously.

(a) Deployed HFRS with affixed PV panel.

(b) Showing breaker box, cellular antenna, and PV power inputs.

Figure 3.4: Parts of the HFRS System

Figure 3.5: Showing charge controller, batteries, and voltage regulator for final stage amplifier, atop the tri-voltage SMPS block.

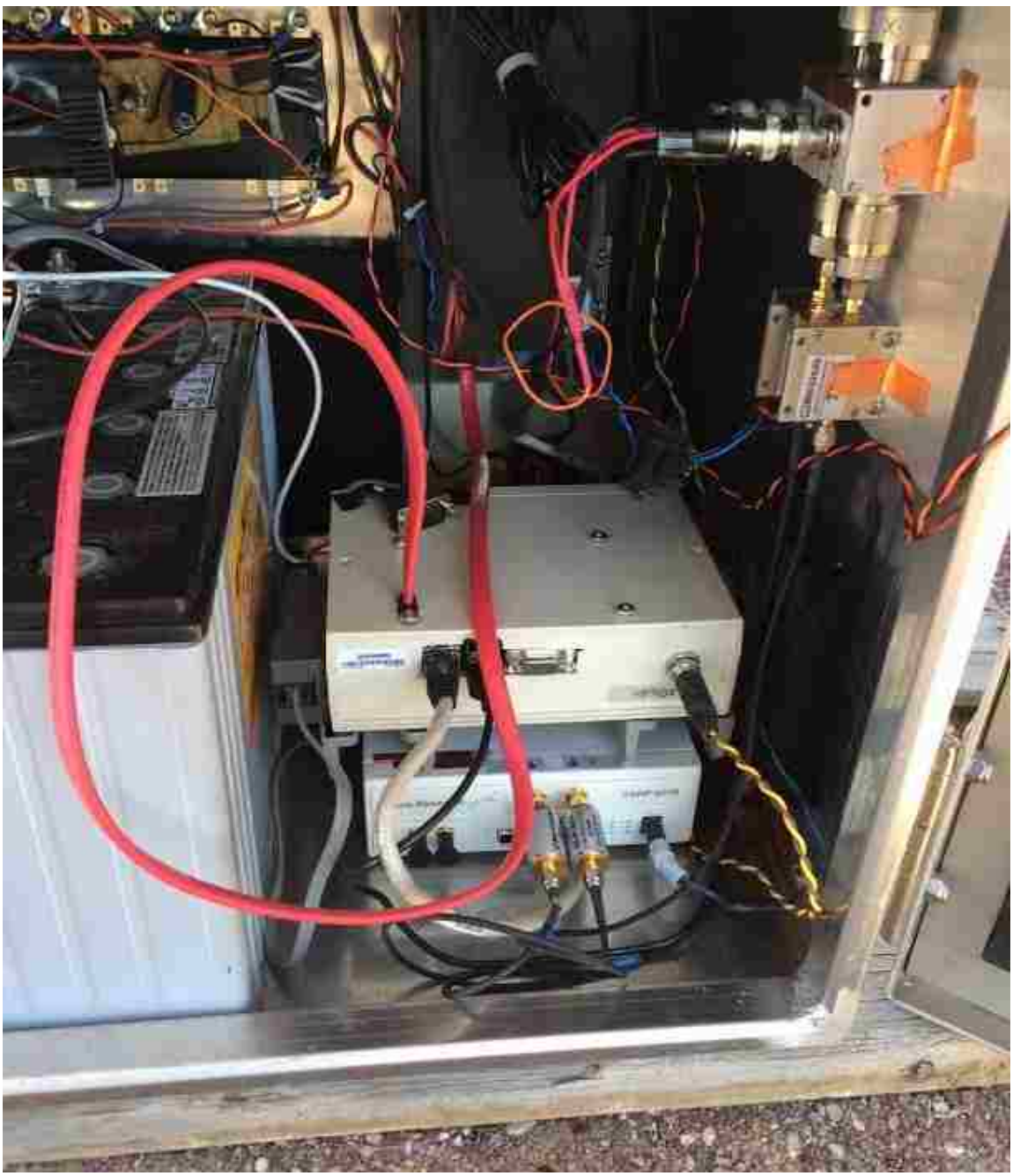

Figure 3.6: Showing computer with custom box, USRP, hard drive vertically mounted on back, and analog back end on side.

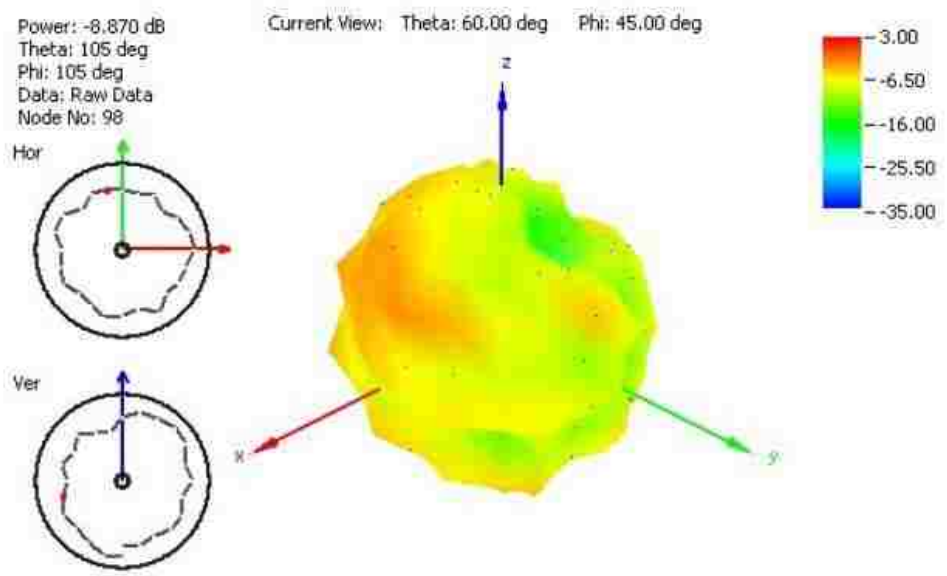

(a) Taoglas radiation pattern for Verizon 3G

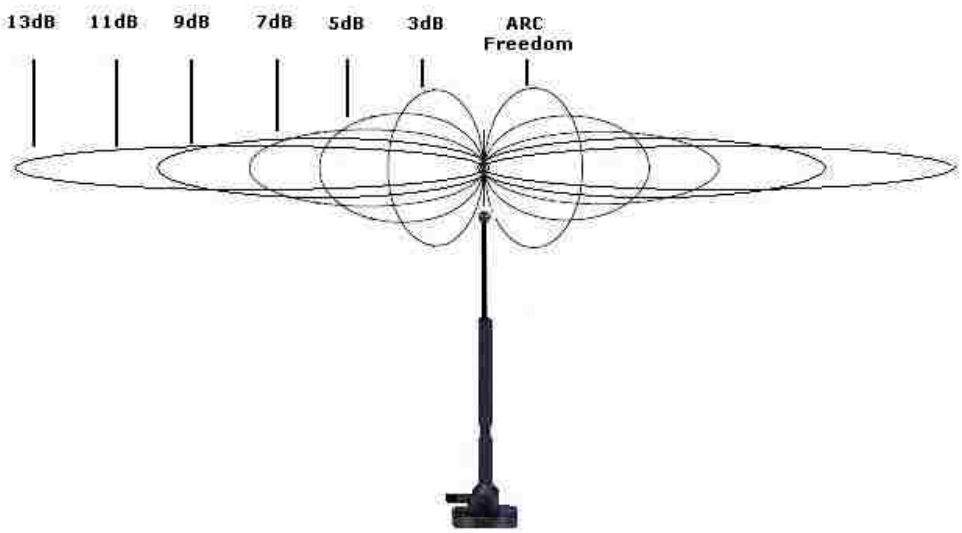

(b) Simplified diagram of AntennaGear's directional 3G antenna

Figure 3.7: Radiation lobe patterns for two different 3G mobile broadband antennas

Product(quantity)	**Manufacturer**	**Description**	**Final Price**
Power System			
Main Enclosure	Affordable Solar (AS)	Model BBA-3	$357.77
Batteries (2)	Affordable Solar	Deka 110 Ah AGM	$519.50
Solar Panel	CSI	250W Poly-Crystalline	$215.60
Solar Panel MC Cable	Affordable Solar	8' run, connecting PV	$10.21
Charge Controller	Morningstar	400W, MPPT	$220.58
Modbus Adapter	Morningstar	Charge Controller Comms.	$30
PV Racking (2)	Unirac	Connecting PV to HFRS	$180.00
DC Breakers (3)	Midnite Solar	5A (2) and 15A (1)	$39
Breaker Box	Midnite Solar	For easy access to breakers	$72
DC/DC SMPS Module	Vicor	24V to 6V,12V,15V module	$440
Distribution Blocks	Digikey	For splitting power wires	$28.00
Load Control			
GPIO Board	Numato Labs	For soft load control	$20
Relay Board	Numato Labs	For load control	$25
Computing			
Computer	Advantech	Atom N2800	$479
Computer Enclosure	Digikey	general purpose	$18
4TB HDD	Seagate	SMART enabled, internal	$190
HDD Enclosure	Rosewill	E-SATA to SATA	$35.00
USRP	Ettus Research	With BasicRX daughterboard	$1,800
USRP GPS	Ettus Research	Internal add-on module	$750
Main Vent Fan	Mouser	120mm X 25mm	$18
Analog			
LWA Antenna	Custom	Includes structure, FEE, dipoles for 2 polarizations	$500
GPS Antenna	Taoglas	Hercules Model	$72.00
Cell Antenna	Antennagear.com	11 dBi, includes FME-F to UML290 comverter	$40
50 MHz Low-pass Filter (2)	Minicircuits	Butterworth	$70.00
Bias-T (2)	Minicircuits.com	ZNBT-60-1W+	$165.90
Medium-Power Amplifier (2)	Minicircuits.com	Obsolete Model	$240
USB 3G/4G Modem	Verizon	UML 290 and USB 760	$20 / month
RFI Mitigation			
Copper Tape	Digikey	1" X 50'	$52.51
RFI Honeycomb Vent (3)	Custom	5" X 5"	salvaged
Conductive Weatherstripping	Mouser	For HFRS door lining	$39.92
20A Feedthrough Filters (7)	Digikey	Anti-RFI for Power Lines	$8.48
Conductive Gasketing	Chomerics	Soft-Shield 4800 Anti-RFI	$60
Machine Shop Services; including labor and parts			
PV panel mounting modifications			$480.40
Electrical equipment mounting and enclosure penetrations			$85
Grand Total, per HFRS			$6,736.47

Table 3.2: Pile-of-Parts cost, per system.

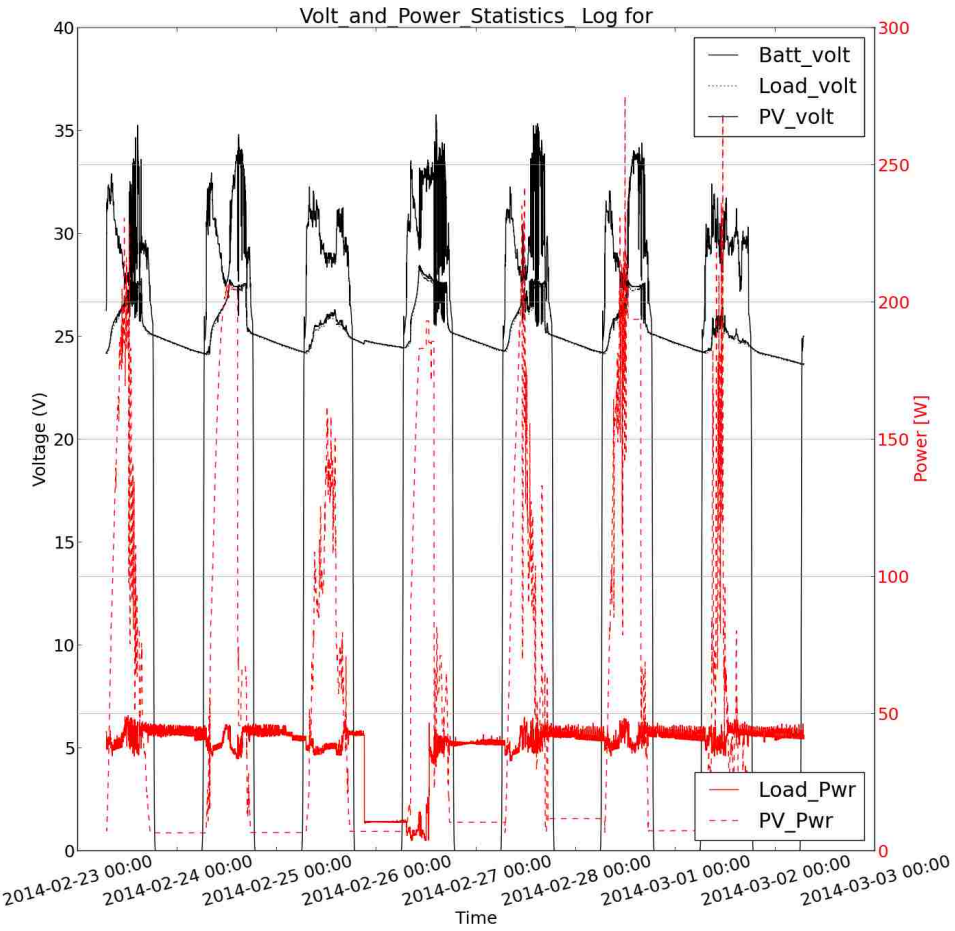

Figure 3.8: Power and voltage behavior during 7 days.

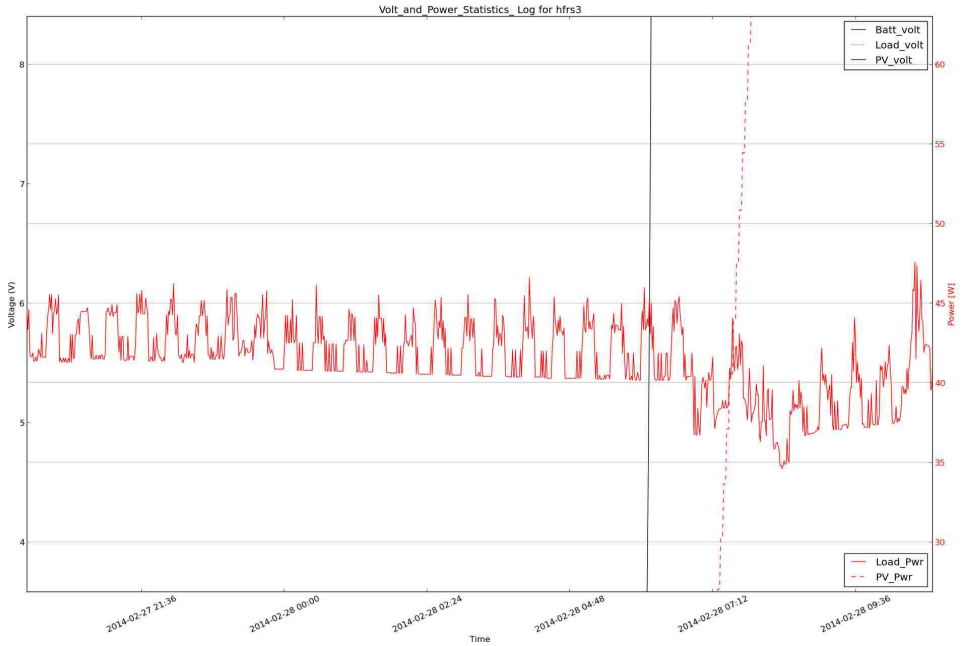

Figure 3.9: Figure3.8 zoomed-in, showing a 5W throttling-back of loads between observations.

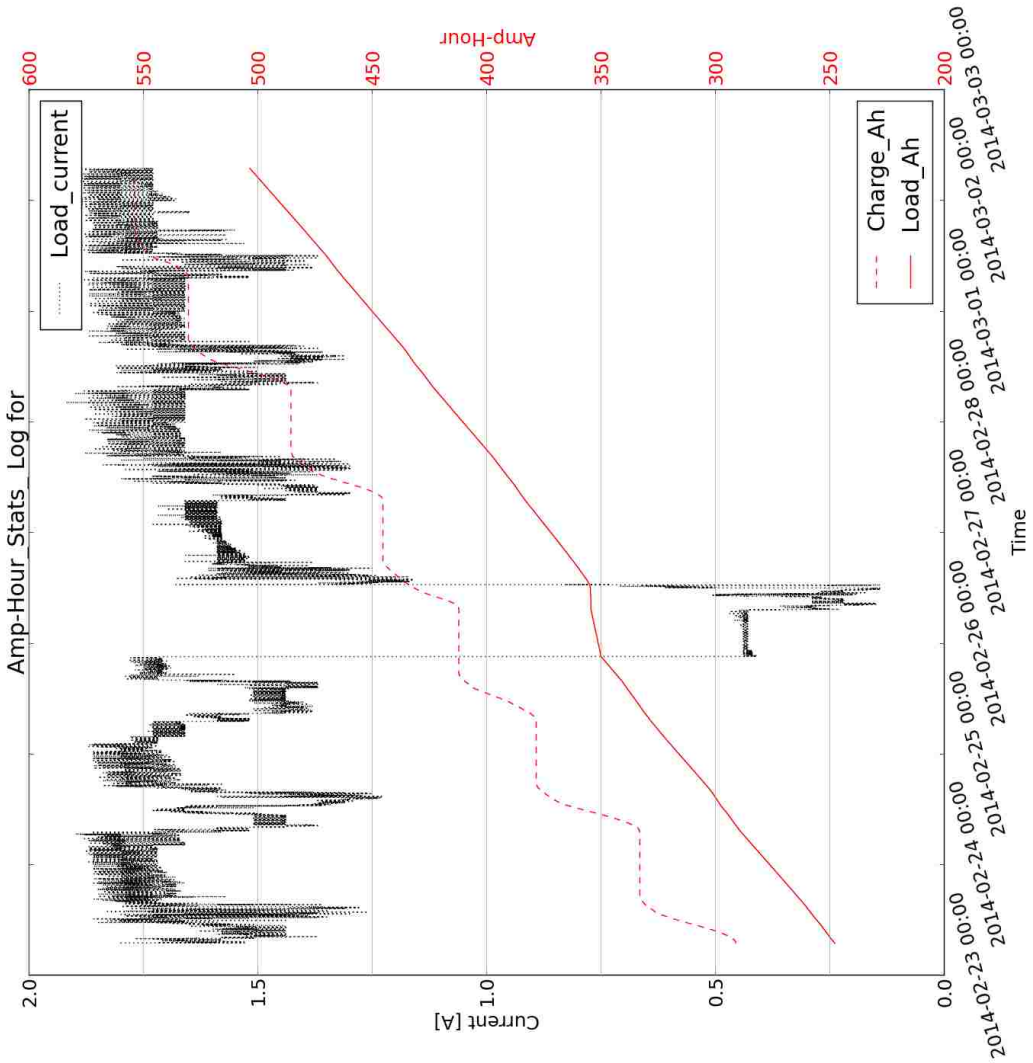

Figure 3.10: Current and charge behavior during 7 days in late February, 2014.

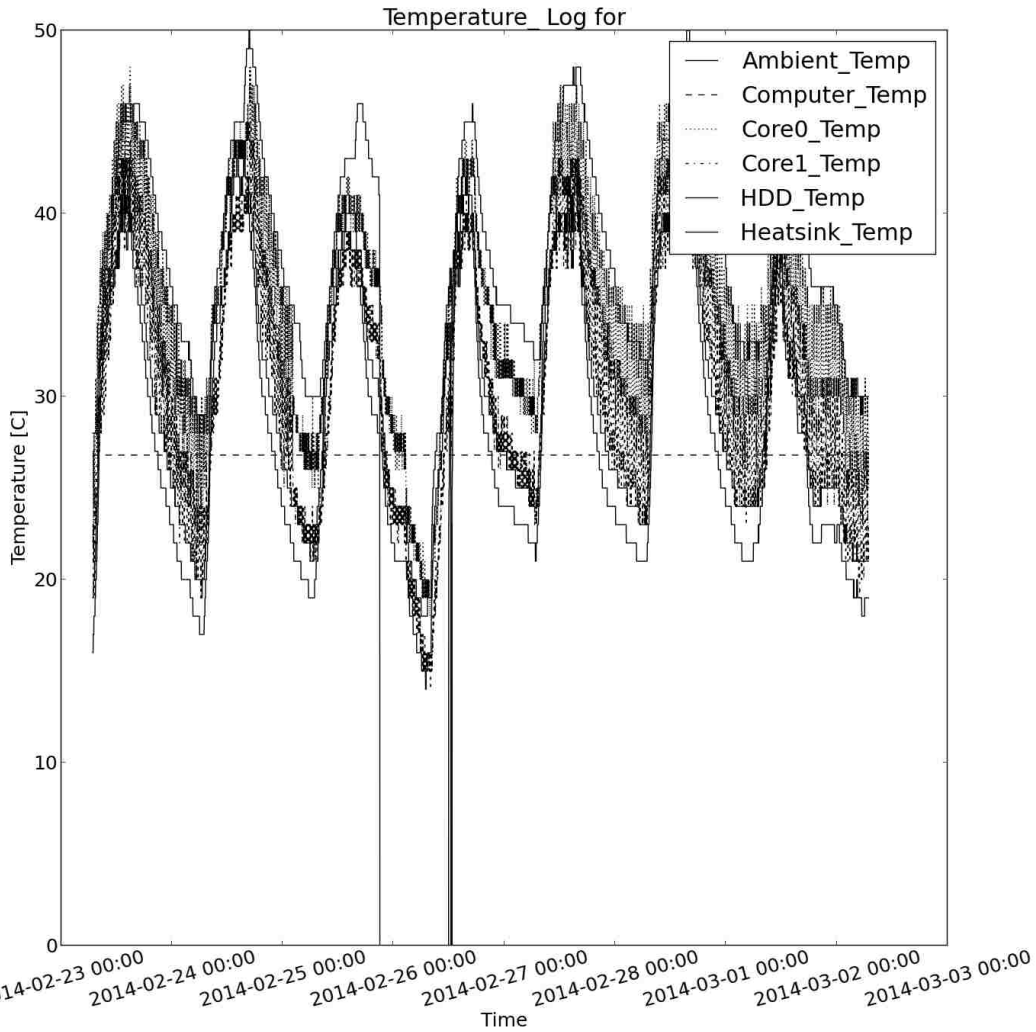

Figure 3.11: Collated temperatures of system during 7 days. Null values are reported when hard drive is off.

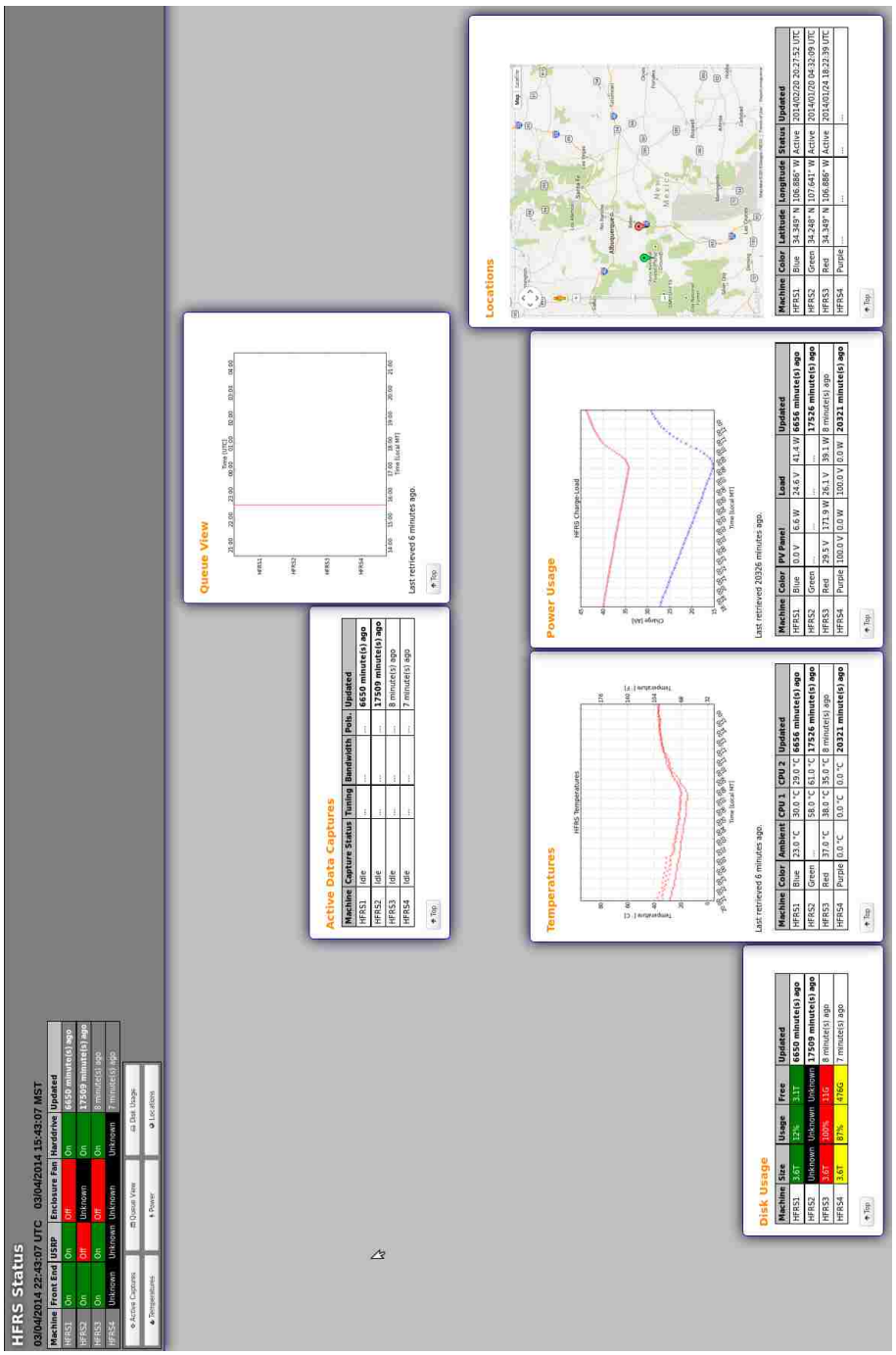

Figure 3.12: HFRS web status.

Chapter 4

EMI Mitigation

The HFRS uses numerous components that can generate RFI, which is coined Electromagnetic Interference (EMI) in the industry and this term is used here to differentiate self-induced RFI from impinging radio signals from non-HFRS sources. The enclosure purchased is rated NEMA-3R, made of aluminum, and is suitable for outdoor placements. The enclosure's seams are only stitch welded and is in need of considerable EMI shielding.

The Very Large Array (VLA) has a reverberation chamber that is designed to test devices for EMI. Unlike an anechoic chamber, the reverberation chamber assures all EMI is picked up from the offending device, emanating from any direction. All electronic devices are required to meet stringent EMI standards before being used in the VLA area. Enclosures designed to attenuate EMI from within are priced beyond the budget of this project. Thus, we are left to modify the enclosure with copper tape, power filters, honeycomb shields, conductive gaskets and strips, as well as RF-absorbing foam.

4.1 Before Modifications, In-Lab

Before modifications, there was an in-lab EMI test as well as a reverberation chamber test. The in-lab test used the spectrum analyzer and a loop antenna to test for EMI from 1 MHz to 60 MHz. The results of the in-lab observations validated the trips out to the VLA for more wideband and more detailed EMI observations. The antenna used is classified as a small loop antenna[1] where the .5 meter circumference is smaller than $\lambda/3$. With this in mind, it is known that the small loop antenna is characterized by a toroid gain pattern with a directivity of approximately 1.5. This is good for almost-omnidirectional observations, and was waved around the enclosure in an arbitrary manner while performing the in-lab observation. The small loop antenna has good receiving properties for this frequency range and has a large effective aperture throughout the 1–60 MHz. Two readings were done: one with all HFRS devices on and the door closed and another done with the door open. A third "ambient" reading was performed with everything in the lab (including lights) off. All three were brought into Python and the ambient reading was subtracted from both HFRS readings. The result shows EMI being emitted from the devices in the HFRS as well as enclosure offering 10–30 dB attenuation. However, without good characterization of the antenna, unavoidable presence of a noisy city and building environment, and imperfect observation techniques, EMI quantification is at best an estimate. Figure 4.1 shows some definite contribution from the HFRS EMI with the door closed when ambient spectra is subtracted. Figure 4.2 shows EMI radiating from the door of the HFRS when open.

4.2 Before Modifications, Reverberation Chamber

The HFRS was placed in the VLA's reverberation chamber both before and after modifications. The equipment in the chamber is reliable from 300 MHz to as high as 10 GHz but since EMI in this case ceases below 4GHz, that's where observations end. The reverberation chamber is equipped with a custom omnidirectional superwideband bi-conical dipole antenna developed at New Mexico Institute of Mining and Technology as well as a "stirrer": huge metallic blades that rotate to eliminate spots of destructive interference that might prevent reception of some EMI at the antenna.

Once the data is collected, it is calibrated and the Effective Isotropically Radiated Power (EIRP) of the EMI can be calculated based on how far the HFRS system will be placed from the nearest VLA antenna. The dashed line in Figure 4.3 is the calculated limit of EMI before interference is of concern to the VLA antennas. Figure 4.3a shows the EMI spectra of the HFRS system before any significant EMI mitigation. As a result, we have implemented a number of modifications to the HFRS system to better mitigate EMI.

4.3 Modifications

It is known that EMI can be considered water in a way - if there is a space for water to leak out, EMI will probably get through as well. The EMI reports were sent back only a month before the beginning of the campaign, so the best in-lab attempts have been made - no time for welding or ordering new enclosures. Firstly, all seams were sealed with conductive copper tape. There are also conductive gas-

kets used for all penetrations, including bolts, door hinges, and the GPS antenna. There are three vent slots on the enclosure, and RFI honeycombs have been affixed with copper tape and a filter media to keep out dust (see Figure 4.4. The door's existing weatherstripping was replaced with conductive, compressive gaskets. Most importantly was the breaker box in the back - all power wires routed through the box and in/out of the enclosure rerouted through EMIs filter rated to 20A and 100 V. EMI is known to travel on wires and thus the power wires could be acting as antennas. Using gaskets and sealed EMI power filters still provide easy user access to the breaker switches (without opening the main enclosure door and reaching in) while preventing EMI from escaping the enclosure. Figure 4.5 shows the bulkhead developed for this purpose.

Even after the modifications, some emission from 1.6 GHz and below exceed the EIRP limit for North Arm location as shown in Figure 4.3b. Fortunately, such EMI did not adversely affect the campaign. It is the author's suspicion that EMI might be leaking out of the unused cellphone portion of the dual purpose cellphone antenna, however there aren't many more modifications that can be done to the existing enclosure to further mitigate EMI.

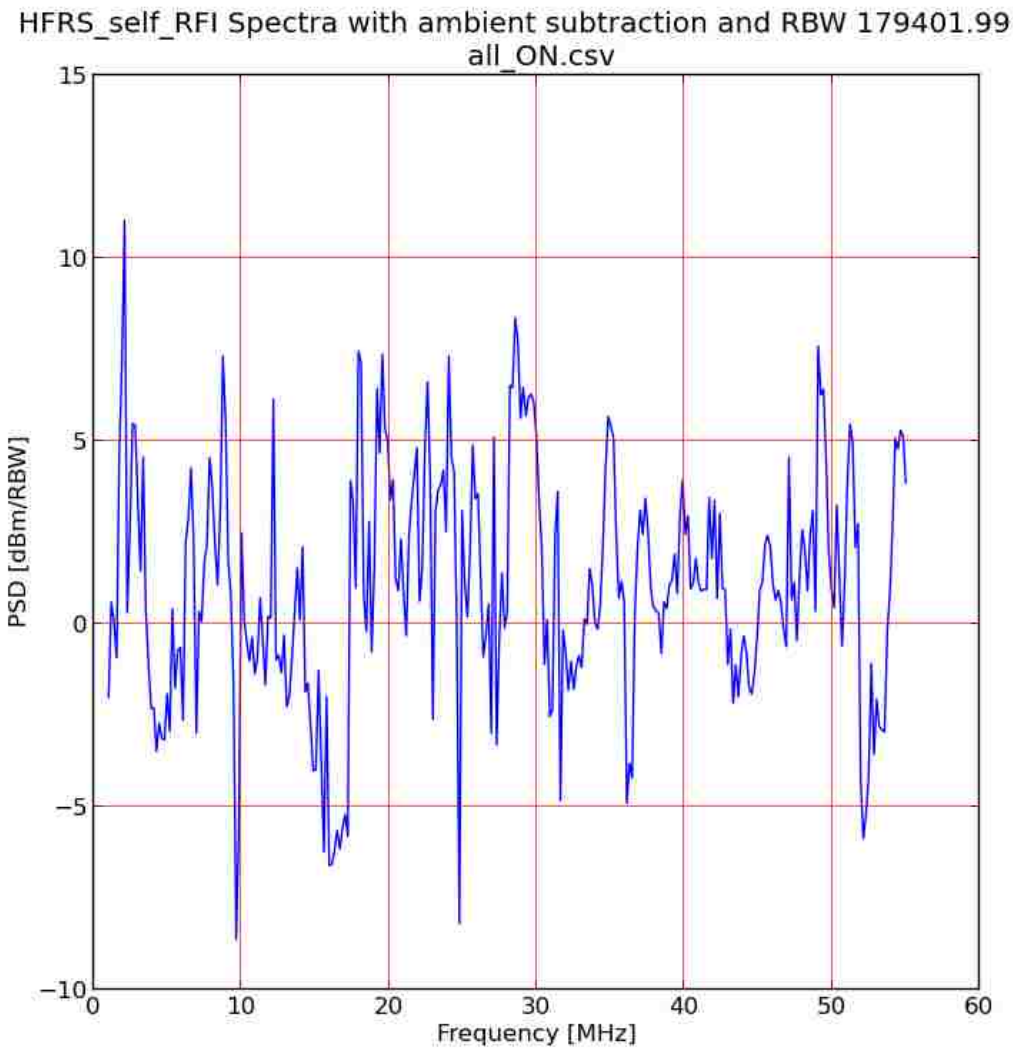

Figure 4.1: In-Lab EMI Spectra with loop antenna, door closed.

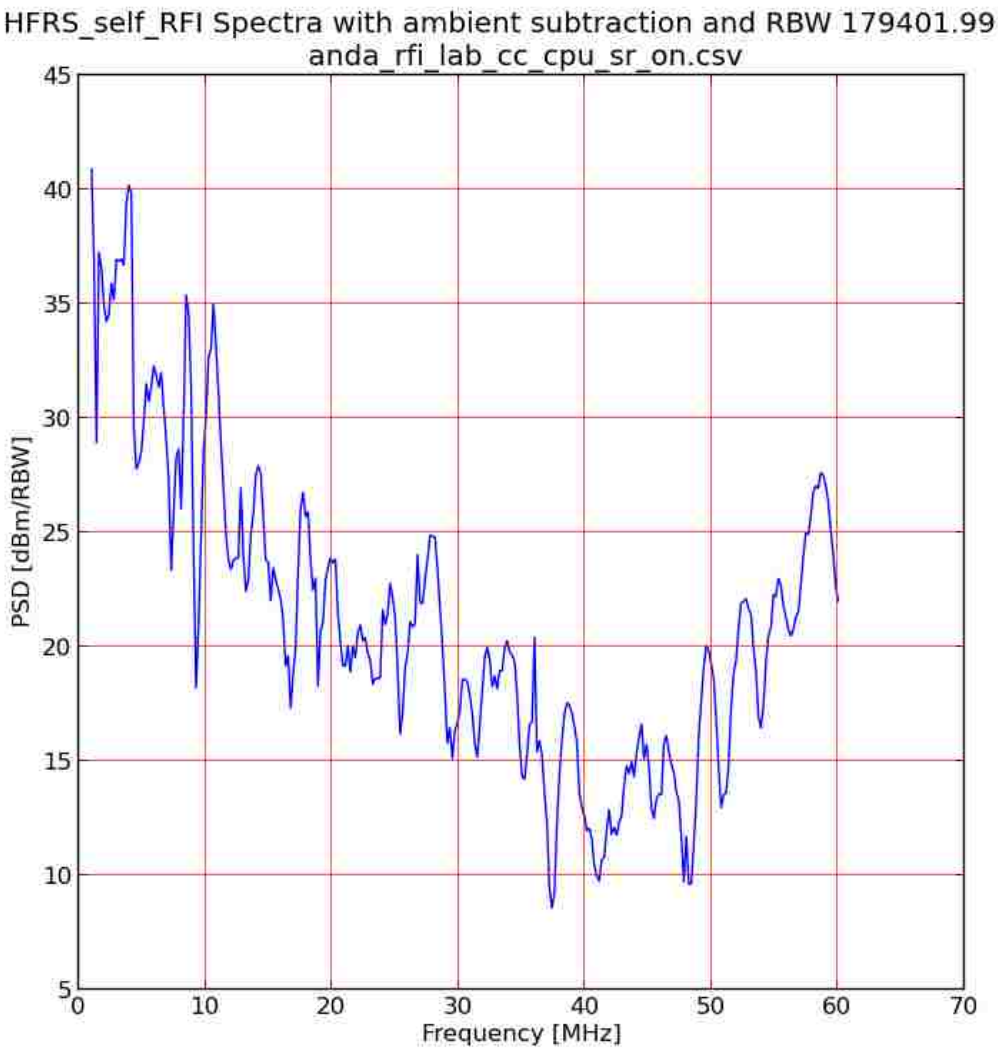

Figure 4.2: In-Lab EMI Spectra with loop antenna, door open.

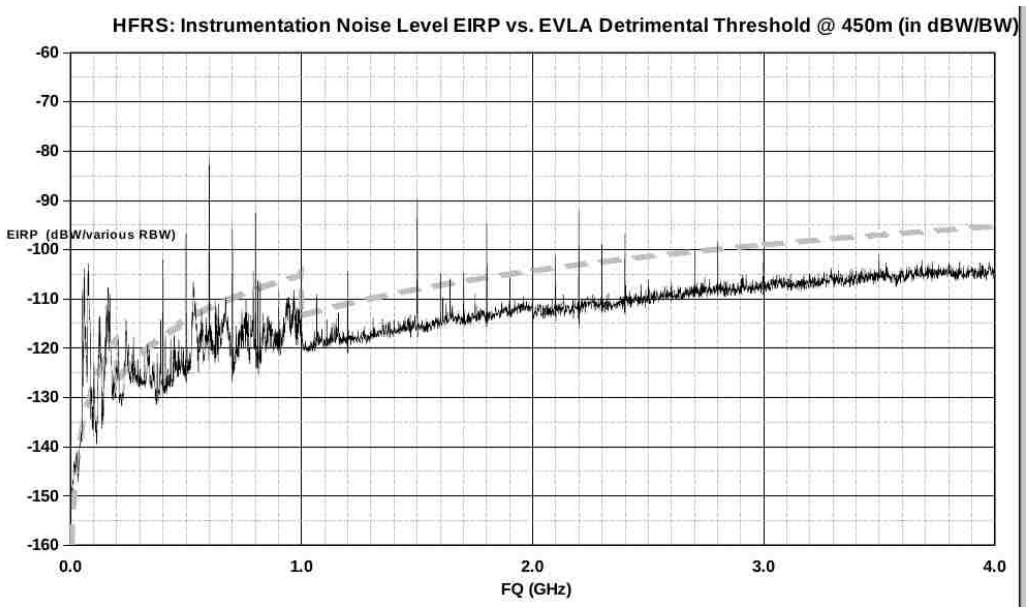

(a) Before

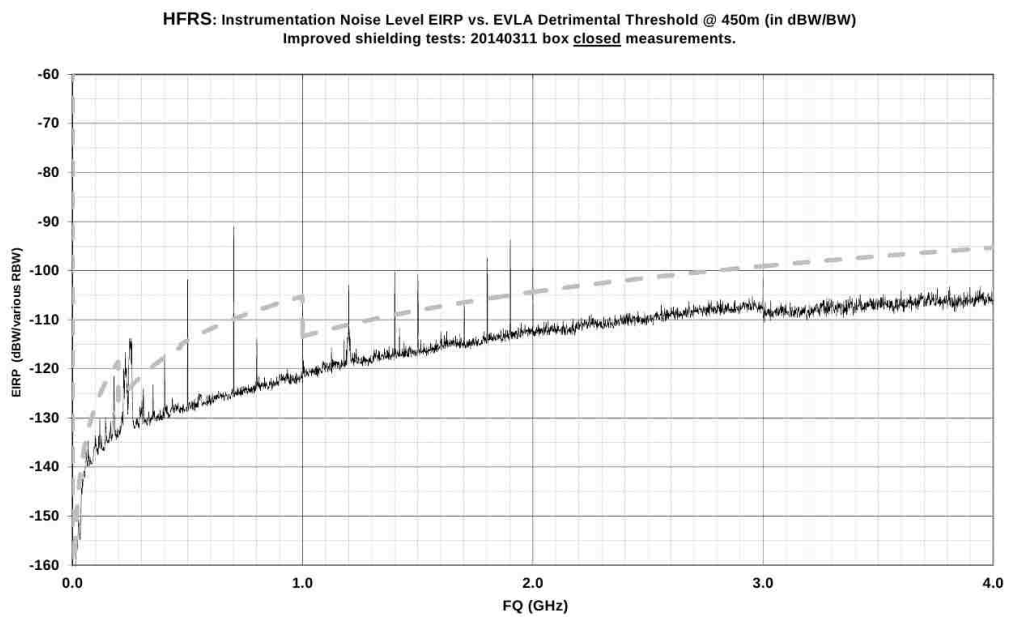

(b) After

Figure 4.3: Chamber Measurements of EMI from the HFRS before and after EMI-mitigation modifications.

Figure 4.4: Vent fan being affixed to RFI Honeycomb, attached to enclosure by copper tape.

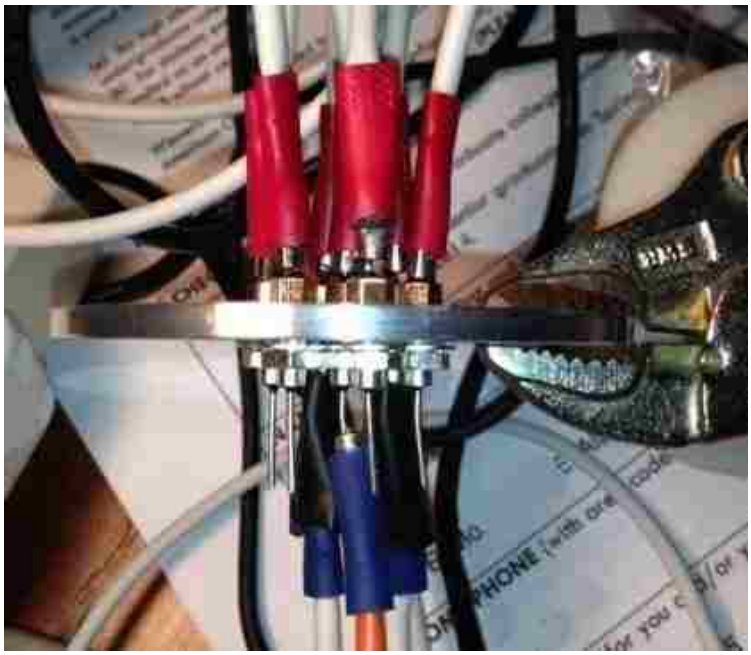

Figure 4.5: Bulkhead developed to pass power wires through the enclosure, into the breaker box.

Chapter 5

RFI Environment Testing

Radio Frequency Interference changes depending on location, and it is important to determine the RFI environment at a field site in order to properly calibrate a radio system. In the case of the HFRS, it is important to determine frequency channels that are notoriously occupied as well as their power levels. These signals can potentially throw the system into compression, and if it occurs often enough, disqualifies the frequencies or site from being used for the observation. The RFI surveys are best run for at least several days continuously, over two polarizations, and should include weekdays and weekends. The information can then be used to optimize the associated HFRS system for the observation. Each HFRS will have its analog RF line optimized based on these surveys, mostly by adjustment of filters and attenuators. Due to the last minute announcements of the field sites, RFI testing took place at only two sites: Sevilleta National Wildlife Refuge and the VLA's North Arm location. The HFRS systems perform the RFI surveys. All recorded data are analyzed by comparing, relatively, impinging signals to each other. For the Sevilleta location, there has been some software calibrations to approximate the power level of RFI signals impinging on the antenna.

5.1 Observation Setup

The RFI observations occurred from 4–88 MHz at Sevilleta and 1–48 MHz at the North Arm. Since the HFRS maximum recordable bandwidth is 3.125 MHz for dual polarization, a sweeping script is implemented so that the USRP sweeps center frequencies. The Nyquist upper limit for the HFRS is 50 MHz, thus for Sevilleta two complete HFRS systems were used: one for 4–50 MHz and the other for 50–88 MHz. The sweeping script holds each observation for 45 seconds before moving to the next center frequency. Each 45 second observation produces two files, one for each polarization, with the timestamps and interleaved headers, just like the campaign. Post processing software developed for this RFI survey uses the meta-data stored in the headers to properly combine the files for statistics and plotting.

5.2 Software-Based Signal Calibration

The processing scripts developed for this RFI survey converts the complex numbers received from the USRP to arbitrary power levels (dimensionless dB). Although displaying these values would be fine, three calibration steps were implemented in order to get more accurate power signals. These calibration steps have been added into the processing scripts, after the FFT. The flowchart is shown in 5.1. To summarize:

1. The USRP outputs unscaled values proportional to the incoming voltage levels and a uniform scaling factor is subtracted to correct for this.

2. The LWA's electronics provides an almost uniform gain throughout the spectrum of interest. These values are subtracted.

3. The LWA antenna's VSWR is representative of power lost per frequency channel before it enters the electronics. This is due to the relationship of wavelength

and antenna geometry.

4. Cable losses are not accounted for, but for under 100 MHz losses do not exceed 5 dB.

A Rohde and Schwarz FSH-3 spectrum analyzer is used as a power-level reference and VSWR measuring device, and its output is measured in dBm. Using a broadband noise source, which is essentially constant throughout 1-100 MHz, we can scale the uncalibrated FFT values to more accurate values to what is actually seen at the USRP's inputs. The FEE gains have also been subtracted from this array using the noise source as a reference input signal into the spectrum analyzer. Thus we are able to estimate, in dBm, signal strength into the FEE from the antenna structure.

Furthermore, we can perform VSWR test on the antenna elements themselves in order to get the frequency-dependent impedance mismatch. As a result, we can get a better estimate on the power level of the impinging signal to the LWA Antenna. Antenna impedance mismatch losses are usually between .5 dB to 9 dB for frequencies above 10 MHz. The loss increases to 20 dB below 10 MHz. Calibrating the data details a more realistic power level of the signals as it enters the FEE.

5.3 Sevilleta RFI

The Sevilleta RFI observations were done between February 21 and March 5, 2014. Sevilleta National Wildlife Refuge is located 20 miles north of Socorro, NM. Sevilleta is a large segment of land west of Interstate 25, and a segment of it is under consideration for a LWA station. Being closer to various transmitters and general civilization than the North Arm and LWA1 site, it is a good idea to perform a survey and compare with the LWA1 site. The GPS coordinates of the HFRS system are 34.34 °N, 106.886 °W. The HFRS systems ran an observation once every 23 to

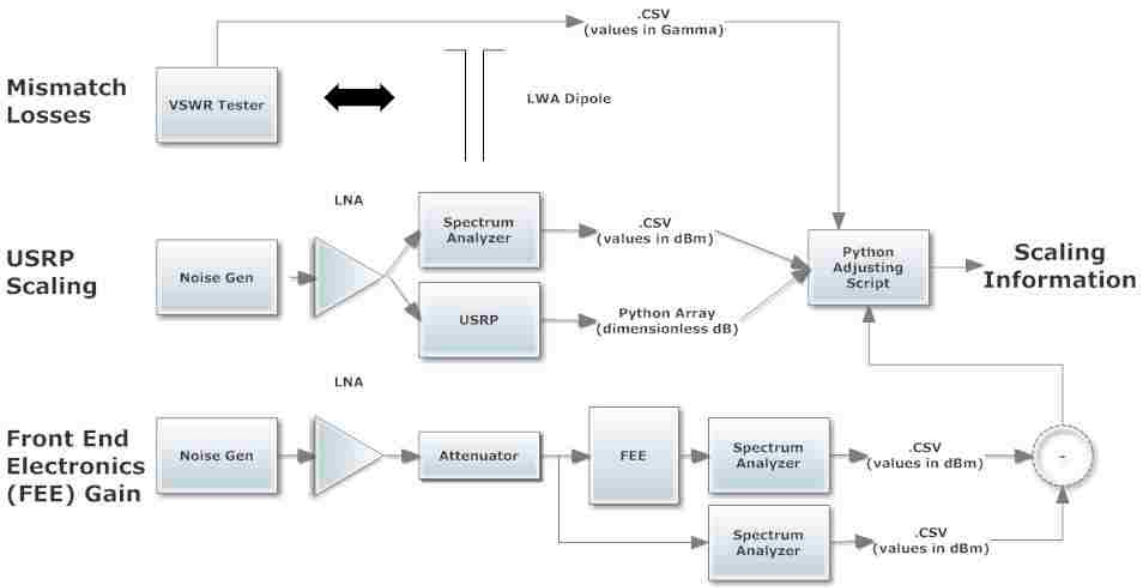

Figure 5.1: The three calibration techniques used to approximate the power levels impinging on the antenna.

30 minutes, with each observation lasting 45 seconds. An observation is a sweep of center frequencies, 3.125 MHz in bandwidth apart, feeding dual polarizations. Polarization X is East/West, and Polarization Y is North/South. Each sweep takes 694 to 750 seconds, with additional "sleep" downtime to gain multiple days' worth of observations on a single 4 TB hard drive. These observations include weekdays and weekends. All data recorded to the two USRP systems are analyzed by comparing, relatively, impinging signals louder than the noise floor. I/Q signals are digitized and sent to the computer in complex integers, each complex number being 32-bits. In practice, the USRP's resolution is 14 bits.

5.4 Setup

The HFRS system used for the lower frequency band was standard issue: a USRP N210 radio, a LWA antenna, and a 50 MHz low-pass filter. The Nyquist rate is limited to 50 MHz[1], and thus the low pass filter is necessary. The USRP N210 radio is dual channel, so observations of both polarizations can be done at the same time. The generalized system gain of the low frequency HFRS is 35 dB.

The higher frequency observations uses a separate HFRS system. Since the observation frequencies were higher than the Nyquist rate, undersampling techniques were employed. Firstly, the antenna's on-board analog 150 MHz low-pass filter was replaced with a Cauer 50 MHz high-pass filter with 20 dB stopbands and sharp rolloff. Secondly, connectorized filters of 52-88 MHz bandpass and DC-90 MHz low-pass were placed in series before the radio to create acceptable rolloffs on both ends of the frequency range. Finally, the second stage amplifier was removed from the Antenna Electronics. Instead, an external, connectorized amplifier was used with 9 dB attenuation. This gives the high frequency HFRS1 system a generalized system gain of 35 dB. Figure 5.2 shows the high frequency receiver setup. The radio's software driver accounts for the mirroring of the aliased frequencies and assures accurate frequency-domain representation of the RFI.

5.5 RFI results: Sevilleta

Observation One: February 21, 22:50 to February 25, 09:11 UTC.

Observation Two: February 27, 17:30 to March 4, 07:11 UTC.

[1]HFRS N210's have Analog to Digital Converters that sample at a constant 100 Msps, and downconversion is done in the FPGA.

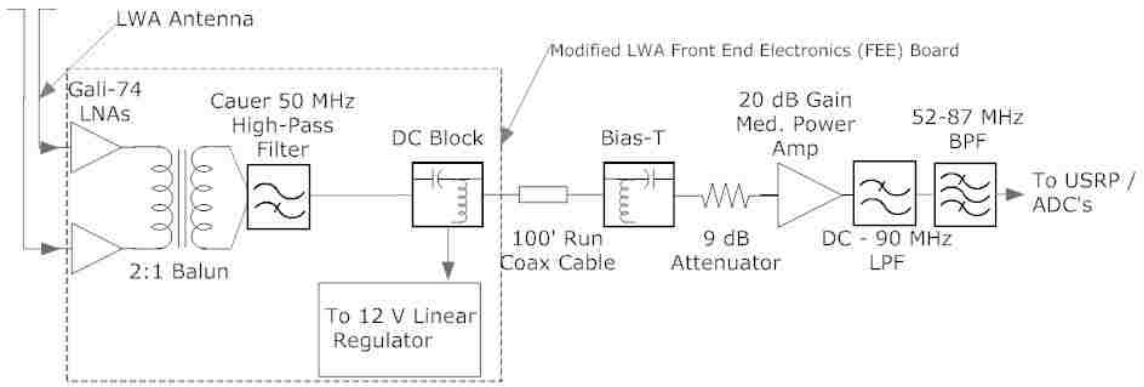

Figure 5.2: Undersampling setup for 50–88 MHz reception using the USRP.

Two tests were run, one for 3 days and 10 hours, and a second one for 6 days and 6.5 hours. Tests include 3 spectral graphs per polarization: average spectra, 80th percentile spectra, and maximal spectra. The 80th percentile observation shows the value in which 80% of the collected spectra falls at or below, per FFT channel. Tests also include a waterfall based on averaged values per polarization. Finally, diurnal observations were taken at the 43 MHz and 63 MHz center frequencies, each being a relatively quiet frequency range throughout the entire observation. This tests the HFRS's stability and sensitivity to the sky noise.

All of the statistics on the spectra are calculated using Python's numpy package, scipy.stats package, and the masking capabilities of numpy to omit blanked data. The waterfall is calculated in a similar manner, reducing the values from each 45 second observation to a one dimensional array of mean values before combining. Tables 5.1, 5.2, and 5.3 list notable RFI and the associated FCC frequency allocation designation[2]. Various modules in the LWA Software Library[6] have been used throughout. RFI occupancy plots are included in this survey to demonstrate the percentage of time each channel is occupied by RFI. In these surveys, RFI is calculated using spectral kurtosis statistics[7]. Essentially, a channel is considered occupied by RFI when kurtosis of a channel exceeds 4 sigma of what is expected of

Gaussian noise.

5.5.1 4–50 MHz

There is considerable RFI below 20 MHz, as well as surrounding the 27 MHz area.

Freq. (MHz)	Description	Freq. (MHz)	Description
1.57	AM Station, KOAZ	1.6	AM Station, KIVA
1.65	Broadcasting	2.5	WWV
3.2	Fixed and Mobile	3.8	Amateur Radio
8.6	Aviation	4.6-4.8	Fixed Mobile
5	WWV	5.09	Fixed and Mobile
5.8	Fixed and Mobile	5.9-6.2	Broadcasting
7.38-7.56	Broadcasting and F&M	9.47-10	Broadcasting and F&M
11.76	Fixed and Mobile	12.1	Fixed and Mobile
15	WWV	15.23-15.6	Broadcasting
19.8	Fixed	20	WWV
21.6-21.8	Broadcasting	21.9	Fixed and Mobile
22.5	Fixed	27	CB and ISM Equipment
30	Fixed	31	Fixed and Mobile
35.2-35.3	Fixed and Mobile	40	ISM
44.6-44.7	Land Mobile	45.7	Fixed and Mobile

Table 5.1: Frequencies of interest for low observation band.

The following graphs show the most useful information from the 4-50 MHz observations. Figures 5.3 and 5.4 show the low frequency observations via dual polarizations and Figures 5.5 and 5.6 show the averaged waterfall for the same observations. The waterfalls give a good temporal view of the data while the spectra shows frequency ranges that are constantly loud. Blank boxes in the waterfalls are either due to computer resource failures while recording to disk or discarding of raw spectra shorter than 43 seconds due to the Python-based processing program used to combine and calibrate the spectra. The first observation shows a lapse of time of about 18 hours towards the end of the observation. This lapse is further detailed in Figure

5.18. Both observations show powerful transmissions from the CB band and perhaps the 40 MHz ISM band as well.

Figure 5.7 shows the RFI occupancy plots for the first and second observations, respectively. Each figure includes both polarizations per frequency channel.

5.5.2 50–88 MHz

Observation One: February 21, 22:40 to February 25, 10:56 UTC.

Observation Two: February 27, 17:32 to March 5, 00:10 UTC.

The observations for the upper frequencies have to take into account the possibility of unwanted aliased signals. Figures 5.8 and 5.9 show the low frequency observations via dual polarizations and figures 5.10 and 5.11 show the waterfall for the same observations. A filter with sharper rolloffs and higher stopband attenuation would have been ideal for this observation, but physical room was not available on the electronic board for a higher-order filter. Thus, we have to analyze the low frequency waterfalls for particularly loud frequencies and check to see if they have aliased over to the corresponding higher frequencies.

The observations between 69 and 73 MHz show aliasing from the 26.6 to 30 MHz, since they occur at the same time on both waterfalls. The FM bands can easily be seen and outside of that, things are relatively quiet. Table 5.2 shows occupied frequencies in this range.

Figure 5.12 shows the RFI occupancy plots for first and second observations, respectively. Each figure includes both polarizations per frequency channel.

Freq. (MHz)	Description	Freq. (MHz)	Description
50	Amateur	50.9	Amateur
51.2-51.5	Amateur	54.3	Broadcasting
55.1-55.5	Broadcasting	57.3	TV Ch. 2
58.1	TV Ch. 2 "KASA-TV"	59.6	TV Ch. 2
59.75	TV Ch. 2	59.9	TV Ch. 2
60	TV Ch. 3 "KENW"	62.4	TV Ch. 2
65	TV Ch. 3	67	TV Ch. 4 "KOB"
70 - 73.6	Aliased Signals	75	Aviation
77	TV Ch. 5 "KNME-TV"	80	TV Ch. 5
82.3-82.6	TV Ch. 6 or Auxiliary	83.2	TV Ch. 6
84	TV Ch. 6	84.38	TV Ch. 6
84.7	TV Ch. 6	85	TV Ch. 6
86.13	TV Ch. 6	87 - 108	FM Broadcast

Table 5.2: Notable occupied frequencies for 50–88 MHz.

5.5.3 March 3, 2014 4–88 MHz Nighttime observations

A nighttime observation between March 3 2014, 3:00 to 10:15, UTC was extracted from the data. This was selected to display the spectra when the 27 MHz broadband interference is not active. Figures 5.13 and 5.14 shows the 4–50 MHz RFI spectra and waterfalls over both polarizations. The 50–88 MHz range shows a more quiet setting via Figures 5.15 and 5.16. The high frequency range show a much quieter situation than the lower end, where most of the RFI can be found below 18 MHz.

In addition, Table 5.3 shows nighttime frequencies of interest above 18 MHz:

5.5.4 Diurnal Observations

In order to test the stability of the HFRS systems, two quiet channels have been selected. In order to not skew the data, the middle 2,000 of 4,096 (the FFT length)

Freq. (MHz)	Description	Freq. (MHz)	Description
20	WWV	20.25	Fixed
21.7	Broadcasting	25	WWV
30	Fixed and Mobile	35.18	Public & Private Mobile
40.08	ISM or Fixed and Mobile	42.7	Fixed and Mobile
44.5	Mobile	44.8	Mobile

Table 5.3: Notable occupied frequencies for low band observations.

frequencies of the channel have been kept, disregarding the DSP - created rolloffs on the 3.125 MHz BW tuning. Time has been converted to local sidereal time, in relation to Sevilleta, NM, and the following graphs represent both polarizations. The stability is proven by folding each observed sidereal day onto itself to distinctly see the digressions throughout the sidereal day. Figure 5.19 shows the HFRS3's stability and Figure 5.20 shows HFRS1's stability throughout the observations. In addition, unfolded diurnal variations can help detect system downtime during observations.

In the cast of the first observation, a system downtime of 9 hours can be seen in Figure 5.18. The break can also be seen in Figure 5.5.

The folded diurnal graph of the low frequency observations, Figures 5.19, show stability variations from 0.1 to 0.3 dB. However, the high frequency observations are more varied. This is partially due to the slightly less sensitive nature of the RF chain, as well as occupied RFI during that time of the sidereal day. The variations outside of 12:00 to 22:00 LST is from 1/10 to 1/5 of a decibel. Both systems detect the diurnal sky noise changes in the sidereal day and are sky noise dominated.

5.5.5 Comparisons With LWA1 RFI Environment

The RFI can be compared between the recent Sevilleta strong RFI survey and the LWA1 survey done in 2011. Although each survey has been done with different recording equipment, the RFI can still be compared relatively. It is found that RFI is prominent 30% or more of the time below 36 MHz at LWA1 and 33 MHz for Sevilleta. However, there are more specific occupied frequencies exceeding 30% throughout the spectrum above 33 MHz at Sevilleta than at LWA1. See Table 5.1.

At LWA1, spectrum occupancy is largely quiet above 33 MHz all the way to 88 MHz with occasional occupied channels. TV channels 2, 3, and 4 can be seen with regularity from both Sevilleta and LWA1. So can CB, amateur radio, and a number of fixed and mobile transmitters throughout the frequencies. These shared RFI occur with approximately the same level of occupancy. The main difference is that there are more occupied bands in the fixed and mobile frequency allocations in the Sevilleta area. Nighttime observation at Sevilleta show a drastically quieter environment above 20 MHz and below the FM bands. A variety of bands through the spectrum, namely the FM bands, CB bands, and several public and private communications below 20 MHz are so powerful that they saturate the HFRS' amplifiers and compress the entire observation bandwidth. Regardless, it is still possible to see the offending frequency in the percentile spectra, but might throw off the RFI occupancy plot towards the high side, due to the combing that may occur with compression.

In addition, a previous RFI survey was performed at Sevilleta at a number of locations. The results of the observation showed no RFI at the 70 to 73 MHz range and thus all signals in that range can be disregarded as aliasing from lower frequencies.

5.6 North Arm RFI Environment

Observation : February 21, 22:51 to February 23, 18:33 UTC for 1–48 MHz.

The North Arm site is located on the northern terminus of the Very Large Array site, near the end of the northerly run of parabolic dish antennas. It is here that UNM has a second LWA field site, currently used for experimentation. The VLA area is located on the San Agustin plains, 25 miles west of Magdalena, NM. The location can be classified as the "Quiet Rural" radio environment[8] category as determined by the International Telecommunication Union. The North Arm is already known to be a very quiet environment, but an additional observation will provide a current update to the area. The HF-optimized antenna has a high pass filter that suppresses the AM bands in series with a 10 dB attenuator. There is no active amplification of the antenna. Only the X (North/South) polarization was connected to the USRP. For calibration, only the USRP scaling calibration was used on both feeds.

AM frequencies were not picked up very well by design on the optimized antenna. However, the AM stations are indeed powerful in this area since without the high pass AM filter, the entire 1–4 MHz band would saturate the USRP's ADCs with the optimized antenna. Table 5.4 shows notable RFI frequencies above 4 MHz.

Figures 5.21a and 5.21b show the local RFI environment with the HF-optimized antenna. The big antenna can probably benefit from a simple RF chain consisting of a low noise amplifier followed by an attenuator, to provide a better dynamic range than in this observation (Figure5.22).

Frequency (MHz)	Description	Frequency (MHz)	Description
15	WWV	17.6	Broadcasting
19.5	Fixed	20	WWV
25	Amateur or Mobile	30	Fixed and Mobile
40	Mobile	40.7	Mobile
44.6 - 44.7	Fixed and Mobile		
45.7 - 45.9	Fixed and Mobile		

Table 5.4: Notable occupied frequencies for 15–48 MHz, North Arm.

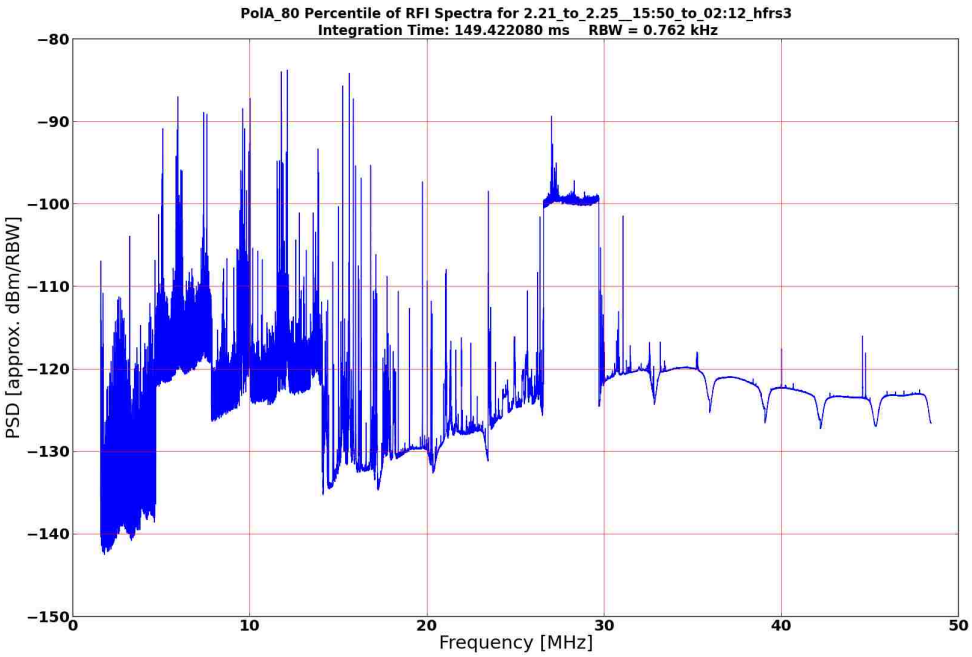

(a) Polarization A, 4–50 MHz

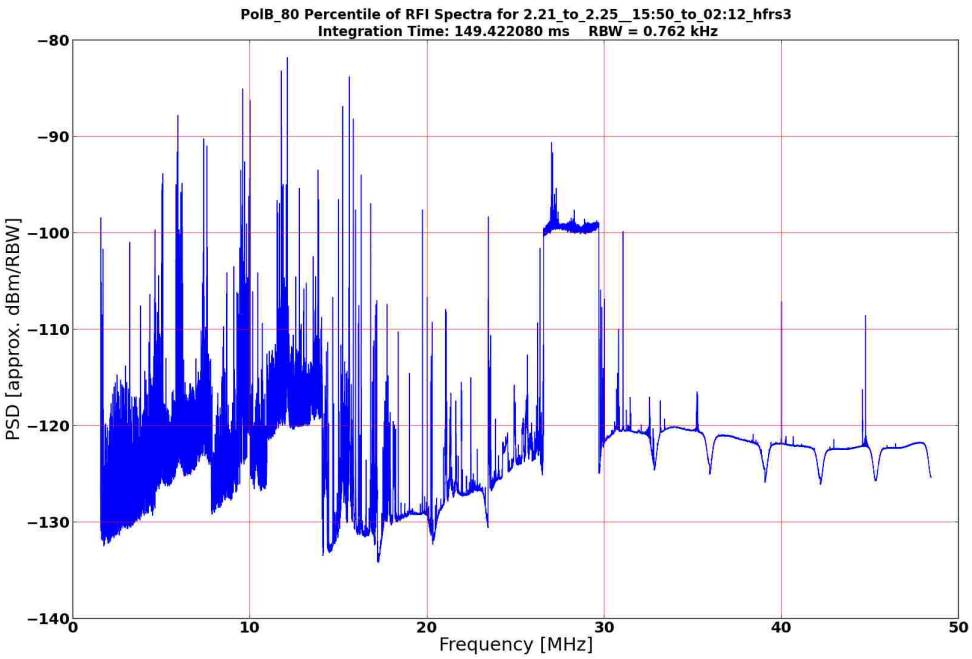

(b) Polarization B, 4–50 MHz

Figure 5.3: 4–50 MHz spectra, first observation, 80th percentile.

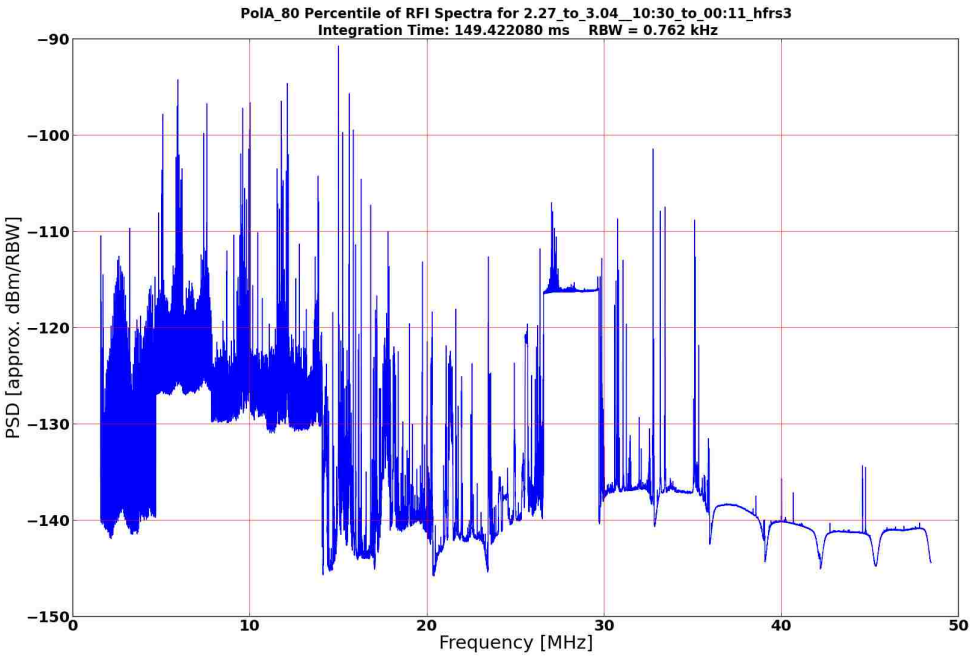

(a) Polarization A, 4–50 MHz

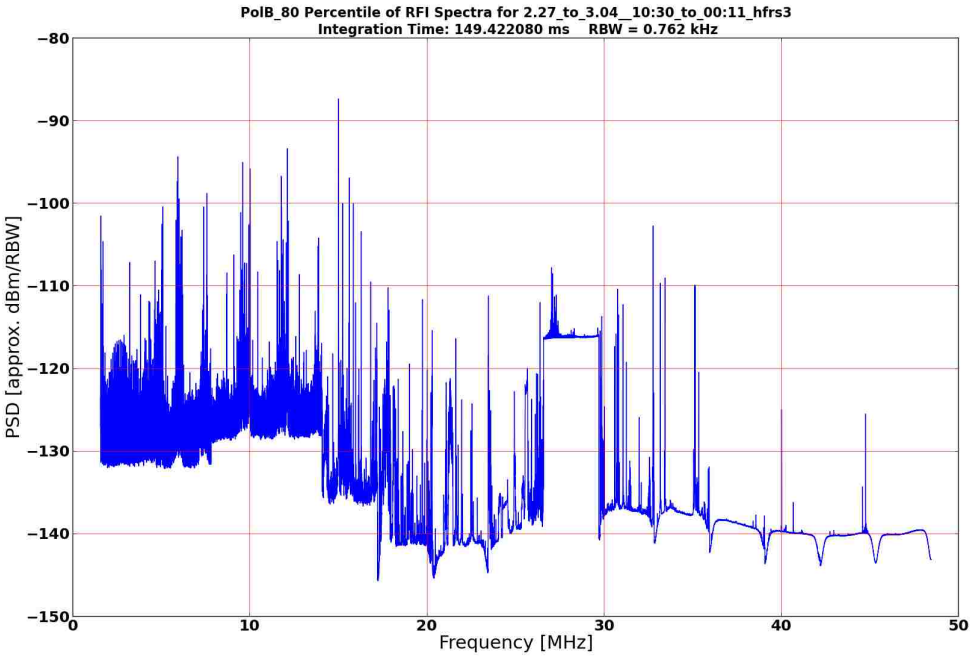

(b) Polarization B, 4–50 MHz

Figure 5.4: 4–50 MHz spectra, second observation, 80th percentile.

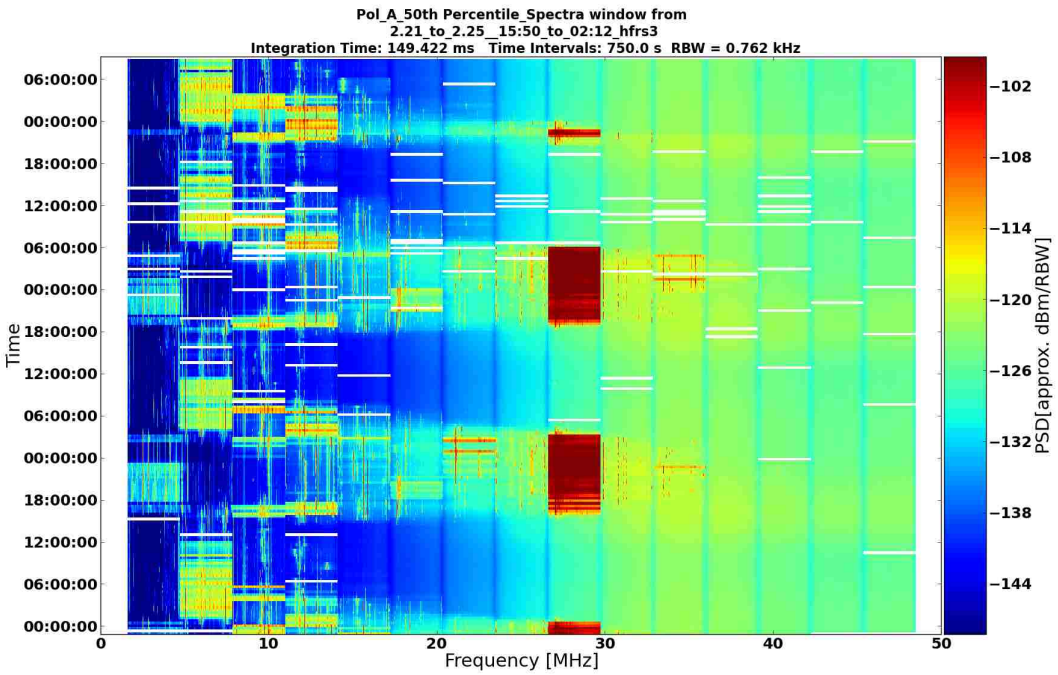

(a) Polarization A, 4–50 MHz

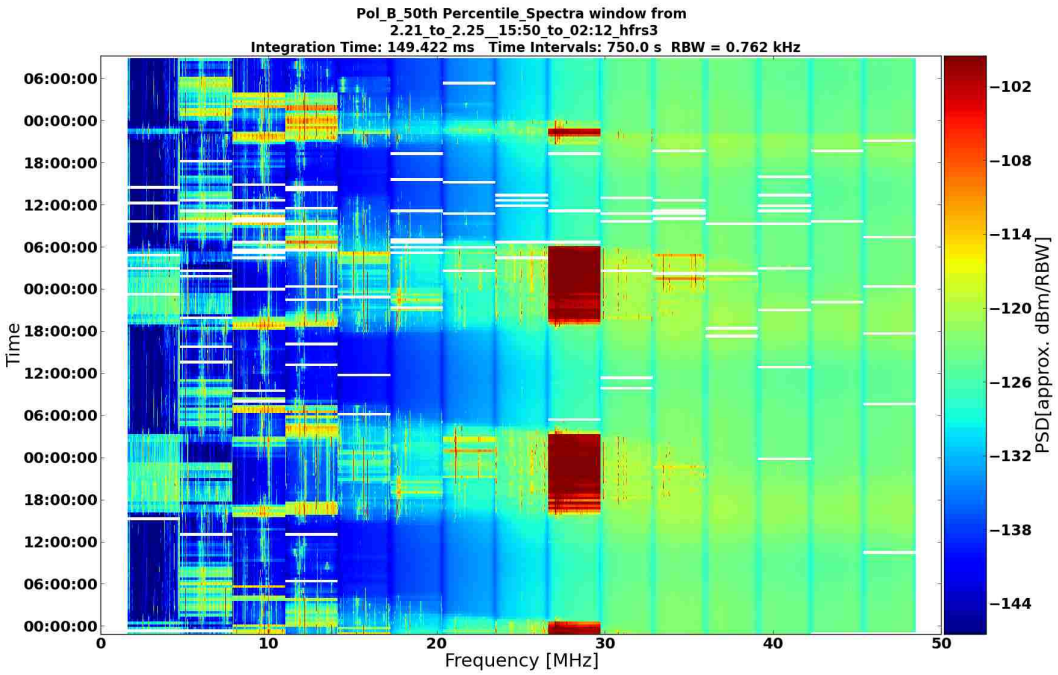

(b) Polarization B, 4–50 MHz.

Figure 5.5: 4–50 MHz waterfalls, first observation, using averaged spectra. There is a lapse in observation towards 20:00 UTC on the last day.

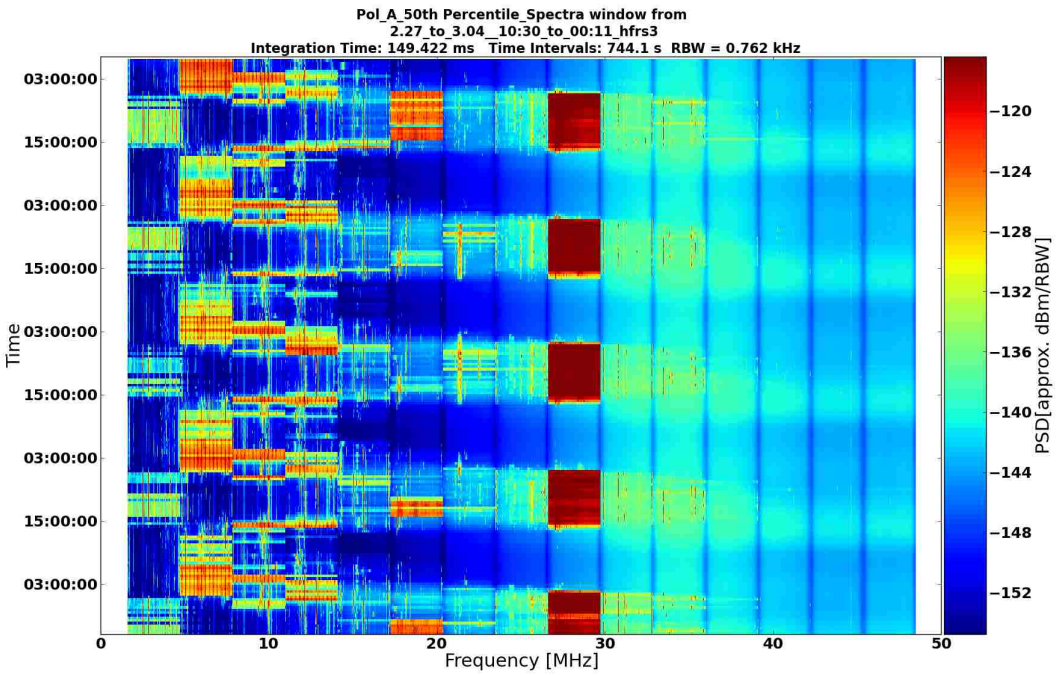

(a) Polarization A, 4–50 MHz

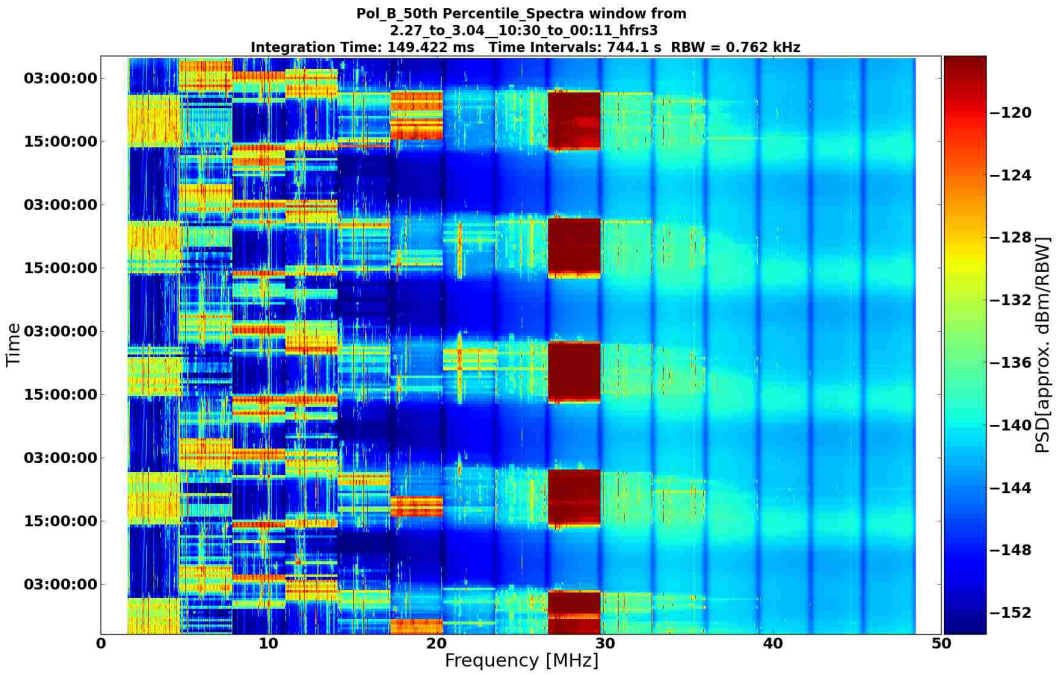

(b) Polarization B, 4–50 MHz

Figure 5.6: 4–50 MHz waterfalls, second observation, using averaged spectra.

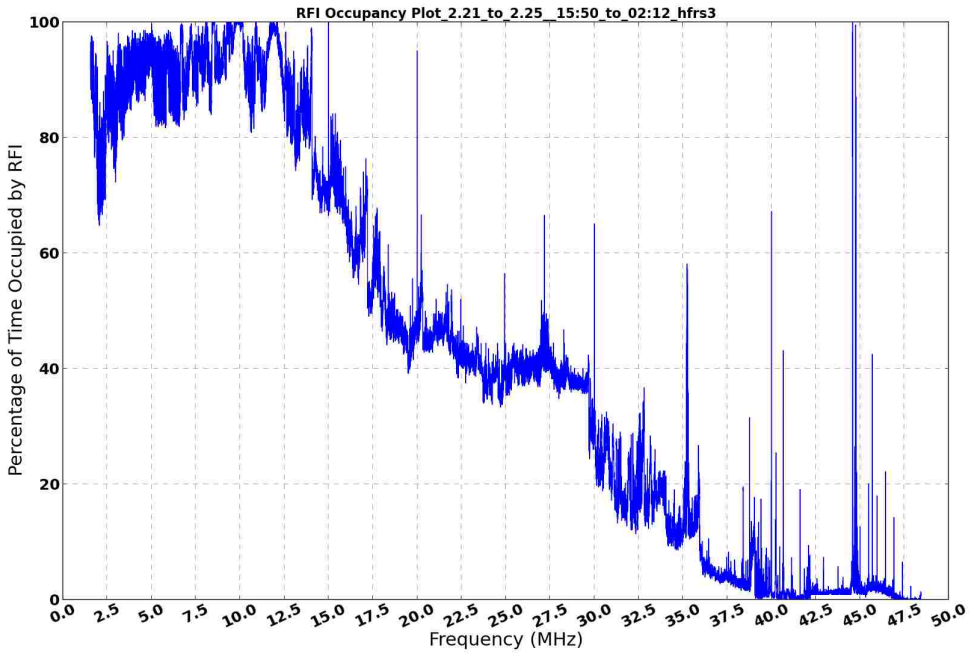

(a) RFI Occupancy Plot, 4–50 MHz, First Observation

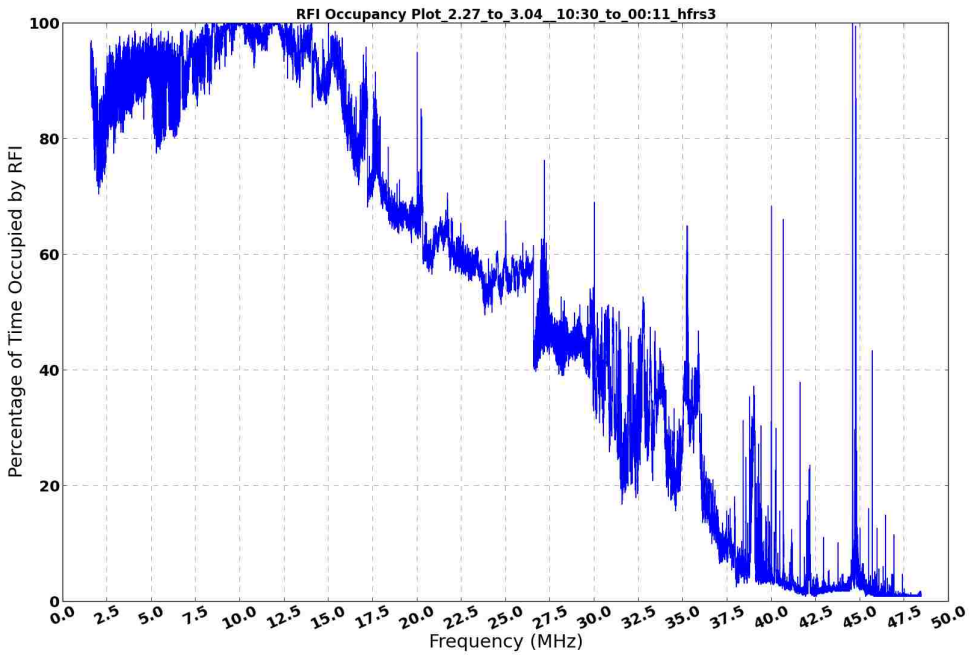

(b) RFI Occupancy Plot, 4–50 MHz, Second Observation

Figure 5.7: Low frequency RFI occupancy plots, both polarizations, using spectral kurtosis.

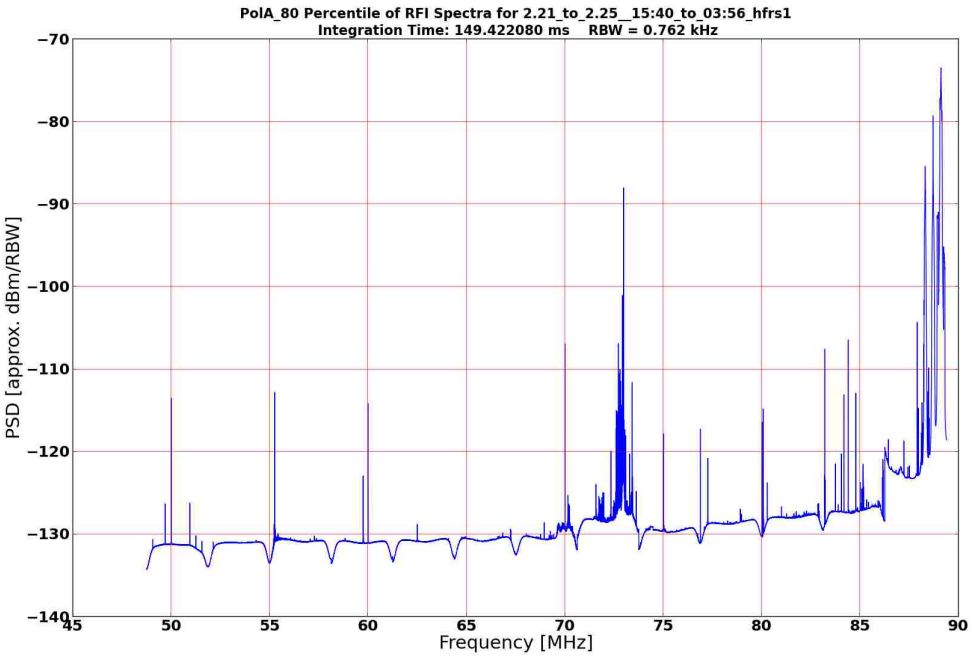

(a) Polarization A, 50-88 MHz

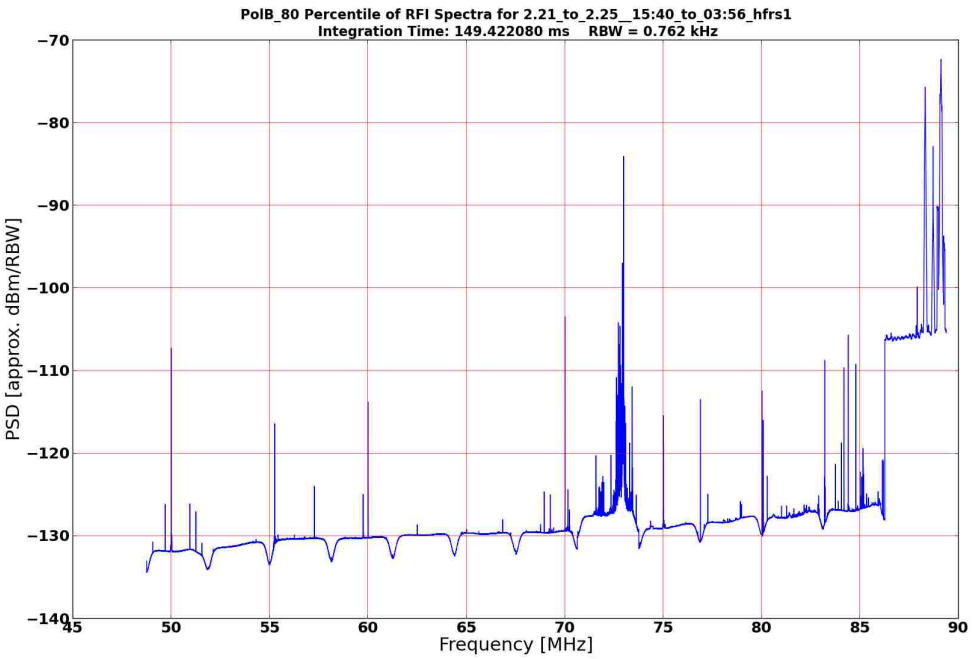

(b) Polarization B, 50-88 MHz

Figure 5.8: 50-88 MHz spectra first observation, 80th percentile.

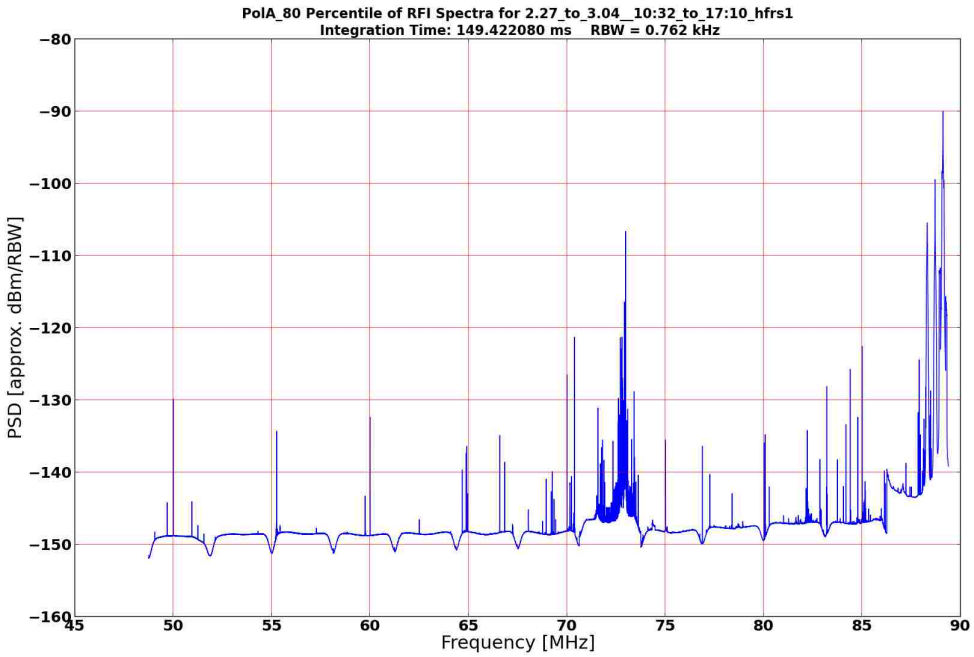

(a) Polarization A, 50-88 MHz

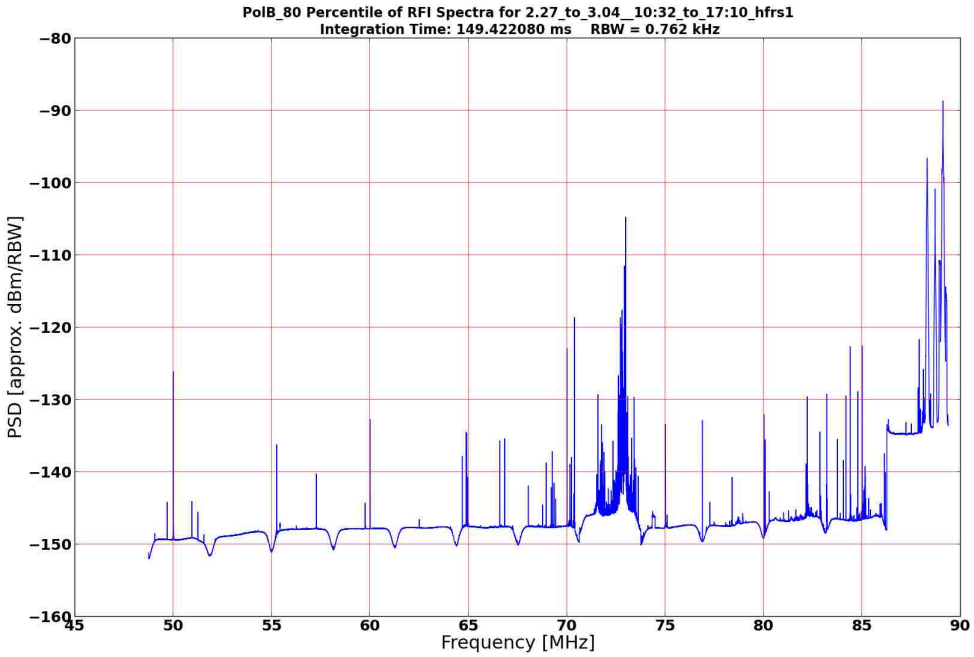

(b) Polarization B, 50-88 MHz

Figure 5.9: 50-88 MHz spectra, second observation, 80th percentile.

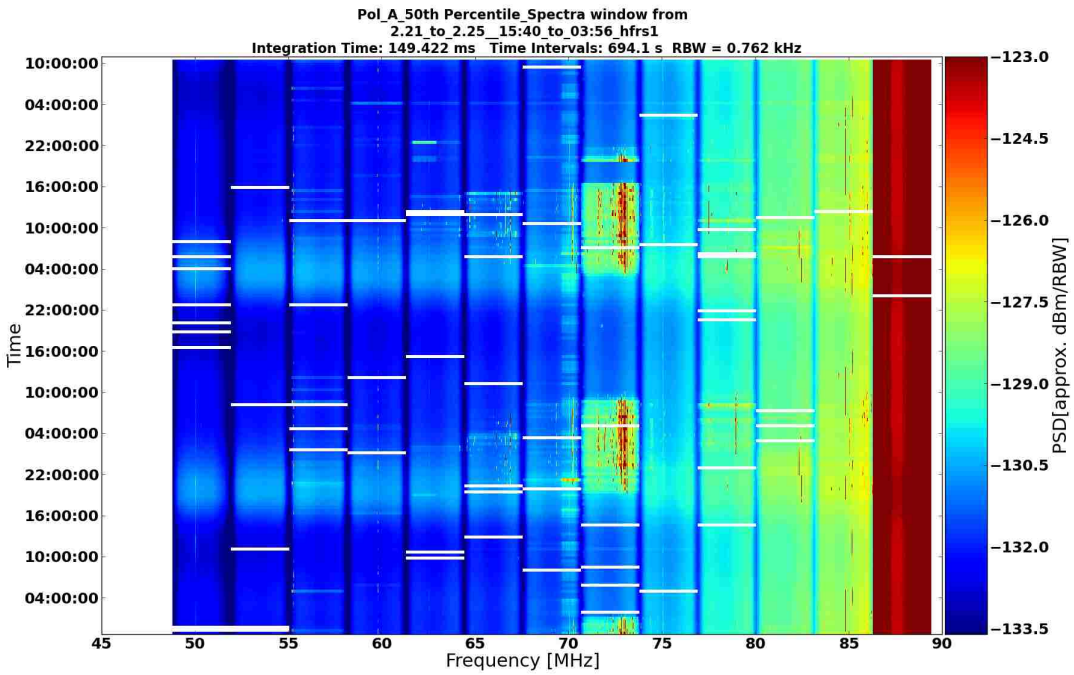

(a) Polarization A, 50-88 MHz

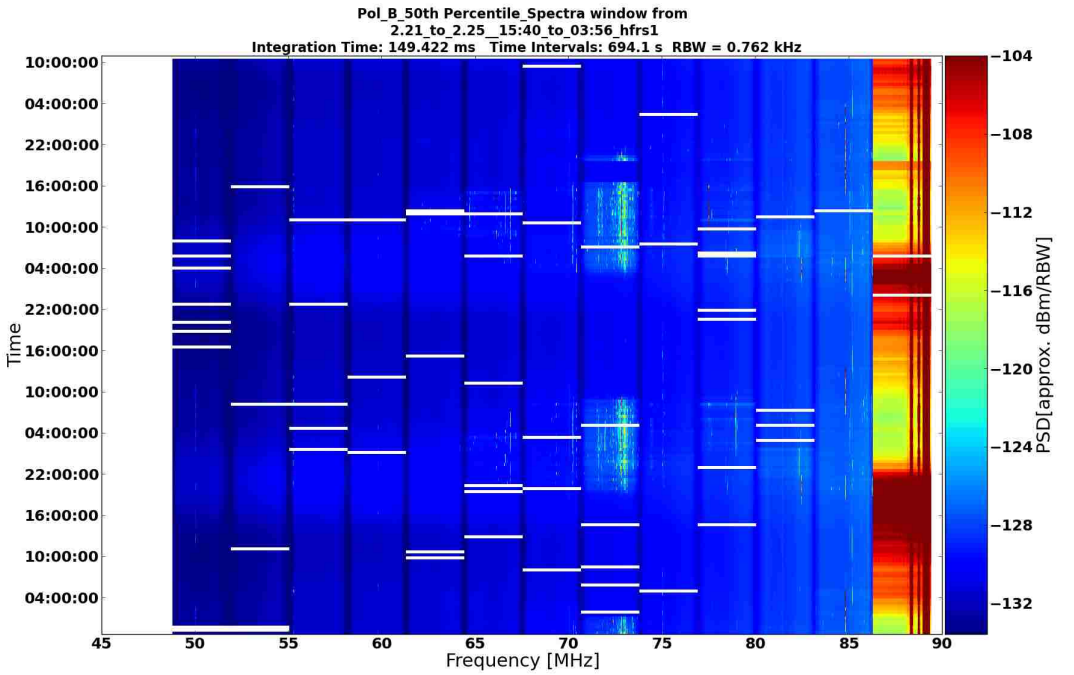

(b) Polarization B, 50-88 MHz

Figure 5.10: 50-88 MHz waterfalls, first observation, using averaged spectra.

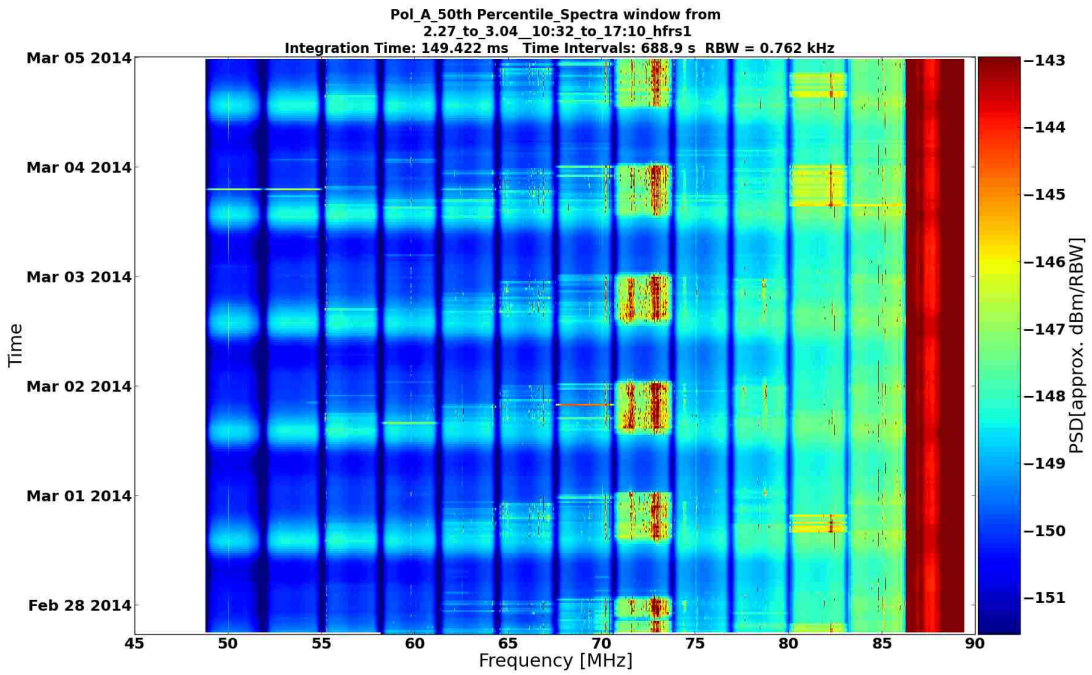

(a) Polarization A, 50-88 MHz

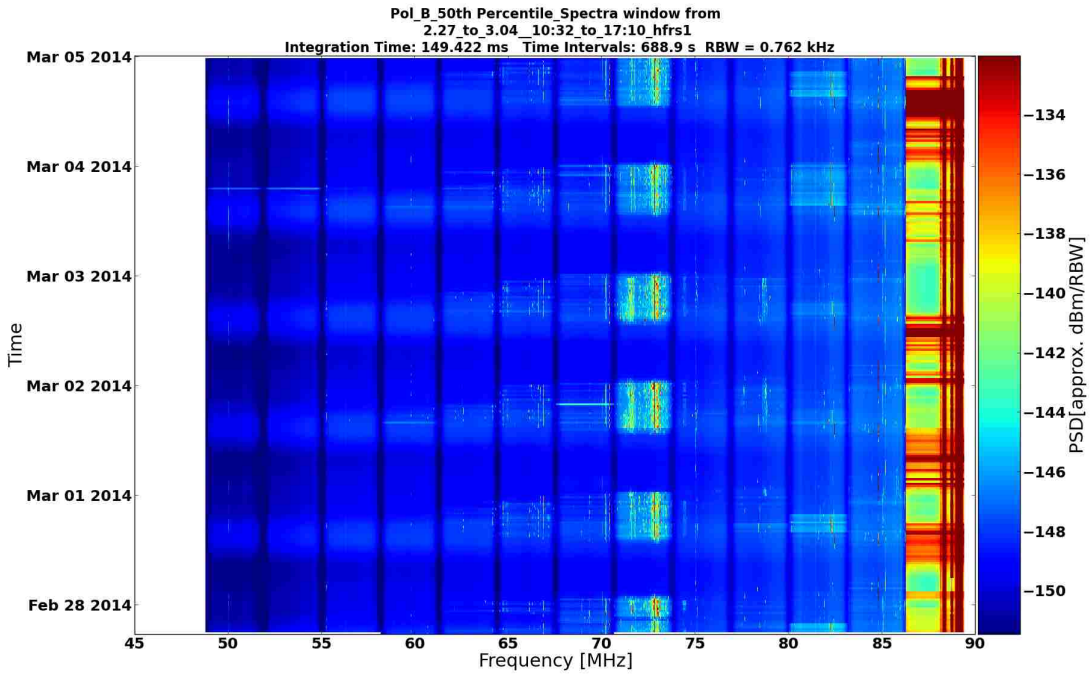

(b) Polarization B, 50-88 MHz

Figure 5.11: 50-88 MHz waterfalls, second observation, using averaged spectra.

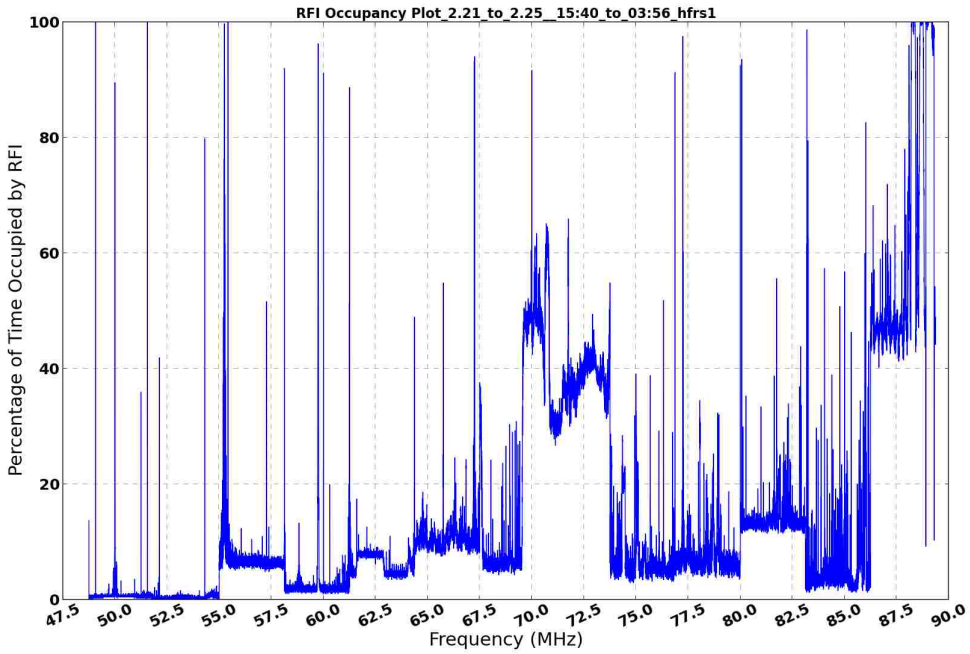

(a) RFI Occupancy Plot, 50–88 MHz, First Observation

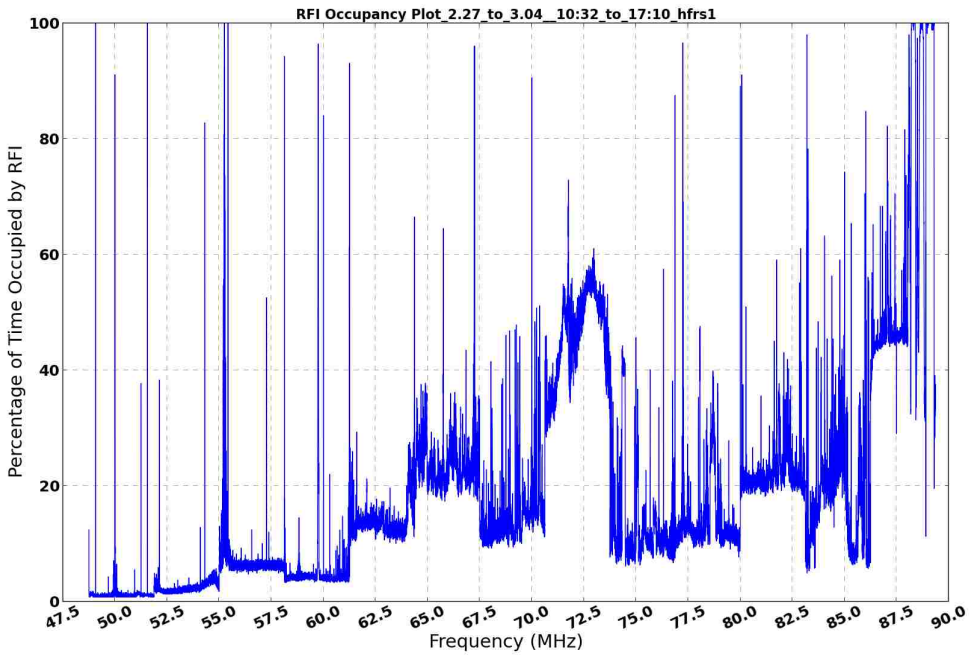

(b) RFI Occupancy Plot, 50–88 MHz, Second Observation

Figure 5.12: High frequency RFI occupancy plots, both polarizations, using spectral kurtosis.

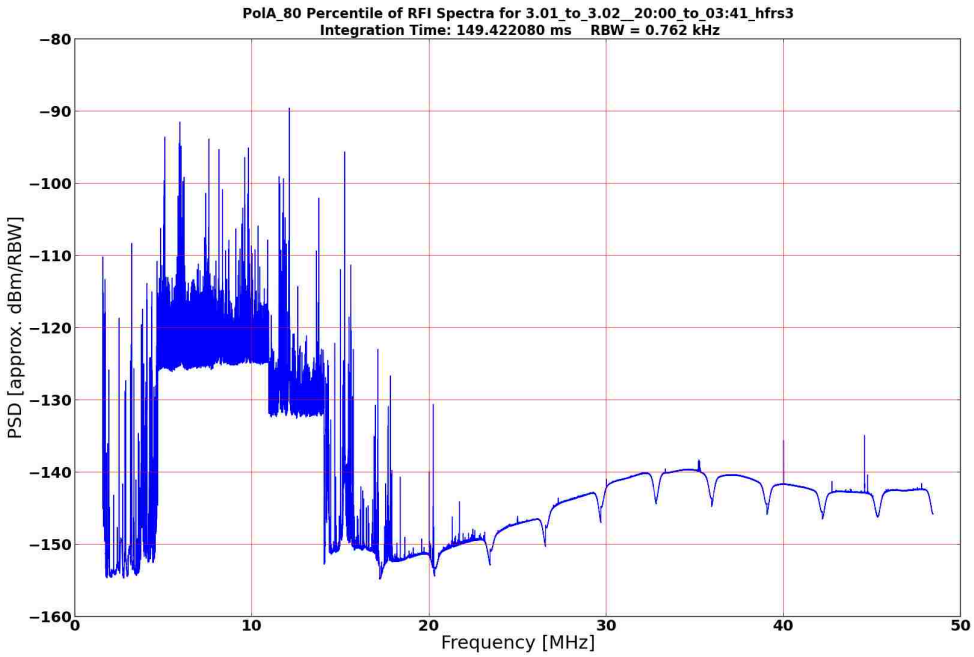

(a) Pol A, 50-88 MHz

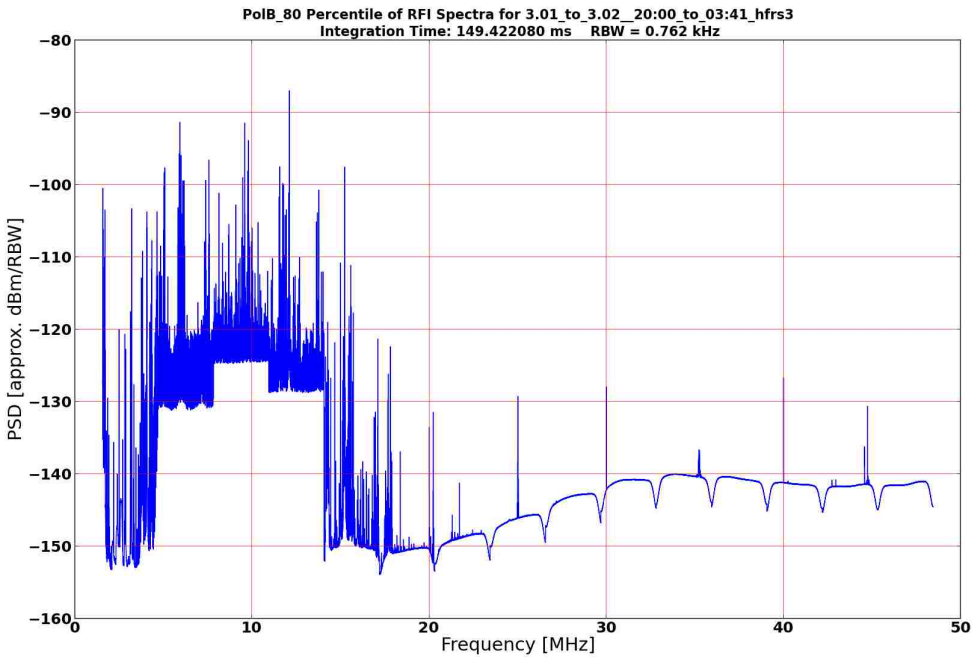

(b) Pol B, 50-88 MHz

Figure 5.13: Dual polarization of March 3, 2014 evening, 80th percentile spectra, 4-50 MHz.

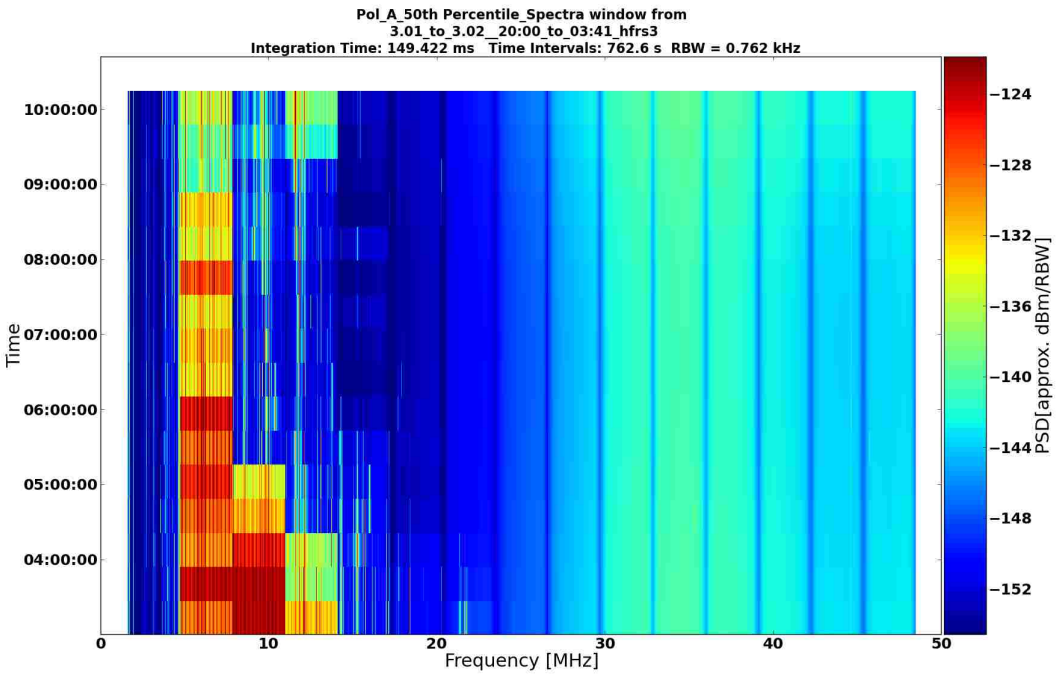

(a) Pol A, 4-50 MHz

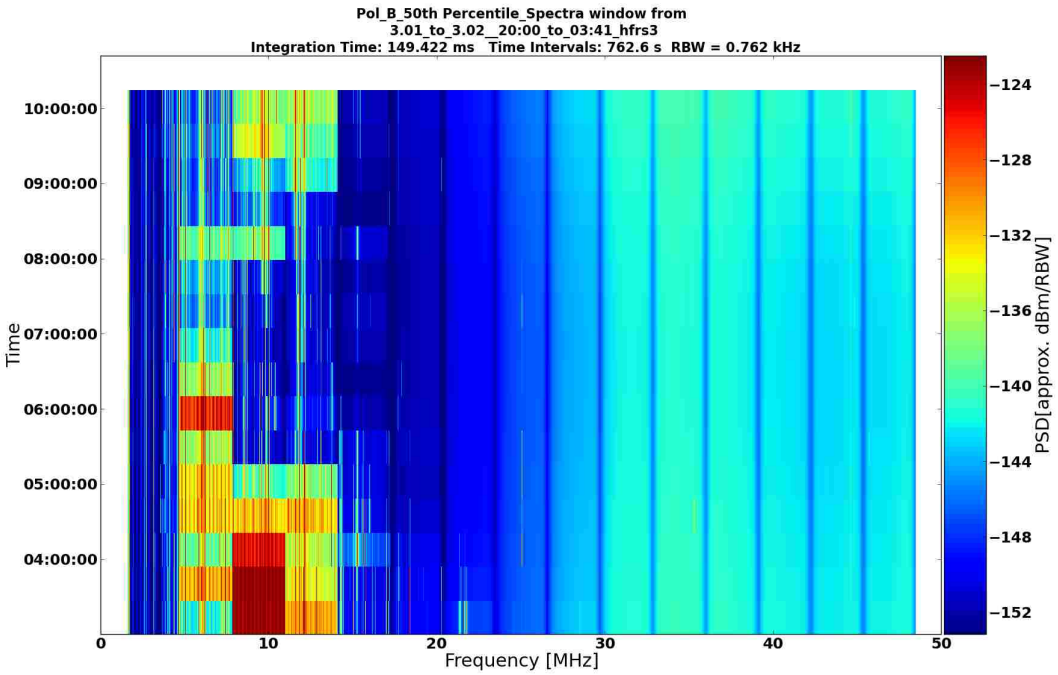

(b) Pol B, 4-50 MHz

Figure 5.14: Dual polarization of March 3, 2014 evening, averaged waterfall, 4-50 MHz.

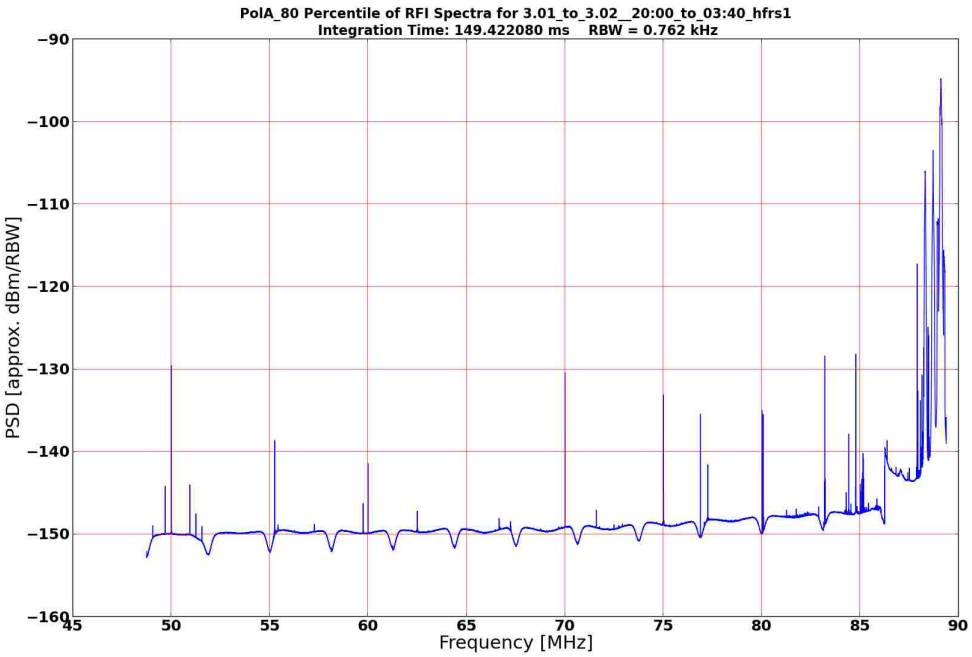

(a) Pol A, 4-50 MHz

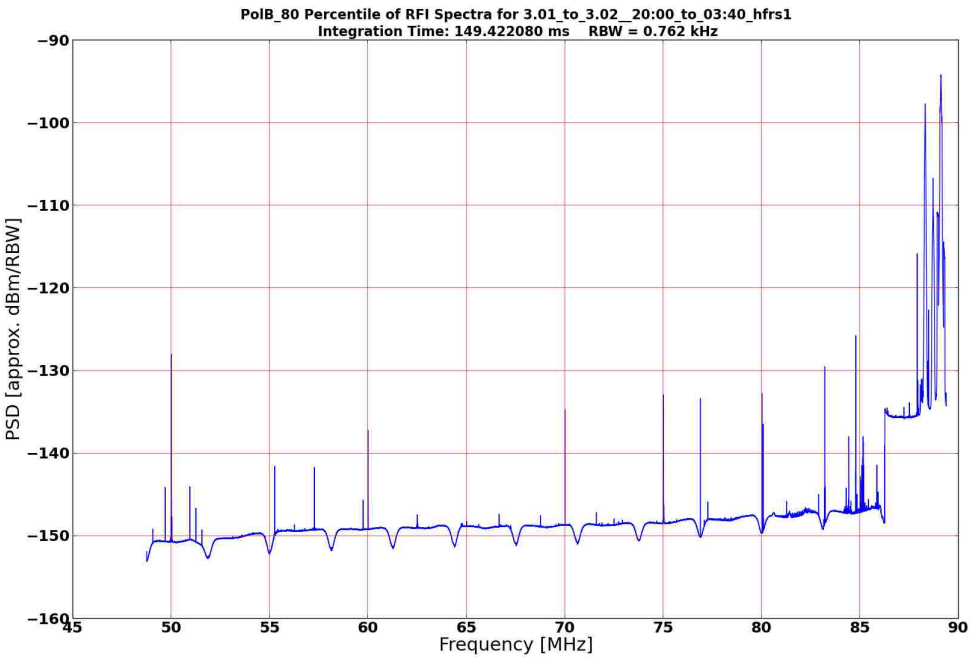

(b) Pol B, 4-50 MHz

Figure 5.15: Dual polarization of March 3, 2014 evening, 80th percentile spectra, 50-88 MHz.

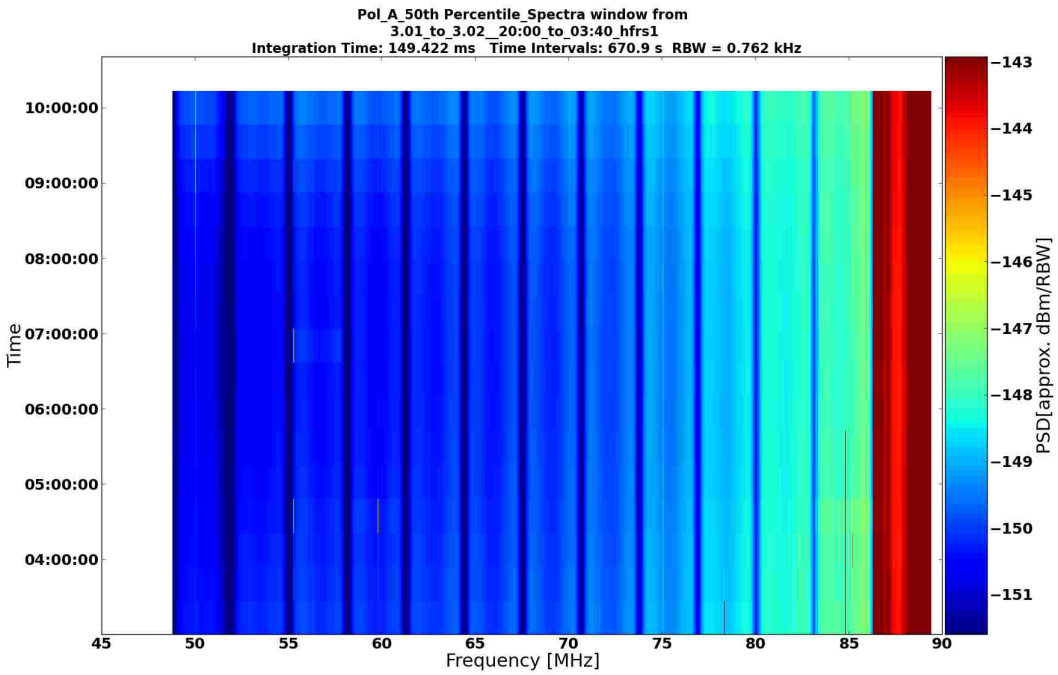

(a) Pol A, 50-88 MHz

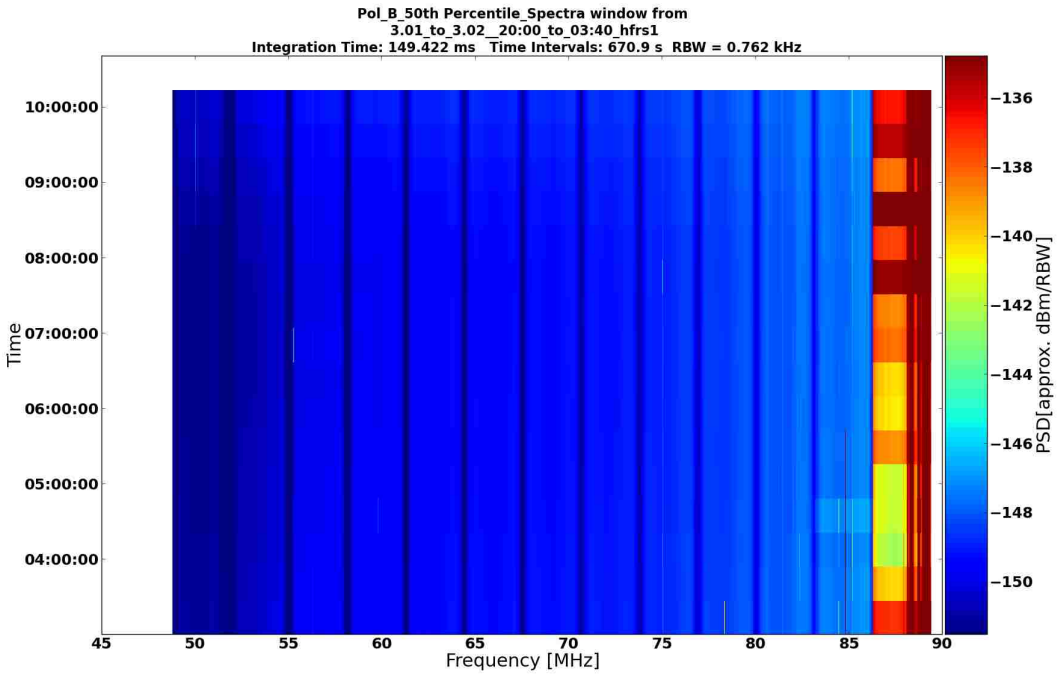

(b) Pol B, 50-88 MHz

Figure 5.16: Dual polarization of March 3, 2014 evening, averaged waterfall, 50-88 MHz.

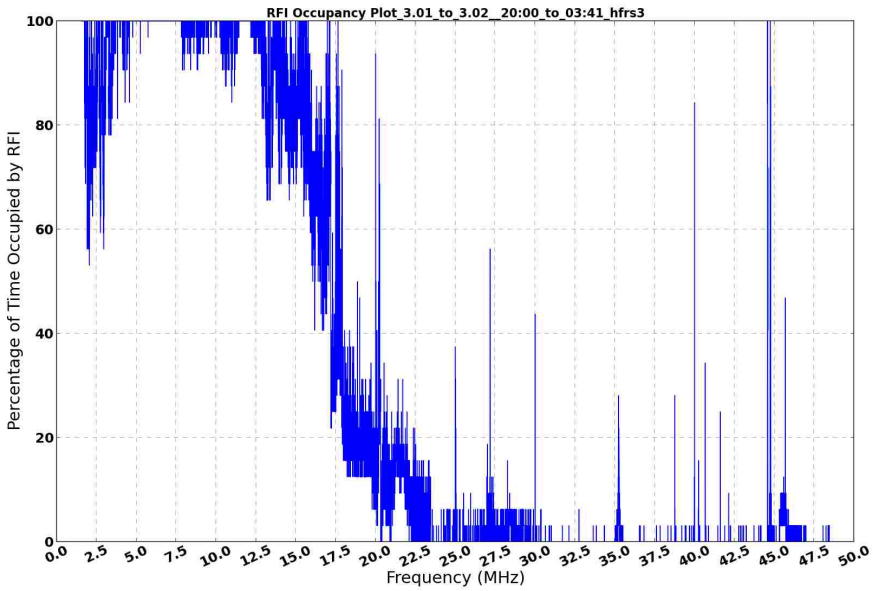

(a) Nighttime RFI Occupancy for 4-50 MHz.

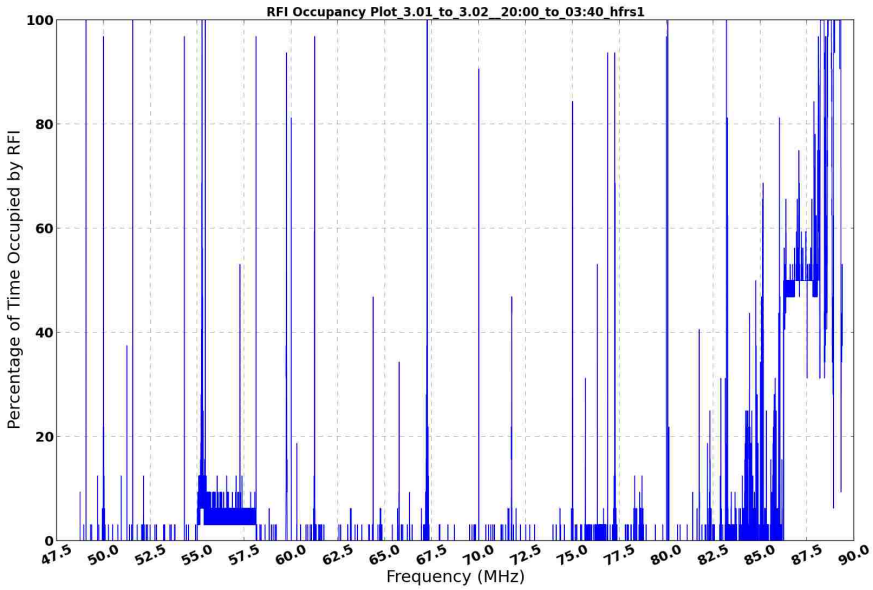

(b) Nighttime RFI Occupancy for 50-88 MHz.

Figure 5.17: RFI occupancy plots for 1-88 MHz during nighttime.

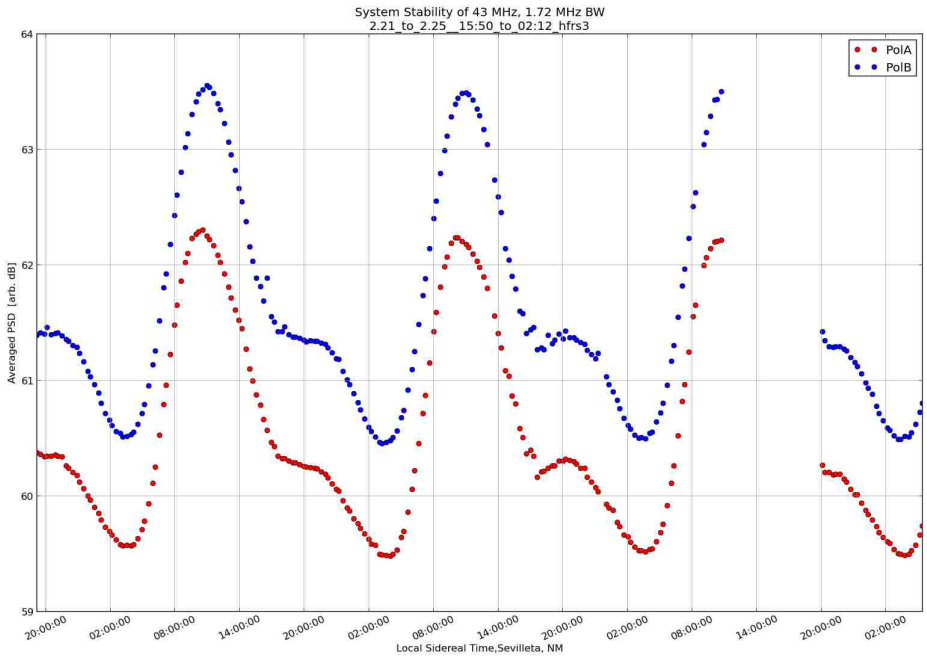

(a) First observation noise floor at 43 MHz of the HFRS3 system, showing system downtime.

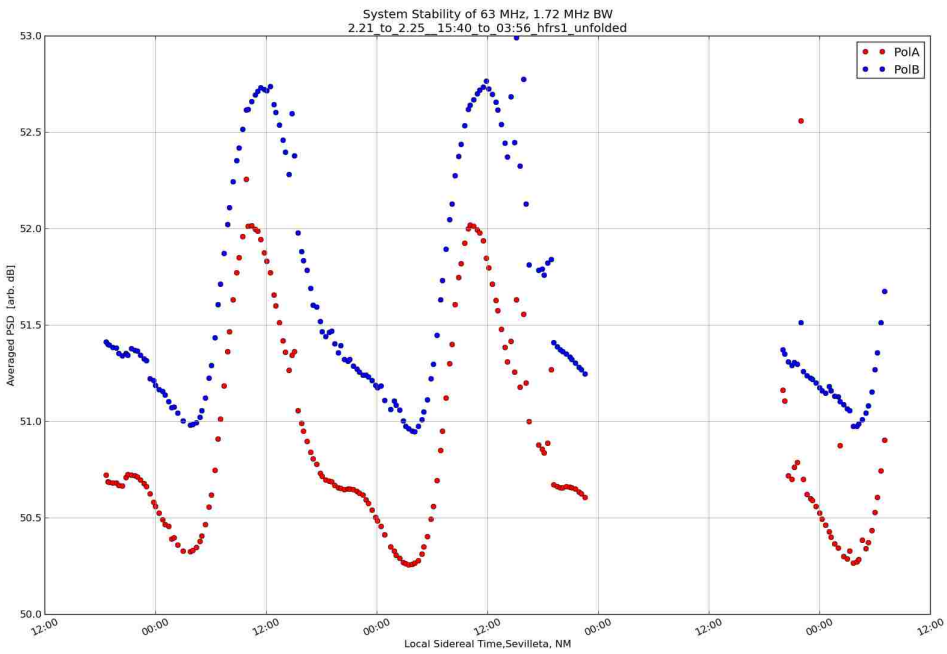

(b) First observation noise floor at 63 MHz of the HFRS1 system, showing system downtime.

Figure 5.18: Unfolded View: First Observation Noise Floor at 43 and 63 MHz.

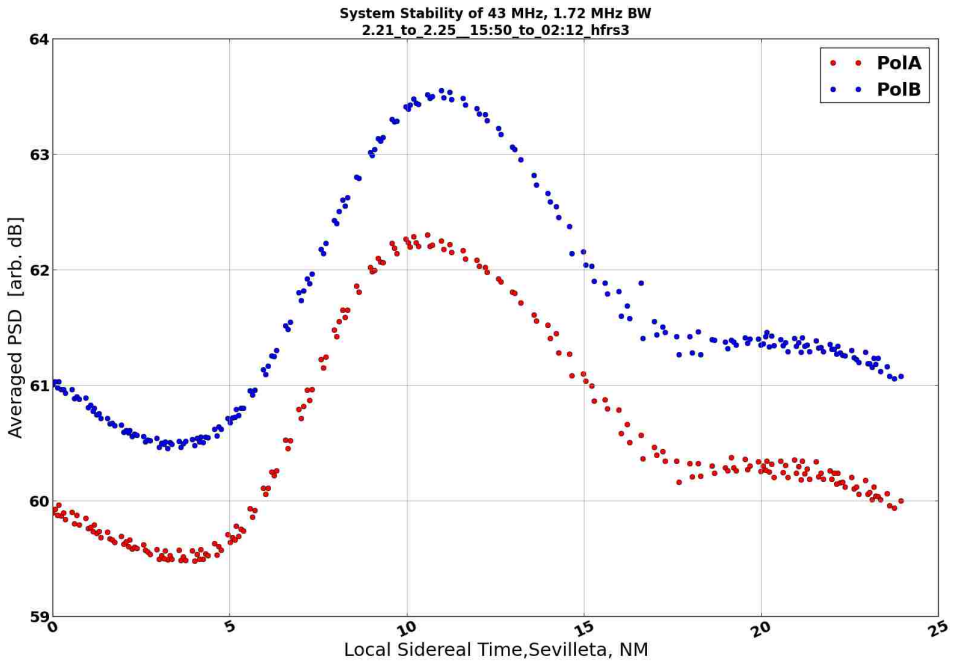

(a) First observation stability at 43 MHz

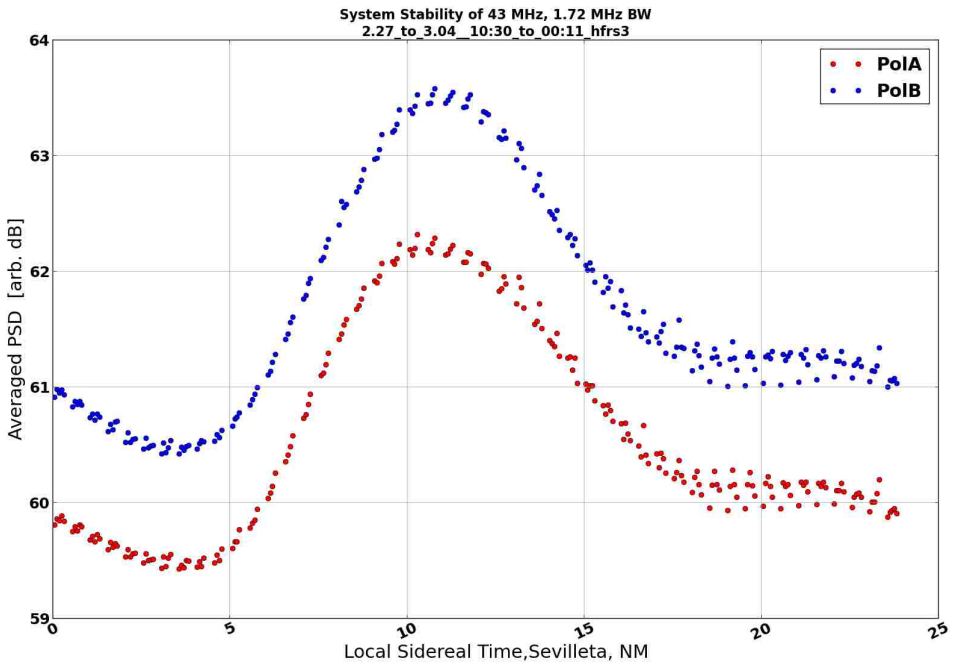

(b) Second-observation stability at 43 MHz

Figure 5.19: System stability at 43 MHz of the HFRS3 (Low Frequency) system.

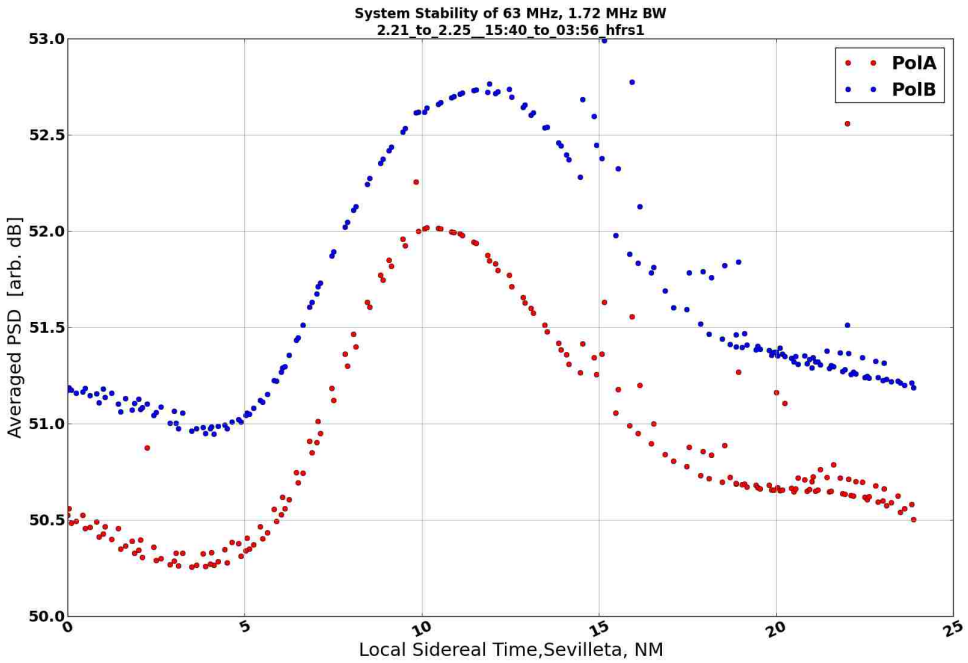

(a) First-observation stability at 63 MHz

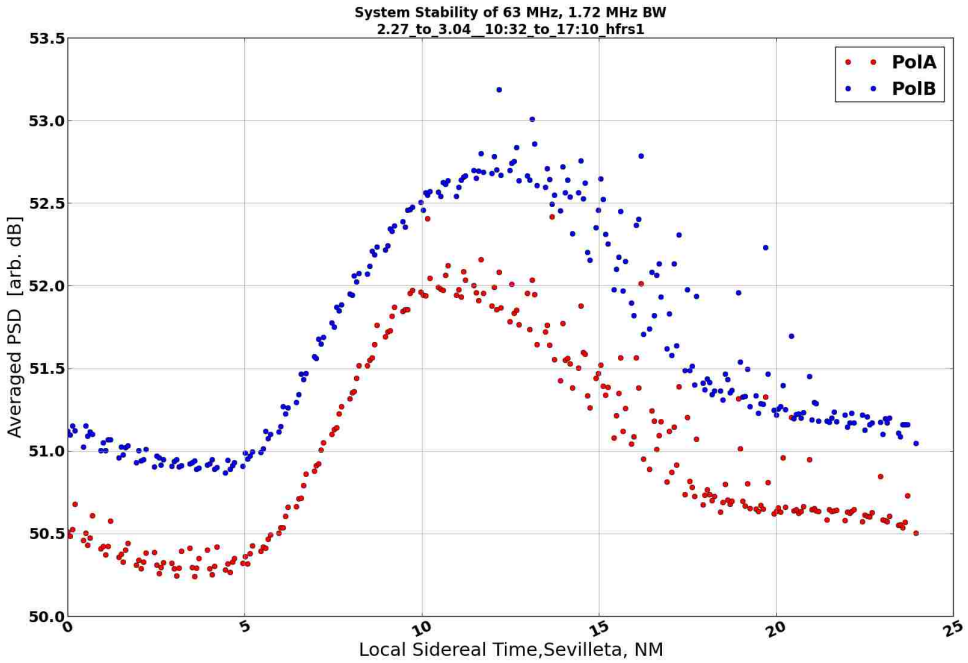

(b) Second-observation stability at 63 MHz

Figure 5.20: System stability at 63 MHz of the HFRS1 (High Frequency) system.

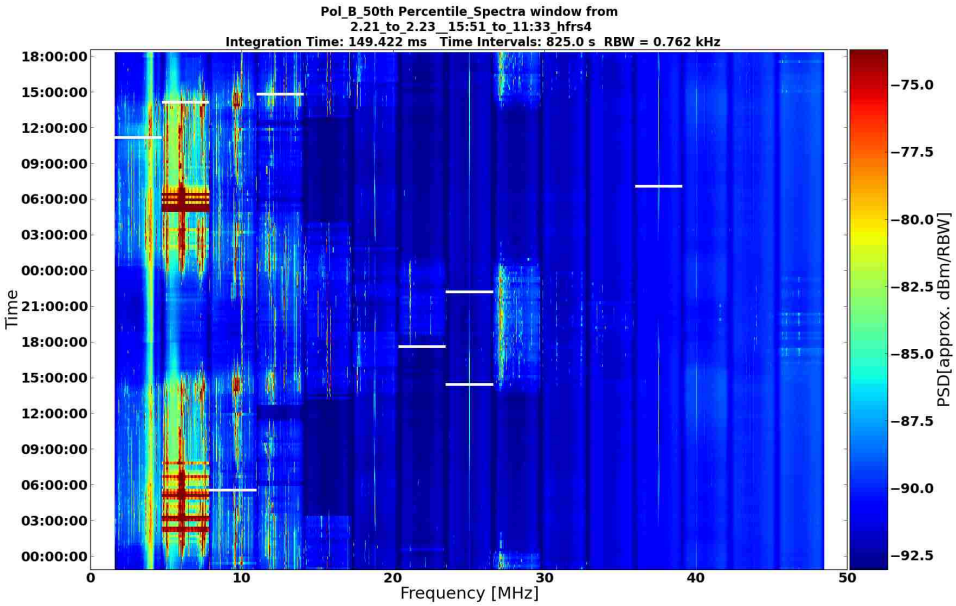

(a) HF-optimized antenna - waterfall, N/S, 1–48 MHz

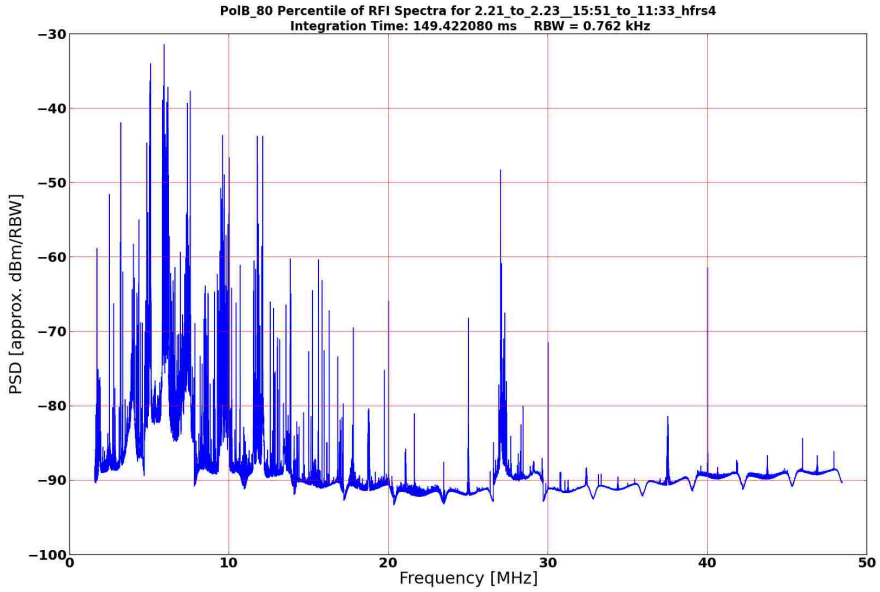

(b) HF-optimized antenna - 80th percentile spectra, N/S, 1–48 MHz

Figure 5.21: Waterfall and 80th percentile spectra using the HF-optimized antenna at the North Arm.

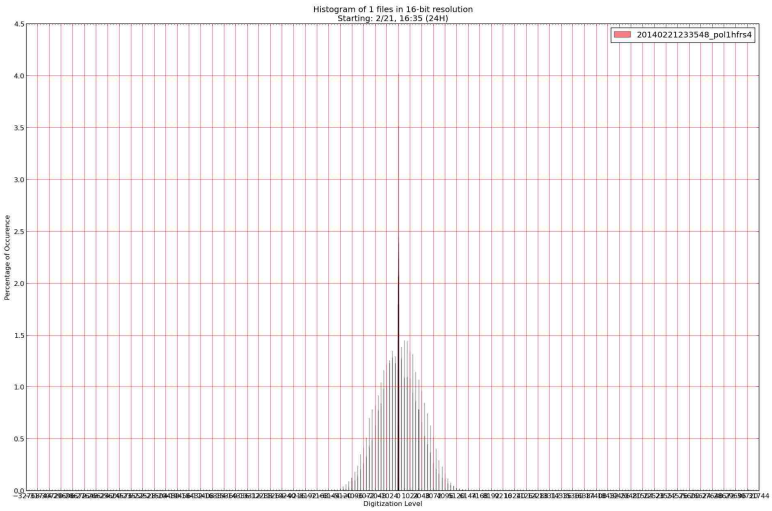

htbp

Figure 5.22: Big Antenna histogram at a loud 12.5 MHz tuning, passive with 10 dB attenuation.

Chapter 6

Conclusions

This document discussed a standalone, field-deployable system that was designed for HF reception and recording. They have been left in the field for more than a month and all sub-systems have proven to be reliable. The most important design objective achieved was a balance between portability, cost, and performance. The HFRS has shown to be successful in the reception of both RFI and ionosonde signals from 1 to 10 MHz. Some other technologies and equipment were considered and some considerations can be made for future design or modifications.

6.1 Future Design

The HFRS possesses much potential for future development. If additional HFRS units were to be constructed, there would be a few critical changes to the hardware.

6.1.1 Power System

GPIO currently works well with the system, but it would be a space saving advantage to utilize the computer's on-board GPIO capabilities instead of an external board solution. A relay board would still be needed for some loads (such as fans and hard drives), but one USB connection can be eliminated. The computer's onboard GPIO hardware is currently not recognized by Linux which necessitates an external GPIO controller.

The power distribution has worked well. The SMPS ordered from Vicor has proven to produce negligible ripples on the voltage line, and additional filtering outside of capacitors was not necessary. Linear voltage regulators, however, will still be used as the final power interface to any analog RF equipment. Overvoltage protection is recommended for the system if left out in the field during seasons that experience electrical storms. A 150V overvoltage suppressor can be installed on the PV positive and battery positive in order to prevent catastrophic damage from stray lightning strikes. This suppressor can be affixed to the breaker box, and wire splices can be made there.

The existing sealed lead-acid battery system is great for this system for a number of reasons: they are cheap, durable, can be used with a number of charge controllers, and are heavy. The weight, as mentioned before, acts as an anchor for the enclosures. However, if a move to smaller, more energy-dense batteries are required, more care will need to be taken in the physical security of the batteries throughout the operating lifetime. They will probably need to be secured to the enclosure and have its temperature more closely monitored. In addition, the HFRS system's health monitoring subsystem will need some way of datalogging voltages, currents, and charges if communication is not available to the specialized charge controller. This health subsystem should also have an alarm function to disconnect all loads from the batteries

in the case of high temperatures if the associated charge controller is not equipped with it.

For safety, it would be a good idea to have a Ground Fault Circuit Interrupter breaker instead of a normal DC breaker between the battery negative and the chassis to further protect against servicing accidents. In the event of a direct short between the battery positive and the grounded chassis, the breaker will sense a current in the battery negative line and break both battery polarizations from the rest of the system.

6.1.2 RF Section

There are a few modifications in the RF section of each system that would make it more versatile in operation and increase its dynamic range and compression point. As a result, a few design changes would be ideal for the next generation of portable antenna recorders. Although the 100' runs of normal coaxial cable exhibited a loss of 3-5 dB from 50 - 100 MHz and can be considered negligible for this type of observation, future systems should be equipped with low-loss cable with a thicker conductor and more hardy insulation. In addition, it would help to extend the run to 200' to assure less EMI from the system as well as preventing any possible metallic coupling to the antenna.

Second, the LWA antenna's FEE would need the first and second stage amplifiers modified to handle a higher compression point, as the existing amplifiers maximize sensitivity for cosmic sources. Third, a digital step attenuator can be placed before the final stage amplifier to assure the best dynamic range for the USRP's ADC. This would be controlled by the computer's GPIO TTL, and can be automated. For example, before each observation, a test stream can be recorded and analyzed for ADC saturation and then the script can increment or decrement the current

attenuation to the final stage amplifier. Perhaps this can be repeated until a suitable Gaussian curve is realized, and then the observation can proceed. This will take some software engineering, especially if the USRP is to stream continuously while adjustment scripts are run.

The last consideration for the RF section of the HFRS is the antenna's resonance. It would be a great asset to maintain the use of a small portable antenna such as that of the LWA for mobile applications, so engineering an antenna tuning subsystem would increase the versatility of the HFRS:

Adjustable Antenna Resonance

An electrically short antenna such as the LWA antenna would need tuning to maximize sensitivity (maximizing VSWR) below 20 MHz. With additional circuitry on the FEE, the unbalanced side of the balun can pass through one of a series of lumped elements or transmission strips via the use of a RF switch. The switch can be toggled using slight voltage changes in the coaxial cable. Inside the enclosure, the 15 V output of the SMPS can instead be routed to a voltage adjuster which can switch between a series of voltages. These series of voltages not only provide power for the FEE, but also as a signal to a comparator which would then toggle the RF switch. The end result is switching the antenna from broadband mode (20–88 MHz) to one of a series of resonant center frequencies. This way, the LWA antenna can enjoy narrowband resonance in a select number of frequencies (which results in better than 2:1 VSWR). The disadvantage is that the FEE will be guaranteed to increase in physical size. The in-enclosure voltage adjuster can be circuitry that is controlled by GPIO from the computer.

6.1.3 Enclosure

The enclosure has done a good job protecting the electronics from the weather. However, even with EMI mitigation techniques, it has proven to still pass some undesired radiation at frequencies below 2 GHz. At the very least, future designs should invest in an enclosure with continuous welds over every seam, fewer penetrations, and a door with multiple latches to apply pressure more evenly on the conductive braid. The computer, USRP, and SMPS have been found to be the more powerful EMI emitters. Although creating a metal enclosure for the computer and power supply would increase the total attenuation of the EMI, the burden still largely relies on the system enclosure to provide the majority of attenuation. There are specially designed EMI-proof enclosures, but they can get upwards of $4,000 for the enclosure size used in this project. Therefore future designs will consider a NEMA 4 or above rated enclosure with the aforementioned design parameters in mind.

6.1.4 RFI Surveys

Future RFI surveys utilizing undersampling techniques will need to use a higher degree Cauer bandpass filter with about 50 or 60 dB stopband attenuation instead of the Cauer high-pass filter with 20 dB stopband used. This would also eliminate the need for additional filters.

6.2 Successful Campaign Results

AFRL has sent back waterfall plots of ionosonde signals picked up by each of the HFRS receiver systems shown in Figure 6.2. Their colormap used for post processing is slightly different. The combing found in the waterfall plots can either be from stray

EMI from the enclosures or the LNAs nearing compression.

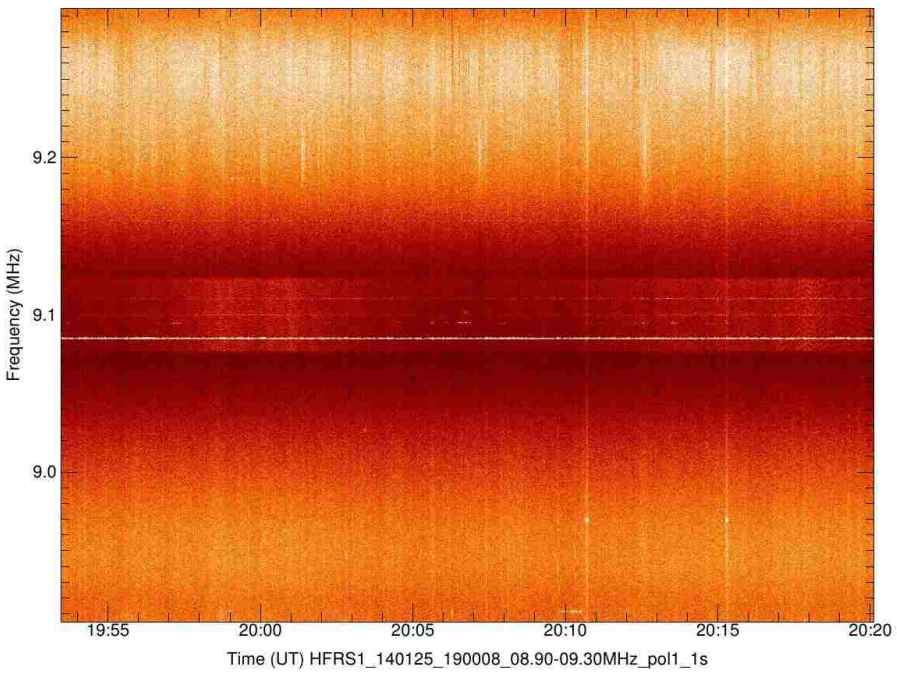

(a) 9.1 MHz Ionosonde observation at Kirtland.

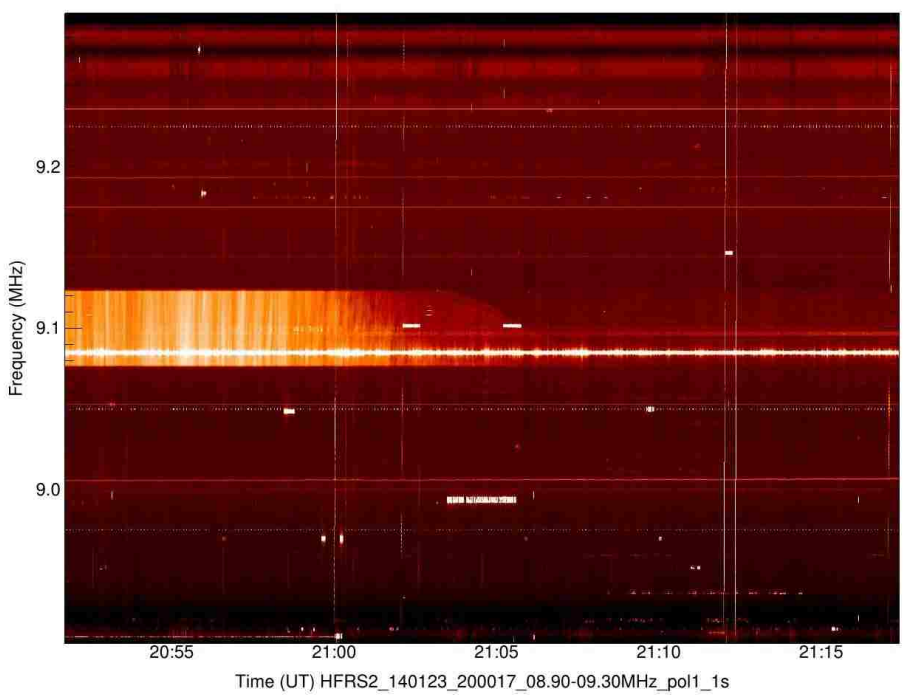

(b) 9.1 MHz Ionosonde observation at North Arm.

Figure 6.1: Waterfalls of ionosonde signal captures during the January-February 2014 campaign.

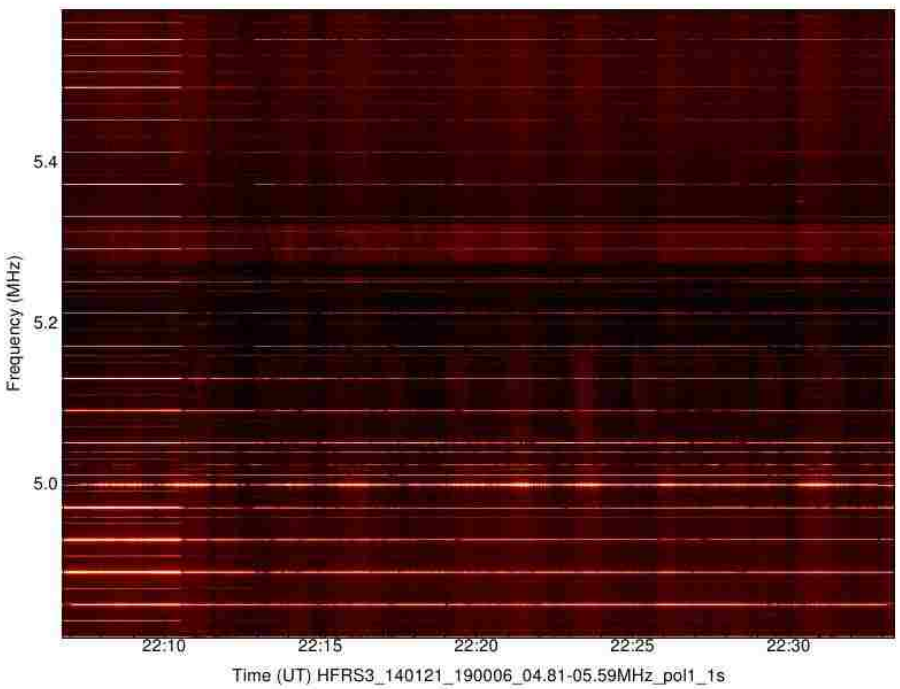

(a) 5.3 MHz Ionosonde observation at Sevilleta.

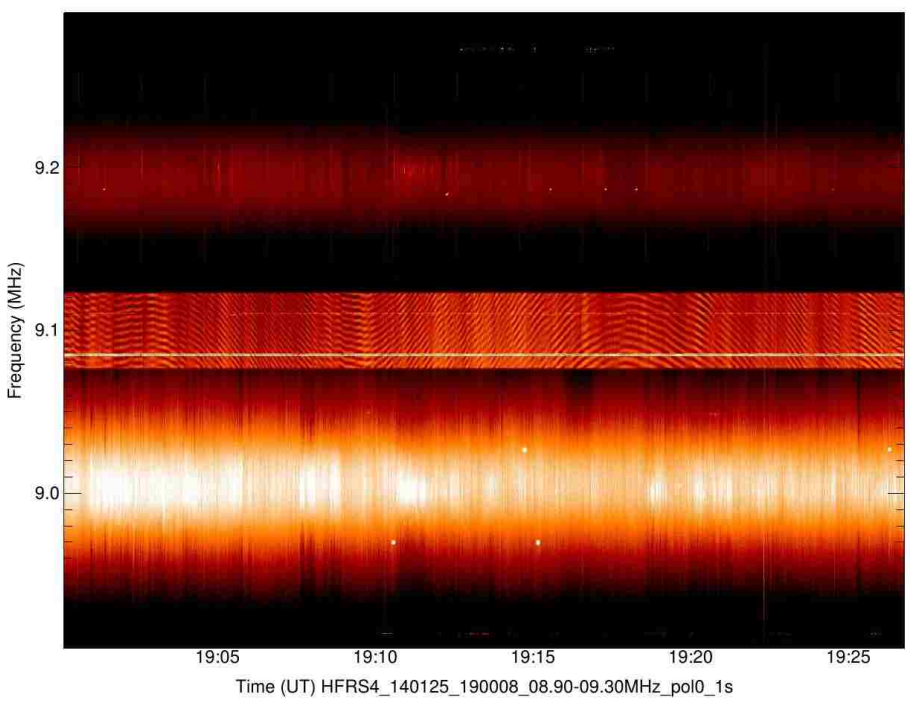

(b) 9.1 MHz Ionosonde observation at Sunspot, near Cloudcroft, New Mexico.

Figure 6.2: Waterfalls of ionosonde signal captures during the January-February 2014 campaign, II.

References

[1] Constantine A. Balanis. *Antenna Theory: Analysis and Design*. Wiley-Interscience, 3 edition, April 2005.

[2] Federal Communications Commission. *FCC Online Table of Frequency Allocations*. FCC Office of Engineering and Technology, Policy and Rules Division, April 2013. http://www.csse.monash.edu.au/documents/bibtex/.

[3] Jayce Dowell. Parametric model for the lwa-1 dipole response as a function of frequency. Dec. 2011. LWA Memo # 178.

[4] Steven W. Ellingson. Antennas for the next generation of low-frequency radio telescopes. *IEEE Transaction on Antennas and Propagation*, 53(8):2480–2489, August 2005.

[5] G.B.Taylor et al. First light for the first station of the long wavelength array. *J. Astron. Instrum.*, 1(1250004). LWA Memo # 185.

[6] Jayce Dowell et al. The long wavelength array software library. *J. Astron. Instrum.*, 1(1250006), 2012. fornax.phys.unm.edu/lwa/trac/wiki.

[7] G.M. Nita & D.E. Gary. Statistics of the spectral kurtosis estimator. *Publications of the Astronomical Society of the Pacific*, 122:595 – 607, May 2010.

[8] International Telecommunication Union. *Radio Noise*. International Telecommunication Union, 1994. ITU-R P.372.6.